

SKB

**TECHNICAL
REPORT**

86-27**Hydraulic testing in crystalline
rock. A comparative study of
single-hole test methods**

Karl-Erik Almén*, Jan-Erik Andersson, Leif Carlsson,
Kent Hansson, Nils-Åke Larsson
Swedish Geological Company

*Since Feb. 1986 with SKB

Uppsala, December 1986

HYDRAULIC TESTING IN CRYSTALLINE ROCK

A COMPARATIVE STUDY OF SINGLE-HOLE TEST METHODS

Karl-Erik Almén*, Jan-Erik Andersson, Leif Carlsson,
Kent Hansson, Nils-Åke Larsson

Swedish Geological Co, Uppsala

*Since Feb. 1986 with SKB

December 1986

This report concerns a study which was conducted for SKB. The conclusions and viewpoints presented in the report are those of the author(s) and do not necessarily coincide with those of the client.

A list of other reports published in this series during 1986 is attached at the end of this report. Information on KBS technical reports from 1977-1978 (TR 121), 1979 (TR 79-28), 1980 (TR 80-26), 1981 (TR 81-17), 1982 (TR 82-28), 1983 (TR 83-77), 1984 (TR 85-01) and 1985 (TR 85-20) is available through SKB.

SWEDISH GEOLOGICAL COMPANY (SGAB)
Division of Engineering Geology
Client: SKB

REPORT
Date: 1986-12-11
ID-no: IRAP 86329

HYDRAULIC TESTING IN CRYSTALLINE ROCK

A COMPARATIVE STUDY OF
SINGLE-HOLE TEST METHODS

Karl-Erik Almén *
Jan-Erik Andersson
Leif Carlsson
Kent Hansson
Nils-Åke Larsson

Sveriges Geologiska AB
December 1986

* Since Feb. 1986 with SKB

ABSTRACT

Swedish Geological Company (SGAB) conducted a literature survey on hydraulic testing in crystalline rock and carried out single-hole hydraulic testing in borehole Fi 6 in the Finnsjön area of central Sweden. The tests were performed during the spring of 1981. The purpose was to make a comprehensive evaluation of different methods applicable in crystalline rocks and to recommend methods for use in current and scheduled investigations in a range of low hydraulic conductivity rocks. A total of eight different methods of testing were compared using the same equipment. This equipment was thoroughly tested as regards the elasticity of the packers and change in volume of the test section. The use of a hydraulically operated down-hole valve enabled all the tests to be conducted.

Twelve different 3-m long sections were tested in borehole Fi 6. The hydraulic conductivity calculated ranged from about 5×10^{-14} m/s to 1×10^{-6} m/s. The methods used were water injection under constant head and then at a constant rate-of-flow, each of which was followed by a pressure fall-off period. Water loss, pressure pulse, slug and drill stem tests were also performed. Interpretation was carried out using standard transient evaluation methods for flow in porous media. The methods used showed themselves to be best suited to specific conductivity ranges. Among the less time-consuming methods, water loss, slug and drill stem tests usually gave somewhat higher hydraulic conductivity values but still comparable to those obtained using the more time-consuming tests. These latter tests, however, provided supplementary information on hydraulic and physical properties and flow conditions, together with hydraulic conductivity values representing a larger volume of rock.

The methods that in 1981 was recommended for use in the standard hydraulic testing programme was two-hour water injection tests under a constant head, followed by a fall-off period of two hours. The selection was based on the criteria of easy handling and evaluation of a large amount of data, applicability in a wide range of hydraulic conductivities, large influence volume and negligible changes in the volume of the section tested.

CONTENTS	Page
ABSTRACT	
INTRODUCTION	1
1. SINGLE-HOLE TESTS, TYPES AND METHODS	4
2. CHARACTERIZATION OF FRACTURED CRYSTALLINE ROCK	8
2.1 General	8
2.2 Conceptual model	8
2.3 Hydraulic properties	10
2.3.1 Hydraulic conductivity	10
2.3.2 Porosity	11
2.3.3 Specific storage coefficient	13
2.3.4 Hydraulic head	15
2.4 Theoretical models of crystalline rocks	16
2.5 Interpretation of single-hole tests	18
3. INFLUENCE OF SKIN AND BOREHOLE STORAGE EFFECTS ON SINGLE-HOLE TESTS	22
3.1 General	22
3.2 Skin effect	22
3.3 Borehole storage effect	25
4. INJECTION/DRAWDOWN TESTS IN HOMOGENEOUS FORMATIONS	28
4.1 General	28
4.2 Radial flow	28
4.2.1 Constant-rate-of-flow tests	28
4.2.2 Constant-pressure tests	37
4.3 Spherical flow	40
4.3.1 Constant-rate-of-flow tests	40
4.3.2 Constant-pressure tests	43
4.4 Steady-state injection tests	44
4.4.1 General	44
4.4.2 Theory and analysis	44
4.4.3 Applications	46

5.	RECOVERY TESTS IN HOMOGENEOUS FORMATIONS	47
5.1	General	47
5.2	Radial flow	47
5.2.1	Tests after a constant-rate-of-flow period	47
5.2.2	Tests after a constant-pressure period	53
5.3	Spherical flow	55
5.3.1	Tests after a constant-rate-of-flow period	55
5.3.2	Tests after a constant-pressure period	57
6.	DUAL-POROSITY FORMATIONS	58
6.1	General	58
6.2	Theoretical models of dual-porosity formations	59
6.3	Theory and test interpretation	61
6.3.1	Constant-rate-of-flow tests	61
6.3.2	Constant-pressure tests	64
7.	BOREHOLES INTERSECTED BY DISCRETE FRACTURES	66
7.1	General	66
7.2	Conceptual models	66
7.3	Theory and interpretation	69
7.3.1	Drawdown and injection tests	69
7.3.2	Build-up (fall-off) tests	76
8.	PULSE RESPONSE TESTS	78
8.1	General	78
8.2	Slug tests	78
8.3	Pressure pulse tests	82
8.4	Drill stem tests (DST)	85
9.	TESTS PERFORMED	88
9.1	General	88
9.2	Description of the test site	89
9.2.1	Finnsjön field research area	89
9.2.2	Borehole Fi 6	90

9.3	Test equipment	91
9.3.1	Measuring probe	92
9.3.2	Flow meters and injection system	93
9.3.3	Performance tests on equipment	94
9.3.4	Elastic properties of the test equipment	95
9.3.5	Correction for the elasticity of the equipment	96
9.4	Test methods	99
9.4.1	Constant-rate-of-flow injection tests	99
9.4.2	Pressure fall-off tests after injection at a constant-rate-of-flow	100
9.4.3	Constant-pressure injection tests	101
9.4.4	Pressure fall-off tests after injection at constant pressure	101
9.4.5	Water loss measurements	101
9.4.6	Slug tests	102
9.4.7	Pressure pulse tests	102
9.4.8	Drill stem tests	103
10.	RESULTS AND COMMENTS	105
10.1	Constant-rate-of-flow injection tests	105
10.1.1	Evaluation	105
10.1.2	Results	107
10.2	Pressure fall-off tests after injection at a constant-rate-of-flow	115
10.2.1	Evaluation	115
10.2.2	Results	116
10.3	Constant-pressure injection tests	117
10.3.1	Evaluation	117
10.3.2	Results	119
10.4	Pressure fall-off tests after injection at constant pressure	124
10.4.1	Evaluation	124
10.4.2	Results	125
10.5	Water loss measurements	126
10.5.1	Evaluation	126
10.5.2	Results	126

10.6	Slug tests	126
10.6.1	Evaluation	126
10.6.2	Results	128
10.7	Pressure pulse tests	129
10.7.1	Evaluation	129
10.7.2	Results	131
10.8	Drill stem tests	134
10.8.1	Evaluation	134
10.8.2	Results	134
11. COMPARISONS OF DIFFERENT METHODS		137
11.1	Summary of results	137
11.2	Section-by-section comparisons	138
11.3	Method comparisons	145
11.4	Conclusions	151
11.4.1	Applicability of the various methods	152
11.4.2	Selection of a method	153
12. HYDRAULIC TESTING FOR SITE CHARACTERIZATION		157
12.1	Hydraulic tests - methods and equipment	157
12.1.1	Test sequence	157
12.1.2	Test equipment	158
12.1.3	Description of graphs plotted	161
12.2	Hydrogeological data base	162
REFERENCES		165
DESIGNATIONS		174
APPENDIX - CORE LOGS		176

INTRODUCTION

At the request of the Swedish Nuclear Fuel and Waste Management Co. (SKB), the Swedish Geological Company (SGAB) conducted a comprehensive study of the methods used to carry out various types of single-hole hydraulic test. The work comprised studies of the theoretical conditions for the tests and their evaluation. On the basis of this work, a field measurement programme was then implemented to test the applicability of the methods.

The method tests were performed in borehole Fi 6 in the Finnsjön test area of northern Uppland in central Sweden during the spring of 1981. The following methods of hydraulic testing were employed:

- o Transient constant-rate-of-flow injection test
- o Pressure fall-off test (after the above test)
- o Transient constant-pressure injection test
- o Pressure fall-off test (after the above test)
- o Water injection test with constant pressure under assumed steady-state conditions (water loss test)
- o Slug test
- o Pressure pulse test
- o Drill stem test

The same equipment, with minor modifications, was used for all method tests. The method tests were preceded by comprehensive tests of the elasticity of the packers and volume changes in the test sections.

The aim of this method study was to gain experience and information on which to base decisions for the selection of methods of hydraulic testing suitable for investigation of low hydraulic conductivity, crystalline bedrock. A basic consideration was, if possible, to select a main method for use in the SKB standard programme for site characterization. Important criteria in the selection of a method included ease of handling, large measuring range (range of hydraulic conductivities), representativeness (large influence volume), volume-stable test section, minimization of instrument and

measurement procedure errors.

Chapter 1 specifies the principles for hydraulic tests, describes various types of test, together with the circumstances under which each is used and what information it provides.

Chapter 2 contains views on the properties of a crystalline bedrock as a groundwater transport medium. Significant hydraulic parameters, such as hydraulic conductivity, porosity and specific storage, are defined and quantified. Finally, different theoretical models for interpretation of single-hole hydraulic tests are discussed.

Skin and borehole storage effects are two factors that may affect the response of a test and which it is important to take into account in the evaluation of a test. These factors and how to keep them to a minimum by the design of tests and instruments are described in Chapter 3.

Chapters 4 and 5 deal with hydraulic tests (injection and draw-down) and recovery tests (build-up and fall-off), evaluated in accordance with assumed homogeneous conditions. Chapters 6 and 7 contain a presentation of alternative methods of evaluating these tests, in which the crystalline rock is assumed to act as a dual-porosity medium and as a single fracture in a porous medium respectively.

Chapter 8 deals with pulse response tests and their evaluation.

Chapters 9 and 10 contain descriptions of the eight methods of testing and the equipment used in the field tests, together with the results and comments on each method. The results from field tests are compared in Chapter 11, both section-by-section for all methods and in pairs of methods. Conclusions are drawn and recommendations given.

Chapter 12 contains a presentation of the selected method of single-hole testing and equipment for site characterization and

the motives for the selection. The scope of data from single-hole hydraulic tests collected hitherto (for the period 1981-1985) is also presented.

1. SINGLE-HOLE TESTS, TYPES AND METHODS

A geological hydraulic test is generally understood to mean the testing of hydraulic conditions in a groundwater reservoir by means of applying some type of controlled disturbance to the reservoir. This disturbance usually involves pumping water into or out of the reservoir. The borehole or well in which the disturbance is introduced is called the active borehole (well). The effect of the disturbance is recorded in the form of water-pressure and/or flow changes, in both time and space. If the effects are only recorded in the active borehole, the test is referred to as a single-hole test. Whenever recording is carried out in surrounding observation boreholes or wells, the term interference test is used.

Hydraulic testing is normally used to determine the hydraulic parameters of a groundwater reservoir, its hydraulic boundaries and its relationship with the surrounding geological and hydraulic features. A disturbance introduced into a reservoir over a long period and under constant conditions may generate new groundwater conditions, in which the effects of the disturbance do not change with time. Such a state is called steady state, whereas the state in which the effects of the disturbance change with time are called transient.

The response, R , to a disturbance, St , in a groundwater reservoir, G , may generally be stated as a function of a large number of factors:

$$R = f(St, G, t, x_i, B_a, B_o, P_i, L_i) \quad (1-1)$$

where St = magnitude and function of the disturbance
 G = hydraulic boundaries of the groundwater reservoir
 t = time
 x_i = space coordinates
 B_a = disturbing effects associated with the active borehole
 B_o = disturbing effects associated with the observation borehole

P_i = hydraulic parameters of the groundwater reservoir
 L_i = leakage into or out of the groundwater reservoir.

To obtain the greatest possible amount of information and the best evaluation conditions, hydraulic tests are carried out under as controlled conditions as possible. This implies that the time part of the disturbance should be completely constant, the recording of the disturbance in time and space good and other geometrical conditions known.

Several types of hydraulic test are used. Basically, they involve injecting water into or removing water from the reservoir for a certain time. In practice, the following three types of hydraulic disturbance may be discerned:

- o Injection of water into (or removal from) a borehole at a constant rate, and recording the effect as a change in the water pressure.
- o Injection of water into (or removal from) a borehole at a constant water pressure, and recording the effect as a change in the rate of flow.
- o Instantaneous injection of a limited volume of water into (or removal of water from) a borehole, or subjecting a borehole section to (positive or negative) water pressure (pulse) and recording the transient decay of the pulse (pulse response tests).

The first type of disturbance is normally used in drawdown (test pumping) and water injection tests. During these tests water is pumped out of or into the borehole (section) at a constant rate and the resulting change in pressure or, alternatively, change in water level in the borehole is recorded continually as a function of time. An injection test normally involves an injection phase, and a pressure-decline (fall-off) phase after completion of injection (cf. recovery tests in Chapter 5). Whenever the pressure change in the latter phase is recorded continually, the test is called a pressure fall-off test.

In other types of hydraulic disturbance, the water pressure is kept constant in the borehole (section) and the amount of injection or removal of water required to maintain the pressure is then recorded continuously as a function of time. Whenever water is removed from the borehole, the test is called a constant draw-down test and when water is injected, it is called an injection test at constant pressure. A variant of this latter type of test is water loss test, in which the flow of water injected at various pressures is recorded under assumed steady-state conditions.

Pulse response tests are tests at which the response of any kind of instantaneous change in the hydrostatic pressure in a borehole (section) is used to determine the hydraulic conductivity. The tests may be divided into slug, pressure pulse and drill stem tests. During a slug test the response is monitored under changing water-level conditions. Usually the hydrostatic pressure in the section tested is observed by measuring the change in the water level in the steel tubing as a function of time. In formations of very low permeability pressure pulse tests may be an alternative as these require shorter test periods since the tests are performed under fully confined conditions. A pressure pulse test is basically a pressurized slug test. The drill stem test, commonly used in the oil-industry, is usually a combination of two slug test periods, with the intervening and subsequent recovery periods under confined conditions.

Common to all transient methods of testing is the recording of the response to an applied controlled disturbance in an existing flow domain. Depending on, among other things, the type of disturbance applied, the response may be influenced by different disturbing factors. The most important is borehole storage, which reflects a change in water volume in the borehole tested due to changes in pressure. In an unconfined test system where the change in head corresponds to a direct change of the water level, the borehole storage coefficient may be 1 000 - 100 000 times greater than in a confined test system. This means that the time required for a hydraulic test in an unconfined system may be about three to five orders of magnitude longer than for the same test in a confined system. Furthermore, the effects of borehole

storage occur only in tests in which the water pressure (and/or water temperature) changes with time. Thus, in general, no effects of borehole storage occur when using injection tests at a constant pressure. Another factor which may affect hydraulic tests is the skin effect, which reflects the hydraulic communication between the borehole and the surrounding rock. The transient response (flow rate and/or pressure) may be affected by the skin effect.

Selection of a method of testing is dependent on, among other things, the magnitude of the hydraulic conductivity. In general, there should be an ambition to reduce the influence of borehole storage or to perform the test in such a manner that the effects of borehole storage can be evaluated. Tests containing transition from unconfined to confined test systems (or vice versa) during the test should be avoided.

The (equivalent) hydraulic conductivity in crystalline bedrock may be determined by analytical methods, developed and used for investigations in porous aquifers with various hydraulic conductivities. In crystalline rocks the hydraulic conductivity is dependent on the fracture frequency and fracture interconnection. The hydraulic conductivity in large parts of the rock may be very low, while in parts with high fracture frequencies, especially fracture zones, the hydraulic conductivity may be rather high. These conditions mean that different methods must be used, depending on the magnitude of the hydraulic conductivity and that the tests have to be carried out with a knowledge of the importance of the disturbing factors that may exert an influence.

2. CHARACTERIZATION OF FRACTURED CRYSTALLINE ROCK

2.1 General

A fractured rock is generally complex, heterogeneous and anisotropic. In order to quantify the groundwater flow behaviour and to treat such systems mathematically, certain idealizations are needed. Basically, two different approaches may be used to model groundwater flow in fractured rocks with a low-permeability matrix, the discrete and the continuum approach. In the discrete approach the groundwater flow is studied in individual fractures, usually by representing each fracture as a conduit formed by two parallel plates. To apply the discrete approach, the geometry of the fracture system must be known. The groundwater flow in the network of discrete fractures is determined by modelling flow through the individual fractures.

In the continuum approach the fractured rock is represented either by an equivalent single-porosity porous medium or by two interacting porous media (fracture continuum and matrix continuum). The latter approach is generally called a dual-porosity model.

2.2 Conceptual model

A fractured crystalline rock is generally divided into several blocks of irregular shape and size by structural features such as fractures and fracture zones. Fracture zones are generally defined as zones of closely-spaced interconnected discrete fractures. Fracture zones may range in width from less than a metre to hundreds of metres. In the concept used in the Swedish site characterization programme the rock has been subdivided into three groups, the regional and local fracture zones and the rock mass. The regional fracture zones are usually topographically marked and extend several kilometres. These zones are separated by approximately 1 to 5 km and part the rock into blocks. The blocks are intersected by the local fracture zones, which vary in width from less than a metre to

tens of metres. The rock mass constitutes the sparsely fractured rock between the local fracture zones (see Fig 2.2.1).

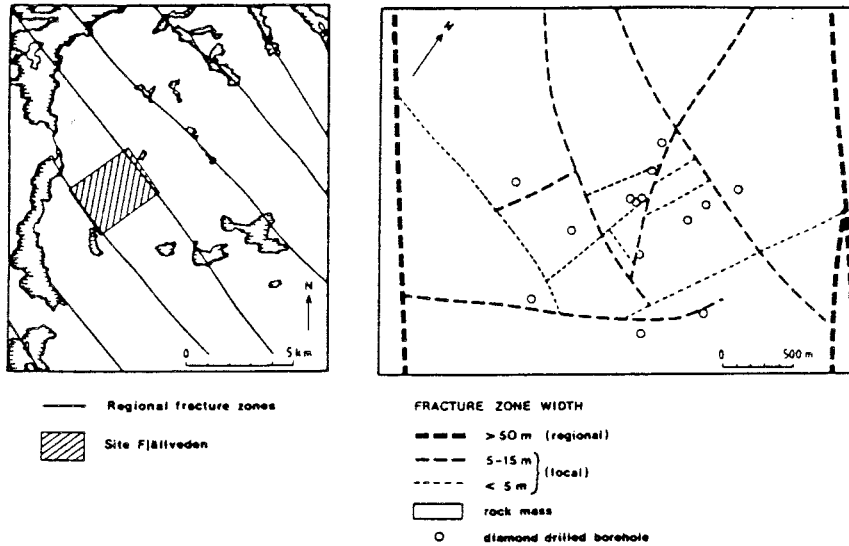


Figure 2.2.1 Rock mass, regional and local fracture zones constituting the different hydraulic units of the different hydraulic units in the Fjällveden test site. After Ahlbom et al (1983a).

With respect to groundwater flow, the rock mass (between the fracture zones) may generally be represented by a large number of intact matrix blocks of irregular shape and size separated by arbitrarily distributed fracture planes of varying size and degree of interconnection. The main groundwater transport flow is assumed to occur in the largest fractures with largest apertures and extents. These fractures, which are marked with arrows in Fig 2.2.2, control the hydraulic conductivity and transmissivity of the rock mass.

The minor fractures do not contribute significantly to the total conductivity but may contribute to the total porosity of

the rock mass by diffusion processes. However, a certain hydraulic conductivity may be present in the minor fractures which are connected to the larger fractures. Thus, all fractures are not interconnected or may have such a small aperture that no flow takes place in these fractures under natural conditions. The blocks of intact, undeformable rock, which are shaded with spots in Fig 2.2.2, may be considered as virtually impermeable. The rock mass may thus be divided into three different regions: the large fractures, the network of minor fractures and the intact matrix blocks (Norton and Knapp, 1977).

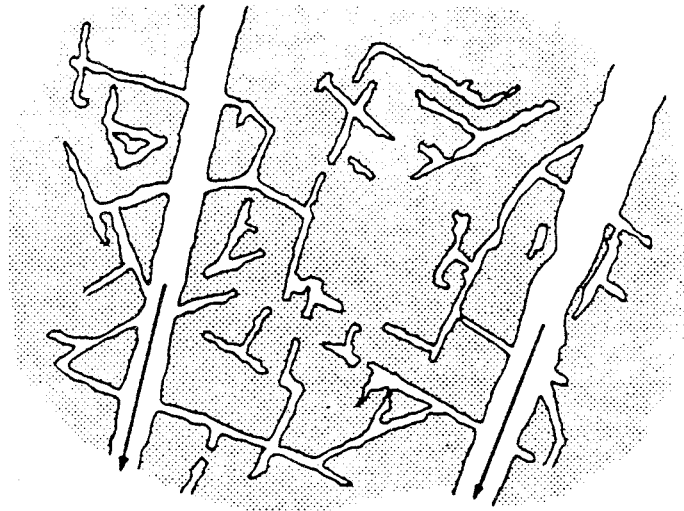


Figure 2.2.2 Schematic representation of different fractures and their geometric relationship in the rock mass. The arrows denote fractures constituting the kinematic porosity (hydraulic fractures). Smaller fractures connected to the hydraulic fractures constitute the diffusion porosity, the remainder the residual porosity. After Norton and Knapp (1977).

2.3 Hydraulic properties

2.3.1 Hydraulic conductivity

The average (bulk) hydraulic conductivity, K , of a rock as described above is dominated by the conductivity of the network

of interconnected larger fractures or flow channels ($K = K_f$). The (intrinsic) hydraulic conductivity of the flow channels can be calculated from tracer tests (Andersson and Klockars, 1985). Here, it is assumed that the transport of water occurs within concentrated flow paths (channels) in a fracture plane rather than using the parallel-plate model of Snow (1968). The resulting hydraulic fracture conductivity, K_e , may either be calculated from the residence time or from the flow rate to the section being tested in an observation borehole.

The ratio between the average hydraulic conductivity of the rock and the hydraulic fracture conductivity, called the kinematic (or flow) porosity, ϕ_k , may be expressed (Andersson and Klockars, 1985) as

$$\phi_k = \frac{K_f}{K_e} \quad (2-1)$$

In general, the hydraulic fracture conductivity is anisotropic and depends on the direction from the active borehole.

2.3.2 Porosity

The total porosity of a crystalline rock may according to Norton and Knapp (1977), be expressed as (Fig 2.2.2)

$$\phi_t = \phi_e + \phi_d + \phi_r \quad (2-2)$$

where ϕ_t = total porosity
 ϕ_e = effective porosity
 ϕ_d = diffusion porosity
 ϕ_r = residual porosity

It should be pointed out that in the paper by Norton and Knapp no distinction was made between kinematic porosity and effective porosity. The effective porosity is here defined as the

volume of interconnected pores through which flow can occur under natural conditions divided by the total bulk volume of the rock. The diffusion porosity is represented by the minor fractures connected to the larger ones and which also interconnects these to each other. Only diffusion transport is possible in the minor fractures, due to the limited aperture and/or lack of interconnection. The pore volume, which is related to neither the flow porosity nor the diffusion porosity, represents the residual porosity.

According to Norton and Knapp (1977), who have compiled data from different investigations, the total porosity is 1 to 2 % for crystalline (granitic) rocks. The effective porosity is about 1 %, the diffusion porosity about 5 % and the residual porosity about 94 % of the total porosity. Thus the effective porosity of intact granitic rocks is in the order of 10^{-4} and may be assumed to vary between 10^{-6} and 10^{-3} (see Table 2.1).

From investigations in a low-permeability crystalline rock mass in the Stripa Mine in Sweden, Andersson and Klockars (1985) determined the effective and kinematic porosity from small-scale tracer tests at a depth of about 360 m below ground level. The corresponding average hydraulic conductivity of the rock is in the order of 10^{-10} m/s. At the Finnsjön test area in Sweden, Gustafsson and Klockars (1981) calculated the flow (or kinematic) porosity in a fracture zone (100 m depth) with a hydraulic conductivity in the order of 10^{-6} m/s from shallow tracer tests. The results are presented in Table 2.1.

Öqvist and Jämtlid (1984) measured the porosity on core samples from crystalline rocks from three different investigation areas in Sweden using geophysical methods. The porosity values determined, which are supposed to represent the sum of the effective and diffusion porosity, vary between 10^{-3} and 10^{-2} , with a mean value of 5×10^{-3} .

Table 2.1 Different porosities in crystalline rock determined by various investigators.

Reference	θ_t	θ_e	θ_k	θ_d	θ_r	Rock unit
Norton & Knapp (1977)	10^{-2}	10^{-4}	-	$5 \cdot 10^{-4}$	$9 \cdot 10^{-2}$?
Heimli (1974)	$10^{-3} - 10^{-2}$					"tight" rock
Andersson & Klockars (1985)		$8 \cdot 10^{-5}$	$3,9 \cdot 10^{-4}$			rock mass
Gustafsson & Klockars (1981)			$8,5 \cdot 10^{-4}$			fracture zone (100 m depth)

2.3.3 Specific storage coefficient

The specific storage coefficient of a rock, which is related to the (effective) porosity of the rock, represents the volume of water that can be released from (or stored in) a unit volume of the (bulk) rock when the hydraulic head is changed by one unit. The volume released depends on both the effective porosity of the rock and the total compressibility of the system (rock plus water). The confined two-dimensional specific storage coefficient of an elastic aquifer may, according to Mc Whorther and Sunada (1977), be expressed:

$$S_s = \rho g (c_b + \theta c_w) \quad (2-3)$$

In this equation, c_b , represents the bulk vertical compressibility and c_w the water compressibility. For hydraulic testing in crystalline rock, θ should represent the effective porosity or the sum of effective and diffusion porosity, depending on the duration of the test. The storage coefficient, S , of a confined section of a borehole with length L is for cylindrical flow defined as $S = S_s L$. The specific storage coefficient of crystalline rock is usually determined from hydraulic field tests and rather few values exist so far (Table 2.2).

Black and Barker (1981) investigated the specific storage capacity in three 300-m deep boreholes in crystalline rocks at Altnabreac in Scotland, using slug and pressure pulse tests. Based on physical properties, such as rock compressibility and porosity, they calculated a minimum value of the equivalent specific storage coefficient for the rock mass to $2 \times 10^{-7} \text{ m}^{-1}$. However, for most of the hydraulic tests, values of the specific storage coefficient below the minimum possible, based on standard porous medium analysis, were determined (see Fig 2.3.1). This Figure indicates that flow may sometimes occur in single fractures or flow channels rather than in an equivalent porous medium.

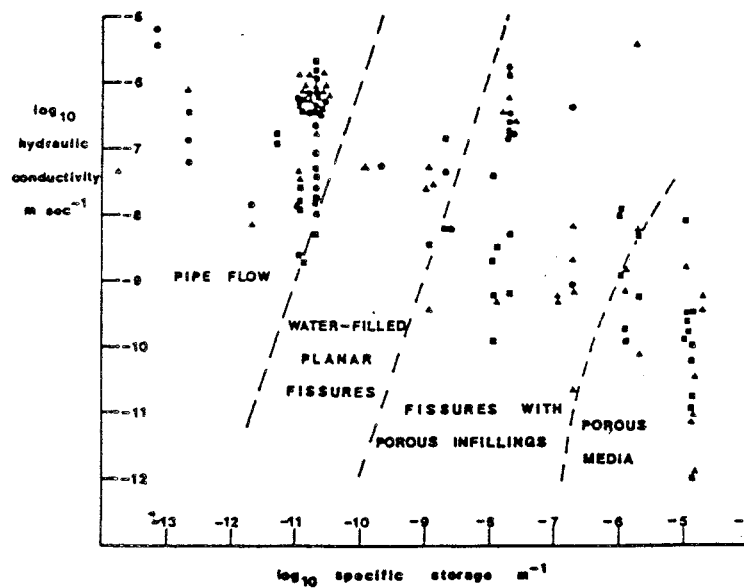


Figure 2.3.1 Results from slug tests in three boreholes at Altnabreac. After Black and Barker (1981).

Specific storage values have been determined from single-hole and interference tests at the Stripa Mine in Sweden by Carlsson and Olsson (1985 a and b). The test site is located about 360 m below ground level. Single-hole tests in a fracture zone about 50 m thick showed a typical dual-porosity pressure response. From these tests the specific storage of the fracture zone was

determined to $1-2 \times 10^{-7} \text{ m}^{-1}$ and for the rock mass $5-8 \times 10^{-7} \text{ m}^{-1}$.

The specific storage has also been determined from cross-hole tests by different authors, e.g. Black et al (1982) at Carwynnen Quarry in Cornwall, Hsieh et al (1985) in the Orachle granite in Arizona and finally in the Swedish site characterization programme (Andersson och Hanson, 1986). The calculated values of specific storage range from $8 \times 10^{-8} \text{ m}^{-1}$ to $5 \times 10^{-6} \text{ m}^{-1}$.

Table 2.2 Specific storage values in crystalline rock, determined from hydraulic tests.

Reference	S_s (m^{-1})	Rock volume (depth)	Test method	
<u>Single-hole tests</u>				
Black & Barker (1981)	$> 2 \cdot 10^{-7}$	bulk rock (0-300 m)	slug & pulse tests	
Carlsson & Olsson (1985)	$1-2 \cdot 10^{-7}$	fracture zone (360 m)	injection tests	
	$5-8 \cdot 10^{-7}$	bulk rock (360 m)	"-	
	$10^{-10}-10^{-6}$	bulk rock (360 m)	build-up tests	
<u>Cross-hole tests</u>				
Black & Holmes (1982)	$8 \cdot 10^{-8}-2 \cdot 10^{-6}$	bulk rock (100-200 m)	const. rate injection test	
Carlsson & Olsson (1985)	$2 \cdot 10^{-7}-2 \cdot 10^{-6}$	fracture zone (360 m)	interference tests (const. rate)	
Neuman et al (1985)	$5 \cdot 10^{-6}$	bulk rock (100 m)	const. head injection	
Test-sites in Sweden	Gideå	$3 \cdot 10^{-6}-10^{-4}$	fracture zone (100 m)	pumping tests
	Svartboberget	$4 \cdot 10^{-6}-10^{-5}$	fracture zone (100 m)	"-
	Fjälliveden	$1-5 \cdot 10^{-7}$	bulk rock (100 m)	"-

2.3.4 Hydraulic head

Apart from hydraulic conductivity and specific storage coefficient, the hydraulic head distribution in the rock is also required to describe the groundwater flow within an area quantitatively. In the uppermost part of the bedrock the hydraulic head and groundwater level in Sweden are generally controlled by the topography. The effect of the topographically

induced hydraulic gradients decreases rapidly with increasing depth in a homogeneous medium. At greater depth, fractures and fracture zones with high hydraulic conductivity have an important effect on the distribution of the hydraulic head. Hydraulic head distributions from several boreholes, determined from hydraulic (injection) tests, have been used in numerical groundwater model studies from three test sites in Sweden by Carlsson et al (1983a). An example of the distribution of the hydraulic head along a borehole is shown in Fig 2.3.2.

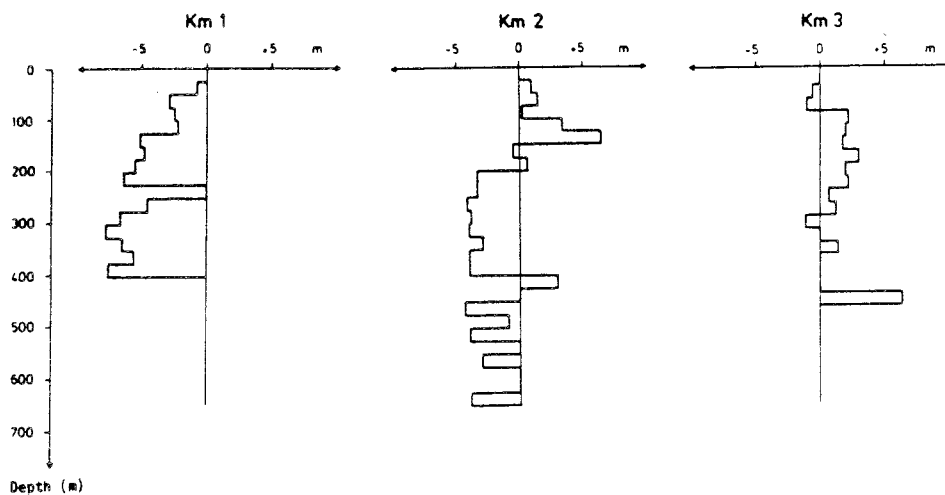


Figure 2.3.2 Hydraulic head in 25-m long sections in boreholes Km 1-3. From Ahlbom et al (1983b).

2.4 Theoretical models of crystalline rocks

In discrete fracture models the rock matrix blocks are generally assumed to be effectively impermeable and the network of interconnected fractures and fracture zones are considered to form the only void space available for groundwater flow (Louis 1969, Maini, 1971, Gale 1975). Using this approach the flow in single fractures is described by an idealized parallel-plate model.

Depending on the scale of investigation in relation to the scale of fracturing the fractures may either be characterized

individually or by using average flow properties within the area investigated. Large scale discontinuities, such as fracture zones, require individual characterization (discrete approach). Smaller scale fractures in the rock mass require an averaged or statistical approach. Statistical models based on fracture orientations and apertures measured in boreholes may be used to generate an equivalent anisotropic porous medium.

In the continuum approach the network of fractures is represented by an equivalent porous medium (fracture continuum). If the matrix blocks are permeable they are represented by another continuum which interacts with the fracture continuum (dual porosity models). If the matrix blocks are impermeable, the fractured rock mass may be represented solely by the fracture continuum. This may either be isotropic or anisotropic.

The theoretical approach that is the most appropriate one depends mainly on the scale of the test with respect to fracture density and size of the flow domain. When fracture density is low, a discrete approach may be required to study small-scale tests. On the other hand, when the fracture density is high and the area investigated rather large the continuum approach may be valid and probably most appropriate. The problem of scale and the connectivity of fracture systems in crystalline rocks has been studied by de Marsily (1985). On a regional scale a stochastic model may be the most relevant approach as discussed by Carnahan et al (1983).

To describe groundwater flow mathematically, both the discrete and continuum approach requires input of detailed information on the three-dimensional distribution of hydraulic properties and hydraulic boundary conditions in the rock. Hydraulic tests, including single-hole and interference tests, can provide hydraulic conductivity and specific storage values for discrete fractures or the rock, and identification of hydraulic boundaries.

2.5 Interpretation of single-hole tests

Most theoretical models used for interpreting hydraulic tests in fractured crystalline rock are based on the assumption that the fractured rock can be represented by an equivalent continuous porous medium, either a single-porosity or a dualporosity medium. This concept is shown schematically in Fig 2.5.1. The fractured rock is represented by a single fracture and as an equivalent porous medium. The corresponding hydraulic conductivities for the single fracture and the porous medium to yield the same flux through the fracture and porous medium respectively are calculated for the given boundary conditions.

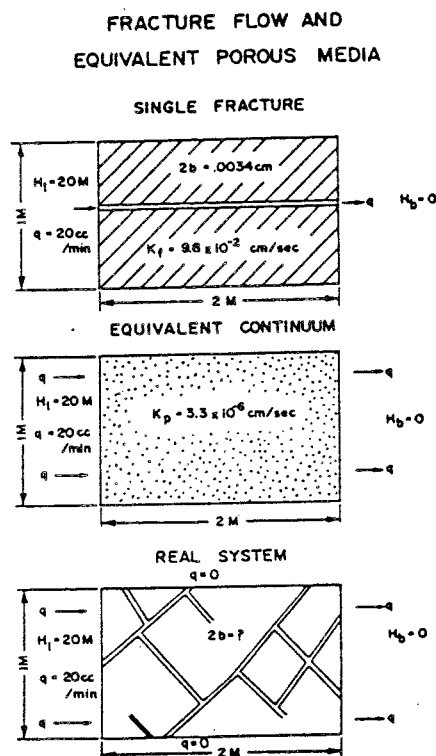


Figure 2.5.1 Illustration of the equivalent continuum concept.
After Gale (1982).

In a real system it is the degree of fracture interconnection that to a great extent determines the total (effective) hydraulic conductivity of the rock. Depending on the estimate of the porosity, the assumption of an equivalent continuum may present a different view of the velocity field than the assumption of continuous single fractures. The true hydraulic

conductivity and flow velocity through a real system of interconnected fractures is likely to lie somewhere between these two extreme assumptions (Gale, 1982).

The size of the investigated volume during a hydraulic test (radius of influence) depends mainly on the hydraulic properties of the rock and the test duration. If possible, the test duration should be selected with respect to the actual magnitude of the hydraulic properties and the fracture distribution to obtain representative parameter values from a particular test, i.e. longer test times in low-permeable rock sections. Ideally, the volume investigated should be large enough to be treated, together with its inhomogeneities, as an equivalent homogeneous and porous medium with representative average values of the hydraulic parameters (Long et al 1982). A representative volume element (REV) of the rock mass is defined as the minimum volume of rock that must be investigated to achieve stable, representative values of the hydraulic parameters. If this volume is increased further, the calculated parameter values will not change significantly. The limitations of standard hydraulic tests are discussed by Carnahan et al (1983).

The assumption of representing the crystalline rock as a dual-porosity medium has been investigated by Black et al (1982) by means of single-hole tests and sinusoidal interference tests. By comparing the actual field test responses with various theoretical models they concluded that the model describing cylindrical flow with interacting slabs of permeable matrix material (dual-porosity model) probably best adhered to the field data. Carlsson and Olsson (1985a) presented results from single-hole tests from the Stripa Mine indicating a dual-porosity response. Such a behaviour is likely to occur during long term testing when two hydraulic units with significantly different properties are present within the volume of rock being tested, e.g. a fracture zone and the surrounding rock.

In Chapters 4 to 8, different theoretical models used for the interpretation of various single-hole transient tests (constant rate, constant pressure, slug tests, pressure pulse tests and

drill stem tests) are presented. All models are based on the assumption that the fractured rock can be represented by an equivalent isotropic porous medium. In order to distinguish between different flow regimes, the test data are generally plotted on various graphs, e.g. linear flow, cylindrical flow and spherical flow plots. The tests may then be analysed according to the theoretical model that best conforms to the actual test data. This technique has been discussed by Gringarten (1982) on evaluation of test data from fractured reservoirs. A detailed discussion of problems in identifying different flow regimes from various graphs is presented by Ershaghi and Woodbury (1985). Typical pressure behaviours for linear, radial and spherical flow regimes in various graphs are shown in Figures 2.5.2 a-c.

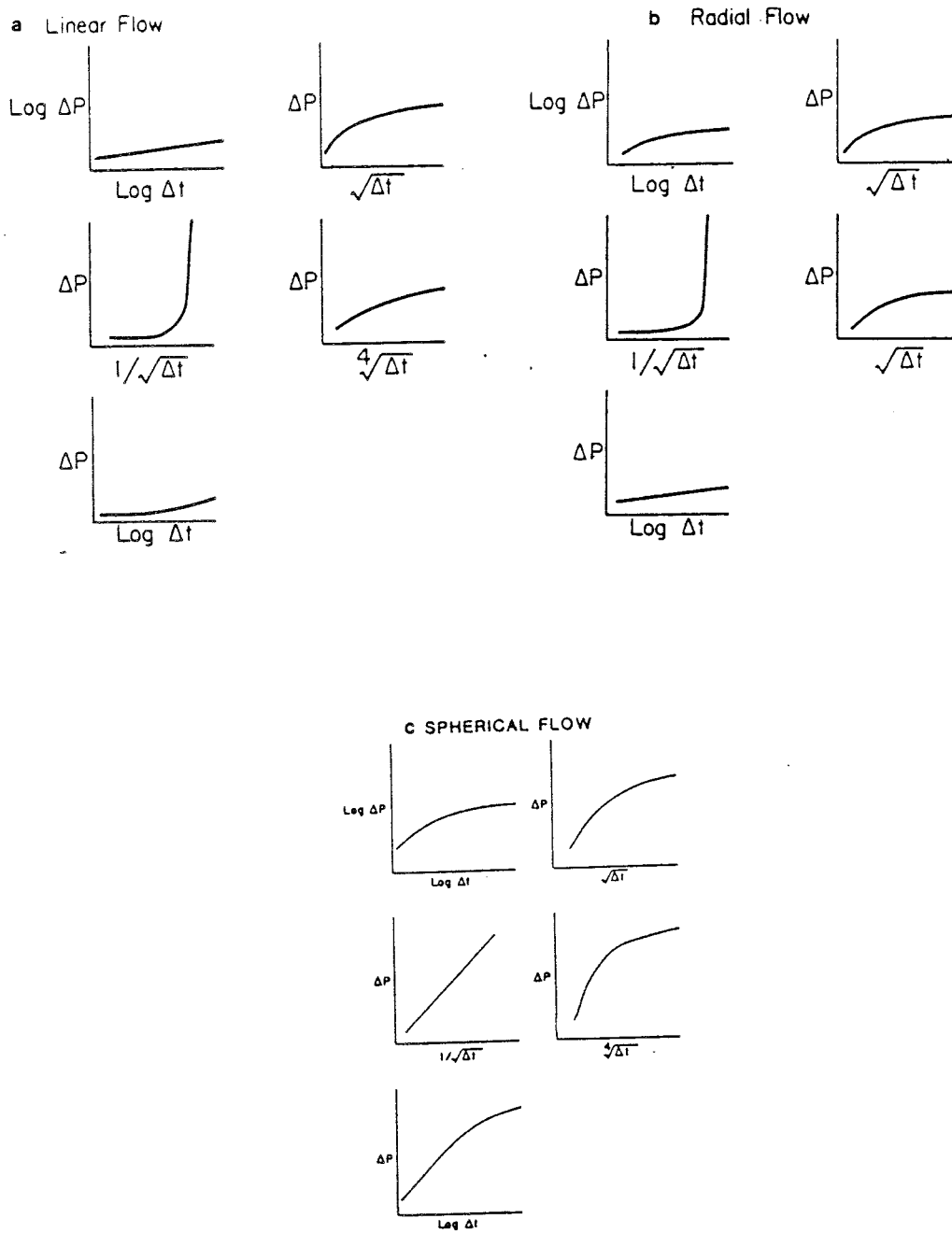


Figure 2.5.2 Pressure behaviour as a function of time during different flow regimes. From Ershaghi and Woodbury (1985)

- a) linear flow
- b) radial flow
- c) spherical flow

3. INFLUENCE OF SKIN AND BOREHOLE STORAGE EFFECTS ON SINGLE-HOLE TESTS

3.1 General

Borehole storage and skin effects may influence the transient pressure response at the active borehole during hydraulic testing. Both effects characterize the hydraulic conditions at or near the active borehole. The skin effect reflects all factors which may affect the hydraulic interaction between the borehole and surrounding rock. These factors include, in general, altered hydraulic conductivity adjacent to the borehole due to drilling, partial penetration and completion, the deviation of the borehole and turbulent flow effects. Skin effects are normally present in all kinds of hydraulic test, both during draw-down (injection) and build-up (fall-off).

Borehole storage effects are caused by the volume of fluid which is stored in the borehole itself or in an isolated section of the borehole. Borehole storage effects normally only occur in constant-rate-of-flow tests, when the pressure is changing during the test, particularly in low-permeability formations. In constant-pressure tests the down-the-hole pressure is kept constant. However, during the buildup (or fall-off) period after constant drawdown (injection) tests borehole storage effects may influence the pressure response.

3.2 Skin effect

The skin effect, which is characterized by the skin factor, represents the effective area connected to the borehole. In relation to the nominal radius of the borehole the area may either be increased, due to natural or induced fractures intersecting the borehole (negative skin), or reduced, due to damage (clogging) or other factors mentioned above (positive skin).

In theory, the skin effect may be treated in one of two ways. In the first approach, the skin is assumed to be concentrated

to an infinitesimally thin zone around the borehole wall in which no storage of fluid can take place (van Everdingen 1953, Hurst 1953). This approach makes the case with negative skin merely a theoretical one. The idealized pressure distribution around an active borehole according to this concept with a positive skin factor is shown in Fig 3.2.1.

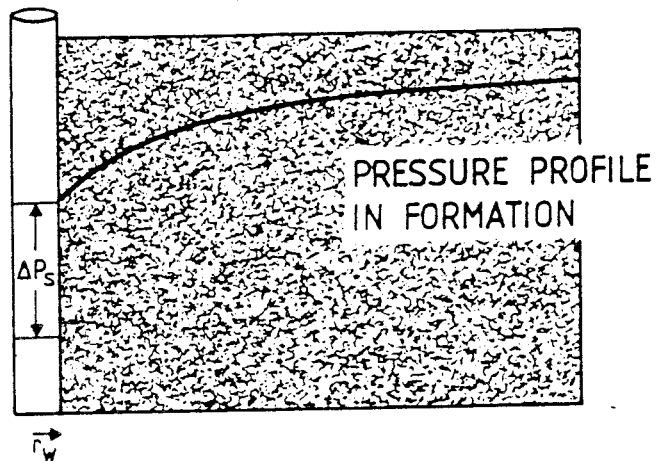


Figure 3.2.1 Pressure distribution around a borehole with a positive skin factor. (Infinitesimally thin skin zone).

The other approach considers the skin effect as being located within a skin zone with a finite radius around the borehole. In this zone, the hydraulic conductivity may either be increased (negative skin factor) or reduced (positive skin factor) (see Fig 3.2.2). This approach is most common for fractured (or stimulated) boreholes, resulting in a skin-zone with increased hydraulic properties (negative skin). In this case, the skin factor may be calculated in analogy with Earlougher (1977):

$$\zeta = (K/K_s - 1) \ln r_s/r_w \quad (3-1)$$

K and K_s represent the hydraulic conductivity of the (unaffected) formation and of the skin-zone, respectively, while r_s and r_w denote the radius of the skin-zone and (nominal) borehole radius, respectively. If the skin factor is known, Eqn. (3-1) may be used to estimate K_s or r_s . It is also possible to define an effective borehole radius, r_{wf} ,

which takes into account the skin effect (Earlougher 1977):

$$r_{wf} = r_w e^{-\zeta} \quad (3-2)$$

Eqn. (3-2) implies that the effective radius is greater than the nominal borehole radius if the skin factor is negative, and vice versa. For boreholes intersected by single fractures, the effective radius is generally a function of the fracture length. According to Earlougher (1977) the skin factor may vary from about -5 for a fractured well to ∞ for a completely clogged well.

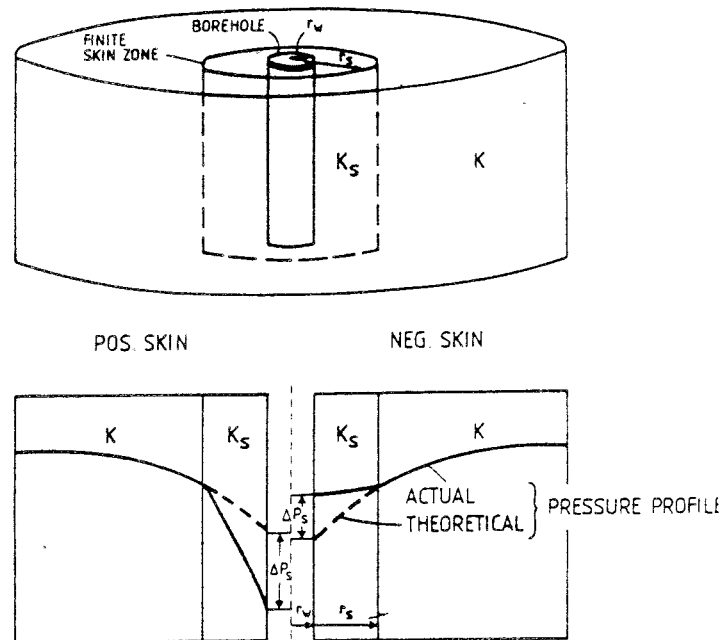


Figure 3.2.2 Pressure distribution around a borehole with a skin zone of finite thickness for a positive and negative skin factor respectively.

For other borehole conditions, such as partially penetrating wells or deviating boreholes, additional so-called pseudo-skin factors can be defined. Theoretical calculations have shown

that turbulent flow effects in pressure testing of groundwater is normally negligible for hydraulic conductivities less than about 10^{-7} m/s with normally occurring flow rates and pressure differences (Andersson and Carlsson, 1980).

3.3 Borehole storage effect

Since water is slightly compressible, the volume of water contained in a borehole (section) will change with time whenever the water pressure in the borehole (section) is changed due to drawdown or injection. In a constant flow-rate drawdown test (in an open borehole) the total flow rate, Q , pumped from the borehole during the beginning of the test is derived partly from the formation and partly from the water stored in the borehole. The contribution of water from the formation, Q_f , increases successively during the test to constitute the total flow rate pumped from the borehole after a certain time. The time at which this happens, depends mainly on the magnitude of the borehole storage capacity, characterized by the borehole storage coefficient, C (Fig 3.3.1). The greater the value of C , the longer the period before the total flow comes from the formation, i.e. $Q_f = Q$.

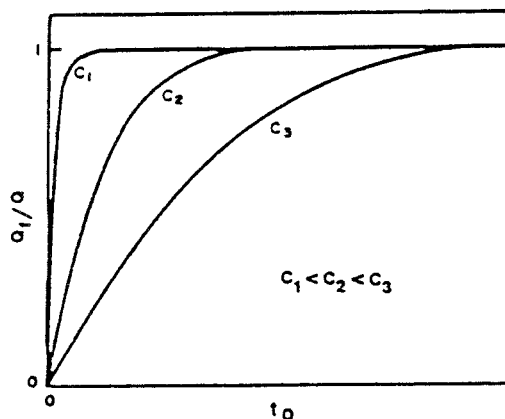


Figure 3.3.1 Relationship between the formation flow rate and the total flow rate for different values of the borehole storage coefficient. After Earlougher (1977).

The borehole storage coefficient, C , is generally defined as (Earlougher 1977):

$$C = \frac{\Delta V}{\Delta p} \quad (3-3)$$

ΔV and Δp are the change in water volume and water pressure in the active borehole (section) respectively. In the metric system, C is expressed in the units m^3/Pa . The volume of water may also be changed due to volume changes in the equipment used for testing (packers, tubes, etc.) as a result of changes in water pressure.

The magnitude of the borehole storage coefficient depends on the actual configuration of the test system. If a free water level in an open borehole without packers changes continuously during the test as a result of drawdown or injection, the borehole storage coefficient, C , is defined (Earlougher 1977) as:

$$C = \frac{V_u}{\rho g} \quad (3-4)$$

V_u is the effective volume per unit length (metre) of the borehole space in which the water level can rise or fall freely.

For confined systems, i.e. sections of the borehole isolated by packers, the borehole storage coefficient is calculated from the following expression (Earlougher 1977):

$$C = V_w c_w = V_u L c_w \quad (3-5)$$

V_w and L is the total volume and length of the confined section, respectively and c_w is the compressibility of water.

The dimensionless borehole storage coefficient, C_D , is defined, in analogy with Earlougher (1977) as:

$$C_D = \frac{C \rho g}{2\pi S_s L r_w^2} \quad (3-6)$$

The borehole storage coefficient for an open test system with a changing water level is normally 10^3 - 10^5 times greater than that of a confined system (Table 3.1). In low-permeability rock, large disturbances of the test data by borehole storage effects are avoided if confined sections of the borehole are tested, particularly for constant-rate-of-flow testing. When the pressure in the borehole is kept constant during the test, borehole storage effects will generally not occur. The effects of borehole storage may also be modified by changing the length of the (confined) test section.

Borehole diameter $2 r_w$ (mm)	Section length L (m)	Borehole storage coefficient C (m^3/Pa)	
		Test system	
		Open	Closed
200	2	} 3 E(-6)	3 E(-11)
	10		2 E(-10)
	50		8 E(-10)
110	2	} 1 E(-6)	9 E(-12)
	10		5 E(-11)
	50		2 E(-10)
76	2	} 5 E(-7)	5 E(-12)
	10		2 E(-11)
	50		1 E(-10)
56	2	} 3 E(-7)	3 E(-12)
	10		1 E(-11)
	50		6 E(-11)
46	2	} 2 E(-7)	2 E(-12)
	10		8 E(-12)
	50		4 E(-11)

Table 3.1 Approximate values of the borehole storage coefficient for different borehole diameters in an open and closed test system respectively.

4. INJECTION/DRAWDOWN TESTS IN HOMOGENEOUS FORMATIONS

4.1 General

In a constant-rate drawdown or production test, water is pumped at a constant rate from a borehole or from an isolated section of the borehole. The pressure response (drawdown) of the water in the formation due to the pumping is monitored in the borehole or in the section of the borehole being tested. Alternatively, the borehole (section) can be subjected to constant drawdown and the decrease in flow rate monitored as a function of time during the test.

In an injection test, water is injected into the borehole or confined section of the borehole. The injection test can be performed either by injection at a constant rate of flow and monitoring the pressure change or, alternatively, by keeping the injection pressure constant and monitoring the change in the rate of flow. All the tests described in this report, except some of the pulse response tests, were performed as injection tests. Since the theory for drawdown and injection tests is analogous they have been treated together in the presentation of the theory.

4.2 Radial flow

4.2.1 Constant-rate of flow tests

The basic differential equation for transient, radial flow in a porous medium (the diffusivity equation) can be expressed:

$$\frac{\partial^2(\Delta p)}{\partial r^2} + \frac{1}{r} \frac{\partial(\Delta p)}{\partial r} = \frac{S_s}{K} \frac{\partial(\Delta p)}{\partial t} \quad (4-1)$$

In Eqn. (4-1), K denotes the hydraulic conductivity and S_s the specific storage coefficient of the reservoir and Δp is the pressure change. The parameters t and r denote the time and

radial distance, respectively. The (line-source) solution to this equation was presented by Theis (1935). Eqn. (4-1) assumes that there are no effects of skin and borehole storage during the test. When such effects influence the test, the equation must be modified accordingly.

Skin effects

The change in head, H , or pressure change at the active borehole, including the skin effect, for a constant rate-of-flow drawdown test can be expressed in analogy with Earlougher (1977) as:

$$H = (p_i - p_{wf}) / \rho g = \frac{Q}{2\pi KL} \left[p_D(t_D) + \zeta \right] \quad (4-2)$$

In Eqn. (4-2), H represents the difference between the initial, static piezometric pressure, p_i , and the actual pressure during the drawdown period, p_{wf} , in the active borehole (section). The other symbols are defined in the list of symbols. The dimensionless change in pressure or head, p_D , is generally a function of the dimensionless test time, t_D , and the dimensionless radial distance from the borehole, r_D . The dimensionless pressure or head change for drawdown tests is defined according to Earlougher (1977) as:

$$p_D = \frac{2\pi KLH}{Q} = \frac{2\pi KL (p_i - p_{wf}) / \rho g}{Q} \quad (4-3)$$

where H is the head change and $p_i - p_{wf}$ the pressure change. For injection tests the pressure change is defined as $p_{wf} - p_i$. The dimensionless time is defined as:

$$t_D = \frac{K t}{S_s r_w^2} \quad (4-4)$$

The dimensionless distance from the active borehole is defined as

$$r_D = \frac{r}{r_w} \quad (4-5)$$

where r is the radial distance from the active borehole and r_w the borehole radius. At the active borehole $r = r_w$ so $r_D = 1$.

Basically, two different (exact) solutions of the $p_D(t_D)$ -function exist. The exponent-integral solution (also called the line-source or Theis solution) assumes that the radius of the active borehole is infinitesimally small ($r_D \rightarrow \infty$), (see Fig 4.2.1). This solution is normally used to analyse interference tests whenever r_D is large. The other solution, called the finite-radius borehole solution or the PDCI solution, assumes that the active borehole has a finite radius. At the active borehole (section) this solution was presented by van Everdingen and Hurst (1949) (see Fig 4.2.1). If $t_D > 100$ the exponential integral solution for the active borehole (in the absence of skin) may be approximated by the following logarithmic expression (Earlougher 1977):

$$p_D = 1.151 (\log t_D + 0.351) \quad (4-6)$$

However, when $t_D > 5$ the difference between the exponential integral solution and the logarithmic approximation is only 2%. In high-permeability formations the condition of $t_D > 100$ at the active borehole is normally reached only after a few minutes of testing. However, in low-permeability formations, t_D may be less than 100 for a substantial part of the test. The finite-radius borehole solution (PDCI), the exponential integral solution and the logarithmic approximation of the latter solution are presented in Fig. 4.2.1. As may be seen from this

figure there are marked differences between the PDCI and the exponential integral solution and the logarithmic approximation for $t_D < 5$. Thus, in low-permeability formations neither the exponential integral solution nor the logarithmic approximation may be applicable.

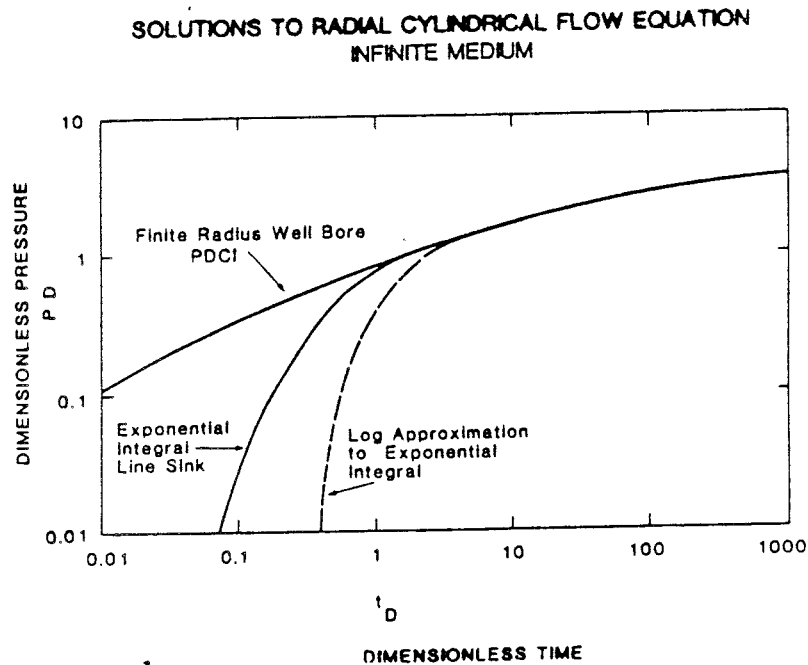


Figure 4.2.1 Solutions to the radial flow equation in an infinite medium. After Morrison (1981).

Using the logarithmic approximation, Eqn. (4-6) may be written in the following form in real parameters including the skin effect:

$$H = \frac{1.15 Q}{2\pi KL} \left[\log \frac{Kt}{r_w^2 S_s} + 0.351 + 0.869 \tau \right] \quad (4-7)$$

Eqn. (4-7) indicates that a plot of the change in head, H , versus $\log t$ should yield a straight line in a semi-log plot ("semi-log straight line"). The hydraulic conductivity of the section tested may be calculated from Eqn. (4-7) in metric units:

$$K = \frac{0.183 Q}{\Delta H \cdot L} \quad (4-8)$$

In Eqn. (4-8), H represents the change in head during a logarithmic time cycle. The skin factor is determined from Eqn. (4-7):

$$\zeta = 1.15 \left[\frac{H_{1 \text{ min}}}{\Delta H} - \log \frac{K}{r_w^2 S_s} - 2.13 \right] \quad (4-9)$$

$H_{1 \text{ min}}$ represents the change in head at $t = 1$ minute. The effective radius of the borehole (section), r_{wf} , can then be calculated from Eqn. (3-2). The additional head change, H_s , due to the skin effect may be expressed from Eqn. (4-2) as follows:

$$H_s = \Delta p_s / \rho g = \frac{Q \zeta}{2\pi KL} \quad (4-10)$$

The radius of influence, r_i , at specific times during the test can for practical situations be estimated from the logarithmic approximation of p_D in Eqn. (4-6) according to Earlougher (1977), in metric units:

$$r_i = \sqrt{\frac{2.25 Kt}{S_s}} \quad (4-11)$$

Using the finite borehole radius solution of p_D , Eqn. (4-2) may be used for type-curve matching. A type-curve may be constructed with p_D as a function of $t_D e^{2\zeta}$ by using the effective borehole radius instead of the nominal radius. The draw-down or injection field data are plotted with $\log H$ as a function of $\log t$. The hydraulic conductivity can be obtained from the pressure (or head) match from Eqn. (4-12) in metric units:

$$k = \frac{0.159 Q}{H_m L} (p_D)_m \quad (4-12)$$

H_m is the change in head at the matchpoint on the data curve corresponding to the value of $(p_D)_m$ on the type curve. The effective borehole radius, r_{wf} , can be obtained from the time match by the definition of the product $t_D e^{2\zeta}$ from Eqns. (4-4) and (3-2). The effective radius is given in metric units by the following expression:

$$r_{wf} = \sqrt{\frac{k t_m}{S_s (t_D e^{2\zeta})_m}} \quad (4-13)$$

In Eqn. (4-13), t_m and $(t_D e^{2\zeta})_m$ denote the time values on the data curve and type curve respectively. The skin factor may be calculated from the estimate of r_{wf} using Eqn. (3-2).

Borehole storage and skin effects

The theoretical pressure behaviour at the active borehole when both skin and borehole storage effects occur was presented by Agarwal et al (1970) in the form of type curves. The solution can be represented by Eqn. (4-3) but p_D is now a function of both t_D and C_D , i.e. $p_D(t_D, C_D)$. The dimensionless borehole storage coefficient, C_D , is defined by Eqn. (3-7).

The type-curve solution is based on a constant rate of flow drawdown (injection) test in a borehole of finite radius. An infinitesimally thin skin-zone surrounds the borehole which is located in a formation of infinite extent. The type curves are plotted with $p_D(t_D, C_D)$ as a function of t_D for different values of C_D with the skin factor as a parameter (see Fig. 4.2.2). The curves marked with $C_D=0$ represent the finite borehole radius solution of p_D for different skin factors but no borehole storage effect.

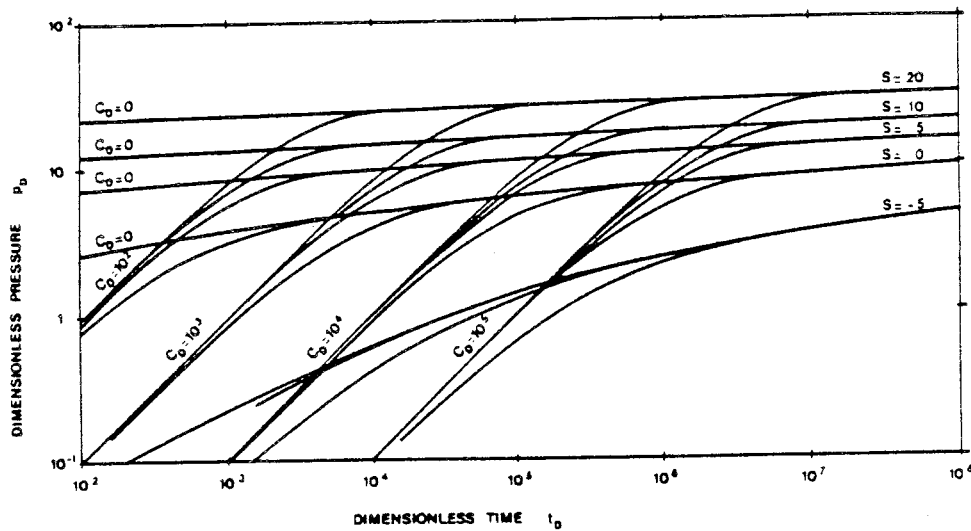


Figure 4.2.2 Type-curves for borehole storage and skin effects.

After Agarwal et al (1970).

As can be seen in Fig 4.2.2, the type curves are initially straight lines of unit slope in a log-log graph. During this period, which is dominated by borehole storage effects, virtually no water is derived from the formation, it comes from the borehole (section) itself. This period may be represented by an infinitely large skin factor. The pressure change during the borehole storage dominated period may be approximated by (Agarwal et al 1970):

$$P_D = \frac{t_D}{C_D} \quad (4-14)$$

Eqn. (4-14) shows that the pressure change is directly proportional to the test duration. During this period, no information about the hydraulic properties of the formation can be obtained. However, the borehole storage coefficient can be calculated from the straight line of unit slope as follows (Earlougher 1977):

$$C = \frac{Q t_1}{\rho g H_1} \quad (4-15)$$

In Eqn. (4-15) t_1 and H_1 are the time and head change at an arbitrarily chosen point on the log-log straight line of unit slope. The value of C , calculated from Eqn. (4-15) should be approximately the same as the one determined from borehole completion data according to Eqn. (3-4) or (3-5).

After a transition period the borehole storage type curves merge with the curves marked $C_D = 0$. At this time the borehole storage effects have ceased. The intersection between the curves represents approximately the time for the start of radial flow in the system and the beginning of the semi-log straight line. To obtain a unique match with these type curves, the C_D -value should be known because of the similar shape of the type curves. If C_D is known, or can be estimated, the hydraulic conductivity may be calculated from the pressure (or head) match using Eqn. (4-12). The skin factor may be estimated as a parameter value. If C_D is not known, a unique match is impossible. In this case the type curves may only be used as a diagnostic tool and to estimate the start of the semi-log straight line (Ramey 1982).

Gringarten et al (1979) presented a modified form of the type curves for borehole storage and skin effects. The type curves are based on the same assumptions as the Agarwal et al (1970) solution. The type curves are presented as $p_D(t_D, C_D)$ versus t_D/C_D with the product $C_D e^{2\zeta}$ as a curve parameter (see Fig. 4.2.3). The limits of the different flow regimes and approximate ranges of various borehole conditions (damaged, fractured) are indicated on the type curves. These curves should better represent fractured boreholes with borehole storage effects (low values of $C_D e^{2\zeta}$). Fractured boreholes are represented by the infinite-conductivity solution (see Chapter 7).

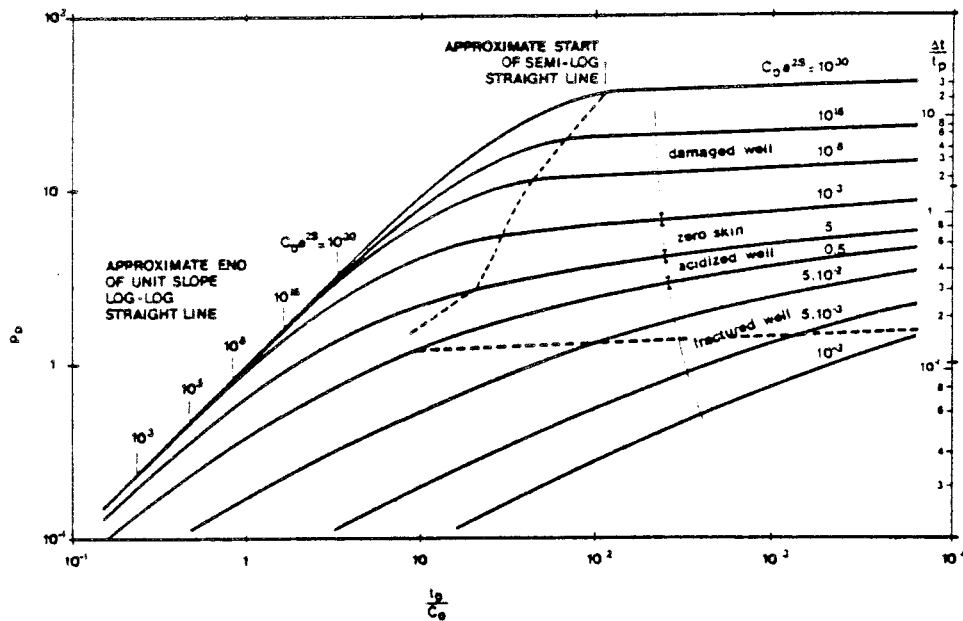


Figure 4.2.3 Modified type-curve for borehole storage and skin effects. After Gringarten et al (1979).

The type curves may be used to calculate the hydraulic conductivity from the pressure (or head) match from Eqn. (4-12). From the time match, the borehole storage coefficient may be calculated using the following expression in metric units:

$$C = \frac{2\pi KL t_m}{\rho g (t_D/C_D)_m} \quad (4-16)$$

If C is known, the skin factor may be determined from the definition of t_D/C_D and the parameter value $(C_D e^{2\zeta})_m$ as follows in metric units:

$$\zeta = 1.15 \log \left[\frac{2\pi r_w^2 S_s L (C_D e^{2\zeta})_m}{C \rho g} \right] \quad (4-17)$$

When the effects of borehole storage have ceased to influence the pressure behaviour and radial flow has started in the formation, analysis can be made on a semi-log plot, provided that the logarithmic approximation of p_D in Eqn. (4-6) is

valid. The head change, H , is plotted as a function of the test time, t , on the data curve. For drawdown and injection tests, the beginning of the semi-log straight line is given by the following condition (Earlougher 1977):

$$t_D \geq (60+3.5\zeta)C_D \quad (4-18)$$

After this time the hydraulic conductivity and skin factor may be calculated from Eqns. (4-8) and (4-9) respectively.

4.2.2 Constant-pressure tests

When a borehole (section) is tested at constant pressure, no borehole storage effects occur since the down-the-hole pressure does not change during the test. However, during the subsequent build-up (fall-off) test borehole storage effects may be important. The solution of the diffusivity equation, regarding the decline in flow rate with time, for the constant-pressure case of radial flow was presented by van Everdingen and Hurst (1949) and Jacob and Lohman (1952). Uraiet and Raghavan (1980 a) included the skin effect in this solution. They considered the skin region to be an annular region concentric with the borehole and with a hydraulic conductivity different (higher or lower) from the formation conductivity.

The reciprocal transient flow rate at the borehole (section) during a constant-pressure test, with the skin effect taken into account, may be expressed as follows in metric units:

$$\frac{1}{Q(t)} = \frac{1}{2\pi K L H_0} \left[\frac{1}{Q_D(t_D)} + \zeta \right] \quad (4-19)$$

H_0 is the constant drawdown or injection head at the borehole (section). The dimensionless flow rate function $Q_D(t_D)$ represents the theoretical solution of Q_D as a function of dimensionless time, t_D , defined by Eqn. (4-4). The effective

borehole radius concept for constant rate of flow tests also applies to the constant-pressure case (Uraiet and Raghavan 1980a). Q_D is defined as follows for constant-pressure tests:

$$Q_D = \frac{Q(t)}{2\pi K L H_0} \quad (4-20)$$

The theoretical solution of Q_D versus t_D can be used for type-curve matching in a logarithmic diagram (see Fig. 4.2.4).

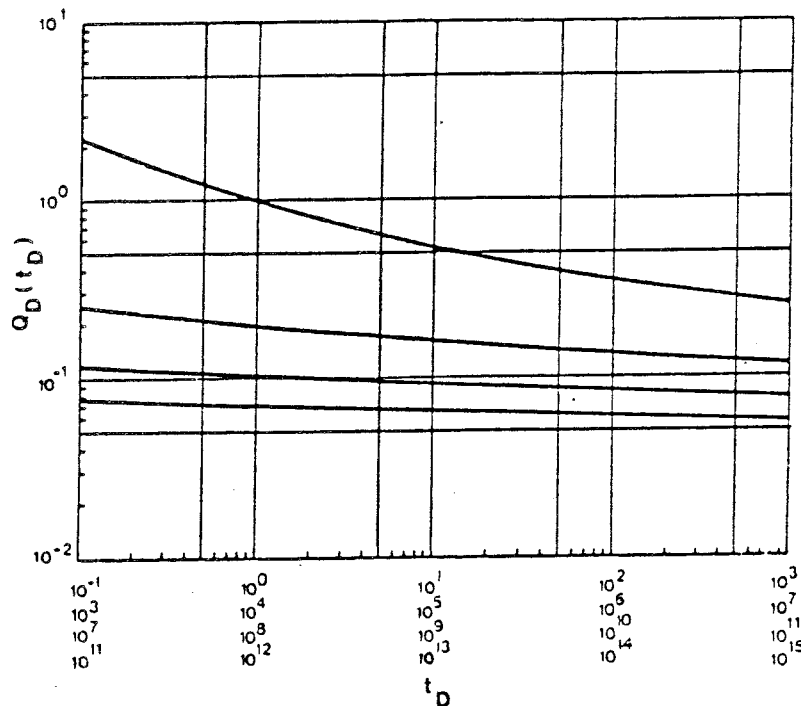


Figure 4.2.4 Type-curve representing $Q_D(t_D)$ as a function of t_D . After Jacob and Lohman (1952).

The decline in flow rate, $Q(t)$, is plotted as a function of the test time, t , in a log-log graph. The type curve shown in Fig. 4.2.4. assumes that the skin factor is zero. However, the skin effect may be incorporated into this figure if t_D is replaced by $t_D e^{2\zeta}$ (or r_w by $r_w e^{-\zeta}$) since the effective radius concept is valid. The hydraulic conductivity may be calculated from Eqn. (4-21) in analogy with Eqn. (4-12) for the constant rate of flow case using the following expression in

metric units:

$$K = \frac{0.159 Q(t)_m}{H_o L Q_D(t_D)_m} \quad (4-21)$$

$Q(t)_m$ and $Q_D(t_D)_m$ are the flow rates at the matchpoint on the data curve and type curve respectively. The effective borehole radius, r_{wf} , and skin factor can be determined from Eqn. (4-13) and Eqn. (3-2) respectively. As may be seen in Fig 4.2.4, the rate of flow declines rapidly at early times ($t_D < 1000$). Then the type curve becomes very flat. Thus, since type-curve matching requires the type curve to be of characteristic shape to obtain a unique match, this method is only suitable at early times ($t_D \leq 1000$).

The dimensionless flow rate $Q_D(t_D)$ may be approximated by $1/p_D$ when $t_D \geq 1000$. If the logarithmic approximation of p_D in Eqn. (4-6) is used, the reciprocal flow rate can, in analogy with Eqn. (4-7), be expressed in metric units (Uraiet and Raghavan 1980a) as:

$$1/Q(t) = \frac{1.15}{2\pi K L H_o} \left[\log \frac{Kt}{r_w^2 S_s} + 0.351 + 0.869 \zeta \right] \quad (4-22)$$

Eqn. (4-22) implies that a semi-log graph of $1/Q(t)$ versus $\log t$ should yield a straight line. The hydraulic conductivity may be calculated from the slope of the straight line in metric units:

$$K = \frac{0.183}{H_o L \Delta(1/Q(t))} \quad (4-23)$$

$\Delta(1/Q(t))$ is the change in flow rate during a logarithmic time cycle. Eqn. (4-23) only provides a reliable value of the hydraulic conductivity if $t_D \geq 1000$. In low-permeability formations t_D may be less than 1000. In such cases, the value of K calculated from Eqn. (4-23) must be corrected according to

a procedure described by Uraiet and Raghavan (1980a). Provided that the logarithmic approximation is valid, the skin factor may be derived from Eqns. (4-22) and (4-23) and is given in metric units by:

$$s = 1.15 \left[\frac{1/Q(t)_{1 \text{ min}}}{\Delta (1/Q(t))} - \log \frac{K}{r_w^2 S_s} - 2.13 \right] \quad (4-24)$$

$1/Q(t)_{1 \text{ min}}$ is obtained by extrapolating the straight line to 1 minute. Eqn. (4-24) is similar to Eqn. (4-9) for the constant-rate case. The skin factor for the constant-pressure case is a measure of the increase or reduction in flow rate due to the skin-zone. This may be expressed as follows (Uraiet and Raghavan 1980a):

$$s = (1/Q_D)_{\text{actual}} - (1/Q_D)_{\text{ideal}} \quad (4-25)$$

4.3 Spherical flow

4.3.1 Constant-rate tests

Particularly if the formation (or part of it) is very thick in relation to the length of the section of borehole tested, a spherical flow regime may occur during the test. The basic partial differential equation for transient, spherical flow in a porous medium may, with spherical coordinates, be expressed as:

$$\frac{\partial^2 (\Delta p)}{\partial r^2} + \frac{2}{r} \frac{\partial (\Delta p)}{\partial r} = \frac{S_s}{K} \frac{\partial (\Delta p)}{\partial t} \quad (4-26)$$

This equation is very similar to the diffusivity equation for transient, radial flow, given by Eqn. (4-1). The head (or pressure) change for spherical flow geometry may, for the constant-rate case, be expressed using Eqn. (4-26) in metric units:

$$H = \frac{P_i - P_{wf}}{\rho g} = \frac{Q}{4\pi K r_{ws}} P_D(t_D, r_D) \quad (4-27)$$

H represents the difference between the initial static pressure, p_i , and the pressure, p_{wf} , at a certain time, t , in the borehole (section) and r_{ws} is the pseudo-spherical borehole radius (Brigham et al 1980). The parameters p_D , t_D and r_D denote dimensionless pressure change, time and distance from the active borehole respectively. The parameter p_D is defined as follows for spherical flow:

$$p_D = \frac{4\pi K r_{ws} H}{Q} \quad (4-28)$$

The definitions of t_D and r_D are the same as for radial flow, given by Eqns. (4-4) and (4-5) respectively, except that they are based on the radius for spherical flow, r_{ws} , in this case (instead of r_w).

The solution of the function $p_D(t_D, r_D)$ for spherical flow is presented in a paper by Onyekonwu and Horne (1983). At the active borehole ($r_D = 1$) this solution may be expressed:

$$p_D = 1 - \frac{1}{\text{erfc} \sqrt{\pi t_D}} \quad (4-29)$$

In Eqn. (4-29) erfc is the complementary error function. For long durations this equation may be approximated as

$$p_D = 1 - e^{-\frac{t_D}{4}} \text{erfc} \sqrt{t_D} \quad (4-30)$$

and for short durations, it may be approximated as

$$P_D = 2 \sqrt{\frac{t_D}{\pi}} \quad (4-31)$$

Eqn. (4-31) assumes that no borehole storage and skin effects occur. Thus, the practical use of the short-term solution is limited (Onyekonwu and Horne, 1983). If borehole storage and skin effects occur, the test data should be analysed using a method presented by Brigham et al (1980). The long-term data may be analysed by plotting the head change, H , versus the reciprocal square root of time, $1/\sqrt{t}$, as indicated by Eqn. (4-30). The data points should fall on a straight line in a linear graph. The hydraulic conductivity may be calculated from the slope of this line by inserting Eqn. (4-30) into Eqn. (4-27) in accordance with the following equation:

$$K = \left(\frac{Q S_s^{1/2}}{4\pi^{3/2} \cdot m} \right)^{2/3} \quad (4-32)$$

where m is the slope of the straight line.

The pseudo-spherical (effective) borehole radius is dependent on many factors, such as borehole conditions, type of well completions, etc. (Brigham et al 1980). According to Culham (1974), the effective borehole radius, r_{ws} , for spherical flow can be expressed:

$$r_{ws} = \frac{L}{2 \ln(L/r_w)} \quad (4-33)$$

L is the length of the section open to flow and r_w is the actual borehole radius. Eqn. (4-33) is derived for steady-state conditions but may also be used under conditions that only approach the steady state (Culham 1974).

4.3.2 Constant-pressure tests

The dimensionless flow rate Q_D for spherical flow conditions is defined for constant-pressure tests by Chatas (1966) similar to Eqn. (4-28) for constant flow-rate tests:

$$Q_D = \frac{Q(t)}{4\pi K r_{ws} H_o} \quad (4-34)$$

Neglecting the skin effect, the change in flow-rate with time, $Q(t)$, at the borehole (section) during a constant-pressure test under spherical flow conditions may be expressed using Eqn. (4-34) in metric units:

$$Q(t) = 4\pi K r_{ws} H_o Q_D(t_D) \quad (4-35)$$

H_o is the constant drawdown or injection head at the active borehole (section) and r_{ws} is the effective borehole radius for spherical flow conditions. The dimensionless time, t_D , is defined by Eqn. (4-4), based on the effective radius, r_{ws} , for spherical flow. The theoretical solution of the function $Q_D(t_D)$ for a constant-pressure test with spherical flow conditions was presented by Chatas (1966):

$$Q_D = 1 + \frac{1}{\sqrt{\pi t_D}} \quad (4-36)$$

Eqn. (4-36) indicates that a plot of the flow rate $Q(t)$ versus $1/\sqrt{t}$ should yield a straight line in a linear graph. The (average) spherical hydraulic conductivity may be calculated

from the slope of this line by combining Eqn. (4-36) and (4-34) as follows:

$$K = \left(\frac{m}{4\pi^{1/2} r_{ws} H_0 S_s^{1/2}} \right)^2 \quad (4-37)$$

where m is the slope of the straight line.

4.4 Steady-state injection tests

4.4.1 General

The constant-head injection test has been widely used to estimate the hydraulic conductivity in geotechnical and groundwater problems. In reality, the flow domain in all groundwater testing is of finite extent. A steady state implies that the groundwater flow is constant in magnitude and direction at all points in the reservoir and does not change with time. A true steady-state situation very seldom occurs in practice. At best, a quasi-steady-state situation may be achieved during a limited period of time. However, methods of analysis based on assumed steady-state conditions are often used. This is due to their mathematical simplicity and also to the fact that they give fairly good agreement with corresponding methods of transient analysis.

4.4.2 Theory and analysis

Under steady-state conditions the right hand side of Eqn (4-1) will be zero as no change in head occurs. The steady-state solution for an injection (or drawdown) test in a confined section of an active borehole may be expressed by:

$$H_0 - h = \frac{Q}{2\pi K L} \ln(r/r_w) \quad (4-38)$$

where H_o = the applied head change in the active borehole section

h = the head change at distance r

r = radial distance from the active borehole section

In Eqn. (4-38) the flow from (or to) the active borehole is assumed to be two-dimensional (radial). At greater distances from the active borehole, particularly when the length of the test section is short, it may be assumed that the flow changes to three-dimensional (spherical) flow. This implies that the head change, h , at a distance r from the active borehole (where spherical flow is assumed) may be calculated, according to Moye (1967), using the expression:

$$h = \frac{Q}{4\pi K r} \quad (4-39)$$

If r is the distance within which the flow is assumed to be radial and beyond which the flow is spherical, Eqn. (4-38) and (4-39) may be combined:

$$H_o = \frac{Q}{2\pi K L} \ln (r/r_w) + \frac{Q}{4\pi K r} \quad (4-40)$$

According to Moye (1967) it may be assumed that $r = L/2$ which implies that

$$H_o = \frac{Q}{K L} \left[\frac{1 + \ln (L/2 r_w)}{2\pi} \right] \quad (4-41)$$

From this expression the average hydraulic conductivity of the test section may be calculated using:

$$K = \frac{Q}{H_o L} \left[\frac{1 + \ln (L/2 r_w)}{2\pi} \right] \quad (4-42)$$

The expression within brackets is generally called Moye's constant. Eqn. (4-42) is normally used to calculate the hydraulic conductivity from steady-state, constant-head injection tests in crystalline rock in Sweden.

4.4.3 Applications

Doe and Remer (1982) presented a theoretical comparison of hydraulic conductivity calculated from steady-state and transient tests in non-porous fractured rock. They found that the hydraulic conductivity is generally overestimated by steady-state methods. They concluded that the error in calculating the hydraulic conductivity by steady-state methods is generally less than one order of magnitude and normally within a factor of about two or three of transient methods.

Andersson and Persson (1985) made a comparison of steady-state and transient analyses using field data from a large number of single-hole tests in crystalline rock in Sweden. They found that the mean value of hydraulic conductivity (423 tests) from steady-state analysis ($t=15$ minutes) was about 2.7 times greater than the corresponding mean value from transient test analysis ($t = 2$ hours). Steady-state analysis occasionally results in 10-20 times higher values than transient analysis. These conclusions are in good agreement with the results obtained by Doe and Remer (1982).

5. BUILD-UP/FALL-OFF TESTS IN HOMOGENEOUS FORMATIONS

5.1 General

When a production or injection test is stopped the pressure change caused by the preceding production or injection phase recovers and the actual pressure approaches the static pressure in the borehole (section). Theoretically, the recovery period is treated as if the production (or injection) goes on continuously and, during the period, an image borehole injects into (or produces from the active borehole at the same rate, i.e. the net flow rate is zero. This implies that the drawdown/injection period and the build-up/fall-off periods are interrelated and that the pressure response during the recovery period is dependent on the duration of the preceding drawdown/injection period (see Fig. 5.1.1). This is true for both constant-flow and constant-pressure tests.

In general, the drawdown (injection) type curves cannot be used directly to analyse recovery data unless the drawdown or injection period is much longer than the longest recovery-time to be analysed. In addition, the correct radial-flow semi-log straight line will not develop during the recovery test if the drawdown or injection period is too short, no matter how long the recovery period is (Raghavan 1980). The theories for build-up and fall-off tests are analogous.

5.2 Radial flow

5.2.1 Tests after a constant-rate-of-flow period

The build-up (or fall-off) data obtained during the recovery period may be represented in two ways, either as the residual drawdown ($p_i - p_{ws}$) or as the actual build-up, $p_{ws} - p_p$, as defined in Fig. 5.1.1. The residual drawdown is generally used for semi-log analysis (the Horner method and the MDH method) whereas the actual pressure change during build-up is more suited for type-curve analysis in a log-log

graph.

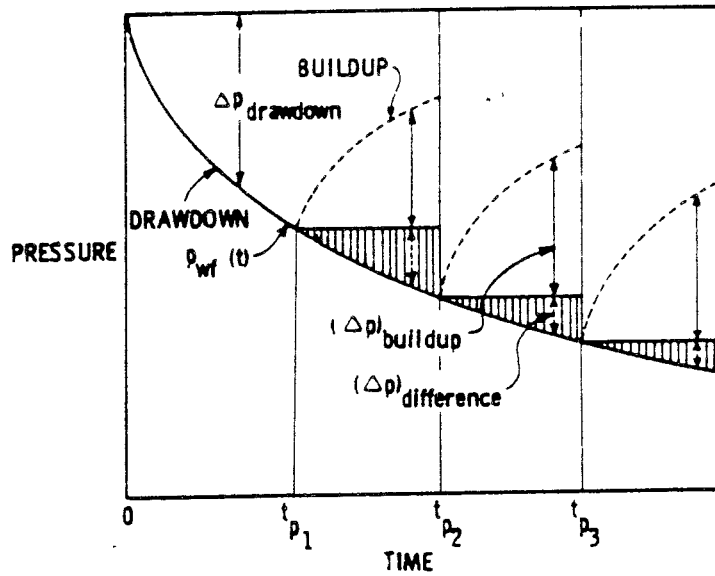


Fig. 5.1.1. Schematic representation of pressure build-up behaviour following a constant rate of drawdown period, t_p . After Agarwal (1980).

Horner method

The basic dimensionless build-up equation, p_{Ds} , in terms of the residual drawdown can be expressed according to the principle of superposition (Earlougher 1977):

$$p_{Ds} = \frac{2\pi KL (p_i - p_{ws})}{Q \rho g} = p_D (t_p + dt)_D - p_D (dt)_D \quad (5-1)$$

The first term in Eqn. (5-1) represents the dimensionless pressure change during the entire drawdown period and its extent during the recovery period (see Fig. 5.1.1). During the recovery period the current time is denoted dt . The drawdown curve is defined by Eqn. (4-3). The second term in Eqn. (5-1) represents the pressure build-up curve during the recovery period, superposed on the drawdown curve. If the semi-log

approximation of P_D in Eqn. (4-6) is applied, then Eqn. (5-1) for the residual drawdown during a build-up test may be expressed as

$$H' = (p_i - p_{ws})/\rho g = \frac{0.183 Q}{KL} \log \left(\frac{t_p + dt}{dt} \right) \quad (5-2)$$

This is the well-known Horner equation in metric units. Eqn. (5-2) indicates that if the residual drawdown is plotted versus the expression $(t_p + dt)/dt$, or its reciprocal value, in a semilog graph, the data points should fall on a straight line. The equation takes into account the production time since t_p is included. However, the theoretical slope of the straight line for radial flow will only exist if the production time is sufficiently long (Raghavan 1980). For a homogeneous formation without borehole storage and skin effects, the drawdown or injection period and also the recovery period must be sufficiently long for the logarithmic approximation of the two terms on the right-hand side of Eqn. (5-1) to be valid. This condition may not always be fulfilled in low-permeability formations (see Section 4.2.1).

If the build-up response is influenced by borehole storage and skin effects, the production time required for the correct semilog straight line to develop is given by the following condition (Raghavan 1980):

$$\frac{t_{pD}}{C_D} = \frac{2\pi KL t_p}{C \rho g} \geq 200 \quad (5-3)$$

In Eqn. (5-3) t_{pD} and C_D represent the dimensionless production or injection time and borehole storage coefficient respectively. The condition in Eqn. (5-3), which is valid for $C_D^{2c} \geq 100$, may be reduced to $t_{pD}/C_D \geq 50$ if an error of 10 % is accepted in the K value. In addition, the recovery period must also be sufficiently long. The time, dt , for the straight line to develop during recovery is given by (Raghavan 1980):

$$\frac{dt_D}{C_D} = \frac{2\pi KL dt}{C \rho g} \geq 60 + 3.5 \zeta \quad (5-4)$$

The hydraulic conductivity may be calculated from the slope of the straight line in the Horner graph from Eqns. (4-8) and (5-2), provided the conditions in Eqns. (5-3) and (5-4) are fulfilled. The skin factor is determined from the following expression for a build-up test (Earlougher 1977):

$$\zeta = 1.151 \left[\frac{(p_{1\min} - p_p)/\rho g}{\Delta H} - \log \left(\frac{K}{r_w^2 S_s} \right) - 2.13 \right] \quad (5-5)$$

In Eqn. (5-5), p_p is the pressure at the stop of the draw-down/injection period and $p_{1\min}$ is the pressure after 1 minute of recovery. This pressure must be taken from the extrapolated straight line. For a pressure fall-off test, the pressure difference in the first term of Eqn. (5-5) should be replaced by $p_p - p_{1\min}$.

The Horner method also permits determination of the initial static pressure, p_i , in the section tested, provided the preceding drawdown or injection period is sufficiently long. This is performed by extrapolating the straight line to an infinite recovery time, i.e. when $(t_p + dt)/dt = 1$ on the time scale (Earlougher 1977). The extrapolated pressure value is generally denoted p^* . If the formation being tested is infinitely large, the extrapolated pressure will be identical to the static pressure. However, if the drawdown or injection time is short, the build-up or fall-off curve will level off towards the static pressure by the end of the test. If effects of depletion occur, e.g. in finite formations, during the drawdown test the average pressure in the formation will generally be lower than the extrapolated pressure.

As already mentioned, the Horner method may not be applicable in very low-permeability formations. The theory of this method

is based on the assumption that the radius of the borehole is

infinitely small and that the logarithmic approximation of p_D in Eqn. (4-6) is valid. Morrison (1981) found that these assumptions may not be valid in tight formations, with errors in the analysis as a result. The special solution of the pressure change in a borehole with a finite radius is called the PDCI solution as discussed in Section 4.2.1. This solution and the logarithmic approximation of p_D are markedly different before $t_D = 25$ and thus the Horner method may give erroneous results (see Fig. 4.2.1). Such low values of t_D may occur in tight formations.

Equivalent-time method

In a Horner diagram, the residual drawdown is plotted on the pressure scale according to Eqn. (5-2). Since this requires knowledge of the initial, static pressure, p_i , which is often not the case, the Horner method is not suitable for type-curve matching in a log-log graph. If Eqns. (4-3) and (5-1) are combined, the dimensionless actual build-up, \bar{p}_{Ds} , based on the pressure at the end of the drawdown period, may be defined (Raghavan 1980) as:

$$\bar{p}_{Ds} = \frac{2\pi KL (p_{ws} - p_p)}{Q \rho g} = p_D(t_{pD}) - p_D(t_p + dt)_D + p_D(dt)_D \quad (5-6)$$

The actual build-up curve is normally used for type-curve analysis. Eqn. (5-6) may be used to calculate a set of specific type curves for different values of the dimensionless production time, t_{pD} (Raghavan 1980). Such type curves may be used for analysis but the disadvantage of this method is that a large number of type curves for different production times are required. To overcome this problem, Agarwal (1980) found that all such type curves may be standardized into one single type curve, provided an equivalent time is plotted on the time scale instead of the actual recovery time.

If the logarithmic approximation of p_D is substituted in Eqn.

(5-6) the following expression is obtained (Agarwal 1980):

$$\bar{p}_{Ds} = 1.15 \left[\log \left(\frac{t_{pD} \times dt_D}{dt_D + t_{pD}} \right) + 0.351 \right] \quad (5-7)$$

Eqn. (5-7) is analogous to the drawdown Eqn. (4-6). Agarwal (1980) demonstrated that replotting a set of type curves for different production times with the time expression in Eqn. (5-7) on the time scale instead of the actual recovery time, dt , resulted in a single curve identical to the drawdown type curve for all values of the production time. Thus, the build-up data may be plotted as a function of the expression $(t_p \times dt)/(t_p + dt)$ in a log-log graph and matched with the corresponding drawdown type curve for all production times. The equivalent time, dt_e , is defined as

$$dt_e = \frac{t_p \times dt}{dt + t_p} \quad (5-8)$$

The equivalent-time method may also be applied to other test conditions and other type curve solutions, such as borehole storage and skin effects, fractured formations, multiple-rate testing as well as to conventional semi-log analysis. If skin damage affects the build-up data a skin factor must be added to the right-hand side of Eqn. (5-7). If both borehole storage and skin effects occur, the corresponding drawdown type curve may still be used and also semi-log analysis if the (dimensionless) production time is sufficiently long and the conditions stated by Eqns. (5-3) and (5-4) are satisfied.

With a skin factor included in Eqn. (5-7), this may in analogy with Eqn. (4-7), be written in the following form:

$$H = (p_{ws} - p_p)/\rho g = \frac{0.183 Q}{KL} \left[\log \left(\frac{t_p \times dt}{dt + t_p} \right) + \log \left(\frac{K}{S_s r_w^2} \right) + 0.869 s \right] \quad (5-9)$$

Eqn. (5-9) indicates that if the absolute build-up pressure, p_{ws} , or the actual build-up pressure difference is plotted versus dt_e in a semi-log graph, a straight line should

develop if the conditions in Eqns. (5-3) and (5-4) are satisfied. This graph is similar to a Horner graph but has the advantage that the build-up data may be plotted on a real time scale both versus dt_e and dt , which permits direct comparison of the curves so that the effect of the production time is visible. The hydraulic conductivity is calculated from the slope of the straight line using Eqn. (4-8). The skin factor may be determined from Eqn. (4-9).

As in the Horner graph, the static pressure, p_s , in the tested interval can be determined in the semi-log graph by extrapolating the straight line to infinite recovery time. This time corresponds in this case to a recovery time in which $dt_e = t_p$ as may be seen from Eqn. (5-8).

5.2.2 Tests after a constant-pressure period

The pressure build-up (or fall-off) behaviour after a period of constant-pressure production (or injection) is similar to the constant-rate case. The dimensionless residual drawdown during recovery for the constant-pressure case is defined by Uraiet and Raghavan (1980 b):

$$p_{Ds} = \frac{2\pi KL (p_i - p_{ws})}{Q_p \rho g} = \frac{2\pi KL H}{Q_p} \quad (5-10)$$

This equation is identical to Eqn. (4-3) for the constant-rate case except that the flow rate, Q , is replaced by Q_p , which is the instantaneous flow rate at the end of the drawdown/injection period.

Horner method

If the residual pressure change during the recovery period after production or injection at constant pressure is plotted in a Horner graph, as described in the previous section, the data points will again fall on a straight line provided the production (or injection) period is sufficiently long. If there are no borehole storage or skin effects, the straight line with correct slope will develop for dimensionless recovery times $dt_D > 40$ if the dimensionless production (or injection) time $t_{pD} > 1000$. When t_{pD} is less than 1000, no extensive straight-line portion can be identified in the Horner graph. For long recovery times the slope of the straight line decreases and will eventually reach zero (horizontal line) when the recovery pressure reaches the static pressure in the section tested (Uraiet and Raghavan 1980 b).

If the two conditions mentioned above are satisfied, the hydraulic conductivity may be calculated in analogy with Eqn. (4-8) as follows:

$$K = \frac{0.183 Q_p}{L \Delta H} \quad (5-11)$$

In Eqn. (5-11), Q_p is the rate of flow at the end of the drawdown/injection period and H is the change in residual head per logarithmic time cycle. If the dimensionless flow time is less than 1000, the maximum slope of the build-up (or falloff) curve should be used to estimate the hydraulic conductivity. If borehole storage and skin effects are present, the recovery time and production time required for the straight line to develop are given by the conditions in Eqns. (5-4) and (5-3) respectively. The hydraulic conductivity is calculated from Eqn. (5-11) and the skin factor for a build-up test from Eqn. (4-9) as for the constant-rate-of-flow case (Uraiet and Raghavan 1980 b). The static pressure in the section tested is estimated by extrapolating the straight line in the Horner

graph, as described in the previous section, unless the static pressure is already reached during the test.

Equivalent-time method

If the build-up (or fall-off) data are plotted on an equivalent time scale, as described in the previous section, type curve matching with drawdown type curves may be performed in a loglog graph. This means that the type curves including borehole storage and skin effect as presented by Agarwal et al (1970) and Gringarten et al (1979) may be used to analyse build-up and fall-off tests after a period of constant-pressure production or injection (see Section 4.2.1). In this case the rate of flow at the end of the drawdown/injection period should be used to calculate the hydraulic conductivity from Eqn. (4-12). The analysis may also be performed on a semi-log graph as described in the previous section. The hydraulic conductivity and skin factor may be determined from Eqns. (5-11) and (4-9) respectively. The method also permits a determination of the static pressure, p_i , of the section tested.

5.3 Spherical flow

5.3.1 Tests after a constant rate of flow period

The basic borehole pressure build-up (and fall-off) equation after a constant flow rate test may be expressed as (Culham 1974):

$$H' = (p_i - p_{ws})/\rho g = \frac{Q\sqrt{S_s}}{4\pi^{3/2} K^{3/2}} \left[\frac{1}{\sqrt{dt}} - \frac{1}{\sqrt{t_p + dt}} \right] \quad (5-12)$$

Eqn. (5-12) indicates that a plot of the residual change in head, H' , in the borehole versus the time expression $(1/\sqrt{dt} - 1/\sqrt{t_p + dt})$ in a linear graph should result in a

straight line with slope, m . From this slope the hydraulic conductivity may be calculated as:

$$K = \left(\frac{Q S_s^{1/2}}{4\pi^{3/2} \cdot m} \right)^{2/3} \quad (5-13)$$

Eqn. (5-13) is identical to Eqn. (4-32) for constant-rate drawdown/injection tests. In Eqn. (5-13) the slope, m , is expressed in metres of water per reciprocal square-root of the time in seconds. By comparing Eqn. (5-12) with Eqn. (4-7) for radial flow it can be seen that no geometrical factor is present in the build-up equation for spherical flow. For radial flow, the geometrical factor is the formation thickness or the length of the section being tested. Thus, for spherical flow, the borehole conditions (perforation, open hole completion, etc.) do not influence the pressure build-up curve. The pressure build-up is instead controlled by the formation some distance from the borehole (Moran and Finklea 1962).

The hydraulic conductivity calculated from Eqn. (5-13) should be regarded as an average value of the spherical volume influenced by the test, including anisotropic properties. As seen from Eqn. (5-13), the hydraulic conductivity is, for spherical flow conditions, independent of both the effective borehole radius and the length of the section tested. The skin factor for spherical flow may be determined in analogy with Culham (1974):

$$\zeta = \sqrt{\frac{S_s r_{ws}^2}{\pi K}} \left[\frac{(p_p - p_1)/\rho g}{m} + \frac{1}{\sqrt{dt_1}} \right] - 1.0 \quad (5-14)$$

In Eqn. (5-14), p_p , is the pressure immediately before the end of the drawdown/injection period and p_1 is the pressure at the recovery time dt_1 . The pressure value, p_1 , is obtained from the (extrapolated) straight line portion of the buildup curve. The effective borehole radius, r_{ws} , for spherical flow should be used in Eqn. (5-14).

The initial, static pressure, p_i , or head in the section tested may also be determined from the build-up curve for spherical flow by extrapolating the straight line to infinite recovery time as for radial flow. In this case, the infinite recovery time corresponds to a zero value of the expression on the time scale.

5.3.2 Tests after a constant-pressure period

According to Moran and Finklea (1962) the build-up Eqn. (5-12) after a period of constant flow may also be used for analysis of build-up (or fall-off) tests after a constant-pressure period for long durations, when the applied pressure or head change, H_o , has returned to within 10-20 % of its (constant) value. This means that the hydraulic conductivity may be calculated from Eqn. (5-13) if Q is replaced by Q_p and the skin factor determined from Eqn. (5-14).

6. DUAL-POROSITY FORMATIONS

6.1 General

A dual-porosity formation is considered to be composed of two interacting porous media regions with both primary and secondary porosity. The primary porosity region is associated with the rock matrix whose hydraulic properties are generally controlled by depositional and lithification processes. The secondary porosity region consists of the fracture system whose hydraulic properties are generally the result of thermal stresses and tectonic processes. In general, the permeability of the matrix blocks is low and the fracture system exhibits high permeability and transmissivity. The storage capacity of the two regions depends on the (effective) porosity of each region.

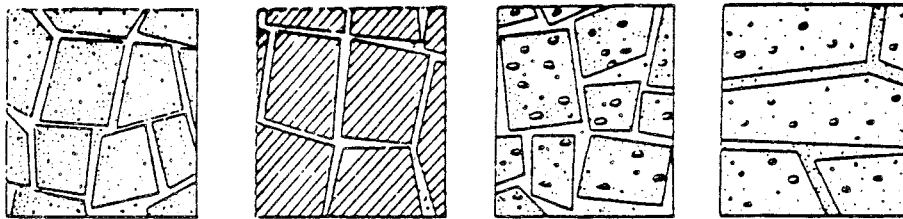


Fig. 6.1.1 Schematic representation of a fractured medium, a purely fractured medium, a dual-porosity medium and a heterogeneous medium. After Mavor and Cinco-Ley (1979).

Dual-porosity formations may be classified into four different categories (Streltsova 1976) (see Fig. 6.1.1). The first category, a fractured medium, consists of a formation whose primary porosity region contains the majority of the storage capacity while the secondary porosity region constitutes the water transmitting capacity of the medium.

The second model, a purely fractured medium, represents a medium whose matrix permeability and matrix porosity are

negligible. Thus, both the storage and transmitting capacity of the medium are due entirely to the fracture network. This category is one limiting form of the behavior of first category.

The third group is a dual porosity medium, in which the storage capacity of the primary and secondary regions of the medium are of the same order of magnitude, while the transmitting capacity is due to the fracture system.

The final category is a heterogeneous medium in which the fractures are filled with a material with a permeability that is lower than that of the matrix.

6.2 Theoretical models of dual-porosity formations

The first category reservoir model in Fig. 6.1.1. is most frequently used in the petroleum industry to describe the pressure behaviour of porous naturally fractured reservoirs. In such theoretical models the storage capacity of the rock is associated with the intergranular, primary or matrix porosity, while the transmitting capacity is attributed almost entirely to the fracture system. The matrix (effective) porosity is generally assumed to be much higher than the fracture (effective) porosity. The category models in cases two and three, described above, may thus be regarded as special cases of this theoretical model. Thus, in the following text the first three cases are grouped together.

In general, the dual-porosity formation is treated as a continuum with the fractures extending throughout the reservoir. Serving as flow channels with high transmissivity, the fractures control the fluid pressure distribution in the rock mass. When the pressure in the fractures is changed, pressure differentials across the matrix blocks are created, resulting in a time-dependent cross-flow between the fractures and matrix blocks. This cross-flow is considered as one-dimensional. The high hydraulic diffusivity of the fractures result in a rapid pressure response along the

fractures, while the rock matrix exhibits a delayed response to pressure changes occurring in surrounding fractures. Ultimately, the pressure in the fractures and matrix will equilibrate, after which the formation acts as a uniform medium with composite properties of both matrix and fracture system.

Several different model geometries have been described in literature to represent dual-porosity formations. The rock matrix may either be divided into parallelepipeds by an orthogonal fracture network (the block model) or, alternatively, into layers by a set of horizontal fractures (the layer model). Other matrix geometries, such as spheres and cylinders, have also been considered. The resulting pressure response is, however, similar for most of these matrix geometries but the actual parameter values calculated for the system may vary according to the different assumed geometries (Najurieta 1980, Moench 1984).

Two different assumptions regarding the nature of the flow in the matrix due to pressure changes at the fracture/matrix interface have been applied in the theoretical models. Firstly, the matrix flow is assumed to be independent of spatial position within the matrix element which implies a pseudo-steadystate cross-flow in the matrix. This assumption neglects the storage capacity of the rock matrix by allowing an instantaneous pressure change throughout the matrix as soon as pressure changes occur in the fractures (Streltsova 1983). According to this assumption, the pressure response of such a medium has a characteristic S-shaped, flat transitional curve with an inflection point in a logarithmic graph.

Secondly, other models assume that the cross-flow between the rock matrix and fractures is transient and can be represented by a one-dimensional diffusivity-type flow equation. This spatially-dependent flow takes into account not only the matrix permeability but also the storage capacity of the matrix. This assumption leads to a different transitional pressure response, both regarding the time of onset and shape of the curve. This model has been adopted by Najurieta (1980), Serra et al (1983), Streltsova (1983) and others. Streltsova also made a critical

examination of the consequences of the two different assumptions regarding the matrix cross-flow. Gringarten (1984) presented a review on theory and practice for reservoirs with "double-porosity" behaviour. He also presented field data from naturally fractured reservoirs whose pressure response is similar to the response resulting from the assumption of pseudo-steady-state cross-flow in the matrix. Moench (1984) explained this behaviour as a result of fracture skin, a thin skin of low-permeability material, deposited on the surfaces of the matrix blocks. The effect of this fracture skin in naturally fractured reservoirs would be to delay the cross-flow between the matrix blocks and the fractures. The pressure response with fracture skin is similar to the one predicted under the assumption of pseudo-steady-state cross-flow (without fracture skin). According to Moench (1984) fracture skin may occur as a result of mineral alteration or deposition created by the flow of groundwater in the fractures.

The hydraulic conductivity, K_f , of the fracture system in a dual-porosity formation is assumed to be approximately equal to the (bulk) hydraulic conductivity, K , of the rock mass since all flow to (or from) the borehole (section) is considered to take place via the fracture system.

6.3 Theory and test interpretation

6.3.1 Constant-rate-of-flow tests

The theoretical pressure behaviour of the model presented by Serra et al (1983) and Streltsova (1983) is adopted in this report. In this model the formation is represented as an isotropic, dual-porosity reservoir of uniform thickness and of infinite extent, bounded by impermeable layers above and below. The matrix is subdivided by a set of parallel horizontal fractures. It is assumed that all production from (or injection into) the borehole is via the fracture system and also that vertical one-dimensional, transient cross-flow occurs in the matrix. The properties of both the matrix and fracture system are assumed to be constant. An infinitesimally thin skin around

the borehole walls is considered but borehole storage and fracture skin effects are neglected. The flow in the fractures is assumed to occur only in the radial direction.

The general differential equation for the groundwater flow in the fracture system may be written in analogy with Streltsova (1983) and Moench (1984):

$$\frac{\partial^2(\Delta p)}{\partial r^2} + \frac{1}{r} \frac{\partial(\Delta p)}{\partial r} = \frac{S_{sf}}{K} \frac{\partial(\Delta p)}{\partial t} + \frac{q_m}{KL} \quad (6-1)$$

In Eqn. (6-1) the parameters S_{sf} and K are based on bulk properties of the rock mass. The flow term, q_m , in Eqn. (6-1) represents the transient cross-flow from the matrix blocks to the fractures. At the matrix/fracture interface ($z=0$) the cross-flow per unit area and unit time may be expressed according to Streltsova (1983):

$$q_m = K_m \frac{\partial(\Delta p_m)}{\partial z} \quad (z=0) \quad (6-2)$$

The corresponding differential equation for the pressure change in the matrix, Δp_m , is expressed by Streltsova (1983):

$$\frac{\partial^2(\Delta p_m)}{\partial z^2} = \frac{S_{sm}}{K_m} \frac{\partial(\Delta p_m)}{\partial t} \quad (6-3)$$

General analytical solutions for the fracture pressure distribution (Eqn. 6-1) and the matrix pressure distribution (Eqn. 6-3) are presented in Laplace space by Streltsova (1983). Serra et al (1983) also derived a similar analytical solution for the same type of dual-porosity model, together with approximate solutions for intermediate and long times. Both types of solution assume transient flow in the matrix rock.

The general solution for the pressure drawdown (or injection) behaviour in the active borehole in dual-porosity formations involves three different flow regimes. Flow regimes 1 and 3 represent the early and late time responses respectively and are characterized by two parallel straight lines in a semi-log graph. If transient cross-flow is assumed the intermediate time flow regime 2 is also characterized by a semi-log straight line, but the slope is approximately half that of flow regimes 1 and 3. The identification of the different flow regimes is important when analysing field data from dual-porosity formations.

During flow regime 1 the pressure response is dominated by the compressible fracture system. During this flow regime the matrix flow has not begun to influence the pressure response. Flow regime 1 constitutes one of the limiting forms of the solution for dual-porosity formations. During flow regime 2 the flow in the matrix, whose response is delayed because of the low matrix permeability, starts to influence the pressure response of the system. This will result in a slower pressure change than during flow regime 1. Flow regime 2 is also characterized by an increase in the total, effective storage of the system due to the matrix storage becoming active.

As time progresses, the matrix blocks near the active borehole become depleted and the pressures in the matrix blocks and fractures equalize. The matrix flow support must then be provided by matrix blocks ever further from the active borehole. At a certain time this results in a delay between the flow transport in the fractures to the borehole and the release of fluid by the distant matrix blocks. After this time the fractured formation behaves as an equivalent uniform medium with a transmissivity corresponding to the fracture system and a composite storage capacity that is the sum of the matrix and fracture storage capacities. This period corresponds to flow regime 3, which forms the second limiting form of the solution for the pressure response in dual-porosity formations.

The hydraulic conductivity of the fracture system (which is assumed to equal the conductivity of the rock mass) and skin

factor can be determined from any of the three flow regimes, if present, in a semi-log graph. From flow periods 1 and 3 the hydraulic conductivity, K , is calculated from the slope of the straight line from Eqn. (4-8), whereas during flow period 2 the conductivity may be calculated from the same equation if the factor 0.183 is replaced by $0.183/2$ since the slope of the straight line is halved.

If the specific storage, S_{sf} , of the fracture system is known, the skin factor can be estimated from flow regime 1 (the first straight line) by Eqn. (4-9) if S_s is replaced by S_{sf} . Accordingly, if the total specific storage capacity of the formation, which is the sum of the specific storage coefficients in the matrix and fracture system, the skin factor may be estimated from flow regime 3 (the second straight line) by the following expression for a drawdown test:

$$\zeta = 1.151 \left[\frac{H_1 \min}{\Delta H} - \log \frac{K}{(S_{sm} + S_{sf}) r_w^2} - 2.13 \right] \quad (6-4)$$

If borehole storage occurs, the pressure data during flow period 1 may be distorted and if the test is short only the intermediate flow regime, 2, may be present (Mavor and Cinco-Ley 1979). To determine the significance of borehole storage effects in dual-porosity formations, the borehole storage type curves presented in Section 4.2.1 may be used for early times.

6.3.2 Constant-pressure tests

Raghavan and Ohaeri (1981) considered theory for constant-pressure tests in dual-porosity formations assuming both the pseudosteady-state and transient flow transfer between the matrix system and the fracture system. The model by Raghavan and Ohaeri (1981) is the same as the one described by Serra et al (1983) for constant-rate-of-flow tests (see Section 6.3.1). In this model it is assumed that the fracture system can be replaced by an equivalent set of horizontal fractures. As in the constant-rate-of-flow case early, intermediate and late

flow periods may be identified for constant-pressure tests. If transient flow transfer is assumed between the fracture system and the matrix, an initial decline in the flow rate will occur. During late times the system behaves as an equivalent homogeneous formation in analogy with constant-rate-of-flow tests.

The analysis of constant-pressure tests in dual-porosity formations is analogous to constant flow rate tests. This means that the test may be analysed in a semi-log graph by plotting the reciprocal flow rate, $1/Q(t)$, versus the test time, t , as described for homogeneous reservoirs in Section 4.2.2. The hydraulic conductivity may be determined from either the early - or the late semi-log straight line using Eqn. (4-23). As for constant-rate-of-flow tests the skin factor may be estimated from the early straight line using Eqn. (4-24) if S_s is replaced by S_{sf} . Alternatively, the skin factor may also be determined from the late straight line from the same equation if the sum $S_{sm} + S_{sf}$ is known or can be estimated.

7. BOREHOLES INTERSECTED BY DISCRETE FRACTURES

7.1 General

When the region near the borehole is dominated by a discrete fracture plane which intersects along the whole or part of the borehole, the early transient flow behaviour is modified compared to a homogeneous medium. This situation is particularly accentuated when a borehole in a low-permeability formation is stimulated by hydraulic fracturing. In crystalline rock, a linear flow type behaviour is sometimes also observed during early times of hydraulic tests, indicating flow to the section tested in naturally discrete fractures near the borehole.

A linear flow type response may also be caused by channeling effects in irregular flow paths in the rock. Such flow paths may have a very large hydraulic conductivity and play an important role from a contaminant migration point of view (Rasmuson and Neretnieks 1986).

7.2 Conceptual models

An analytical model for flow in fracture-dominated reservoirs has recently been presented by Karasaki et al (1985). This model is based on a composite system with two concentric regions. The inner region contains a vertical (or parallel) fracture of finite length which intersects the borehole (section) tested. Water enters this fracture primarily from intersections with other fractures. The water then flows linearly into (or out of) the borehole (see Fig. 7.2.1). The outer region is considered as a porous medium in which only radial flow takes place. Thus, the conceptual model of this system consists of an inner zone with linear flow and certain hydraulic properties and an outer zone with radial flow and separate hydraulic properties (see Fig. 7.2.2). No borehole storage or skin effects are considered in this model. Under favourable conditions the hydraulic parameters for each region may be estimated from type-curve matching using this model.

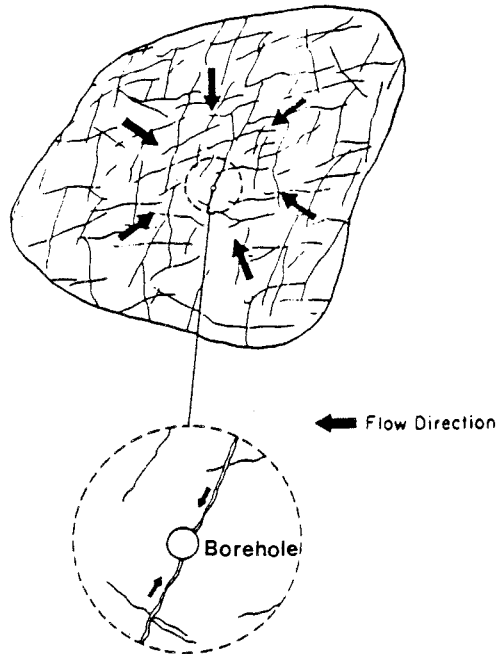


Figure 7.2.1 Flow to a borehole intersected by a discrete fracture. After Karasaki et al (1985).

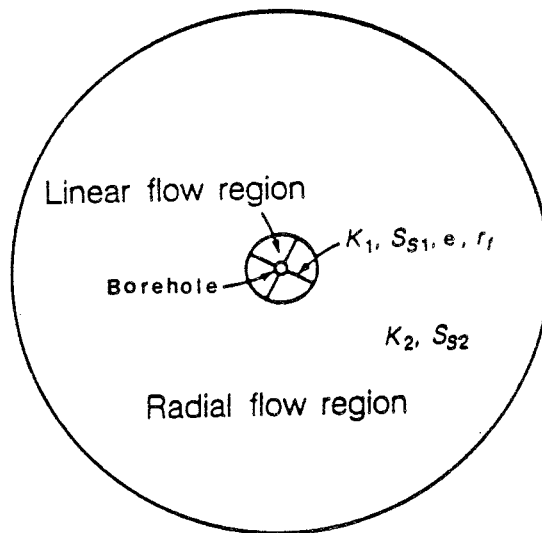


Figure 7.2.2 Composite model of linear-radial flow. After Karasaki et al (1985).

A model for the pressure behaviour of boreholes intersected by a single (vertical) fracture plane of limited horizontal extent was developed by Cinco-Ley et al (1978) and Cinco-Ley and Samaniego (1981) (see Fig. 7.2.3). It is assumed that water from the surrounding formation flows horizontally and perpendicular towards the fracture plane which then acts as a flow channel to the borehole. Both the fracture and the formation are treated as porous media regions. The model suggested by Karasaki et al (1985) is a modification of this latter model. Only high-conductivity fractures are considered.

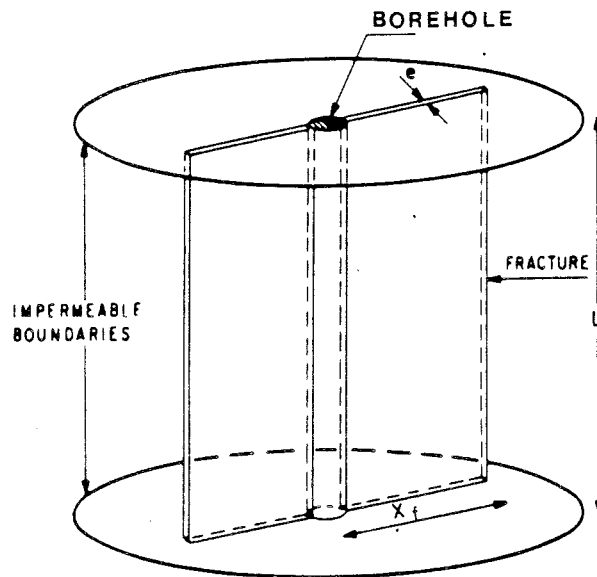


Figure 7.2.3 Borehole intersected by a vertical fracture with finite conductivity. The groundwater reservoir has impermeable upper and lower boundaries and the horizontal extent is infinite. After Cinco-Ley et al (1978).

7.3 Theory and interpretation

7.3.1 Drawdown and injection tests

Constant-rate-of-flow tests

Cinco-Ley et al (1978) defined a number of dimensionless parameters. The dimensionless pressure is defined according to Eqn. (4-3), in Section 4.2.1. The dimensionless time, t_{Df} , generally defined by Eqn. (4-4), is in this case based on the fracture half-length, x_f :

$$t_{Df} = \frac{K t}{S_s x_f^2} \quad (7-1)$$

The dimensionless fracture conductivity, F_{cD} , is defined:

$$F_{cD} = \frac{K_f e}{K x_f} \quad (7-2)$$

In Eqn. (7-2), K_f and K denote the hydraulic conductivity of the fracture and formation respectively and e is the fracture width (aperture).

Figs. 7.3.1 and 7.3.2 show the pressure change during a constant-rate-of-flow test in an active borehole intersected by a single vertical fracture in semi-log and log-log representation respectively. As the parameter F_{cD} increases, the curves approach the infinite-conductivity solution by Gringarten et al (1974). This solution is also included in the graphs. As can be seen from Fig. 7.3.2 the curves form straight lines with a slope of 0.25 for short times in the log-log graph. For large values of F_{cD} the curves approach a straight line with a slope of 0.5 (infinite-conductivity fractures). For long times the curves form straight lines in the semi-log graph.

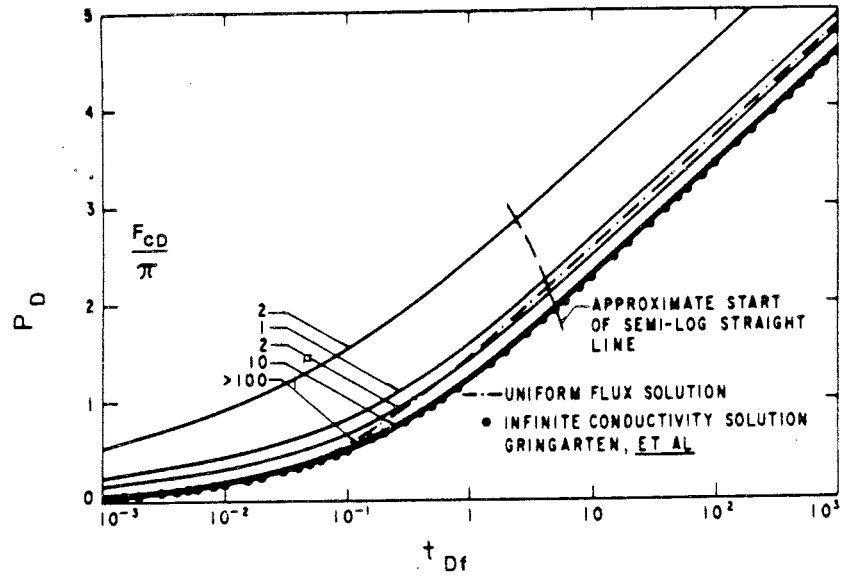


Figure 7.3.1 Type-curves with dimensionless pressure as a function of dimensionless time in a semi-log plot for an active borehole intersected by a vertical fracture. After Cinco-Ley et al (1978).

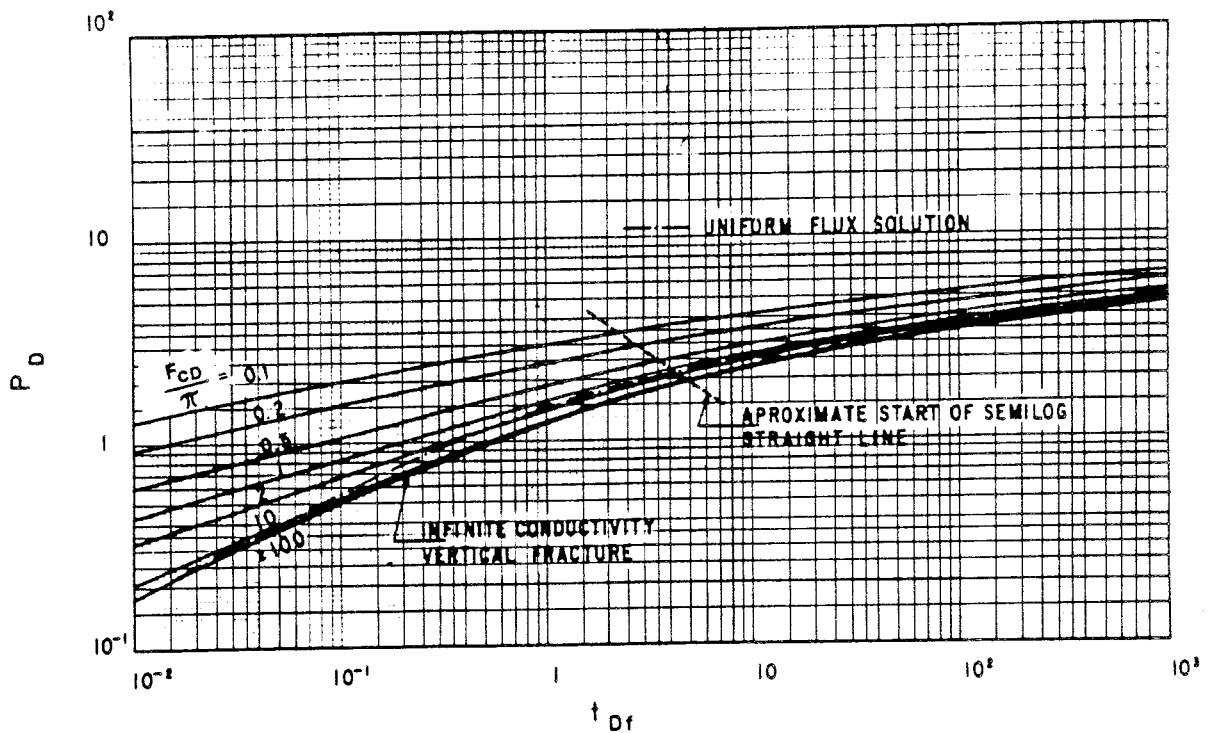


Figure 7.3.2 The same type-curves as in Fig. 7.3.1 in log-log representation. After Cinco-Ley et al (1978).

Generally, the transient pressure response for boreholes intersected by a single vertical fracture plane can be divided into four different flow periods (see Fig. 7.3.3). During very early times, there is a pressure response within the fracture, resulting in a flow which is essentially linear (see Fig. 7.3.3a). This linear fracture flow period is characterized by a straight line with a slope of 0.5 in a log-log graph. However, this flow period occurs too early to be of practical use in the test analysis.

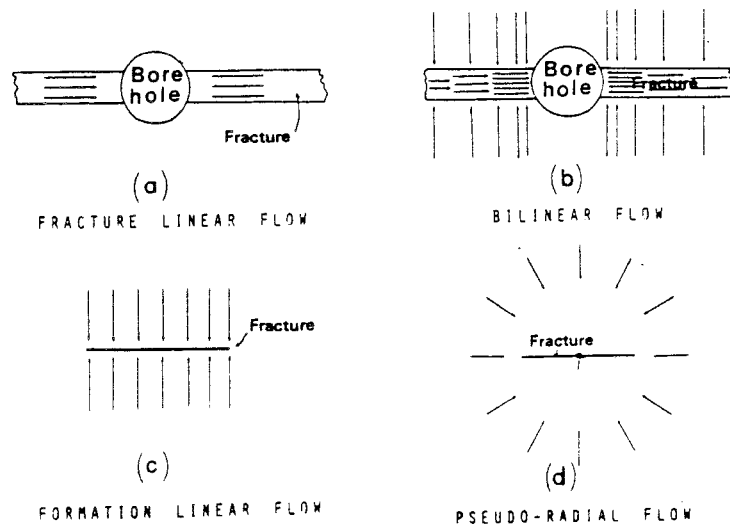


Figure 7.3.3 Flow regimes for an active borehole intersected by a vertical fracture with finite conductivity. After Cinco-Ley and Samaniego (1981).

After a transition flow period, the bilinear flow period may develop (Fig. 7.3.3b). During this period, two flows occur simultaneously. One flow is linear, incompressible flow within the fracture and the other is a linear compressible flow in the formation. This flow period is characterized by a straight line with a slope of 0.25 in a log-log graph (see Fig. 7.3.2). The duration of the bilinear flow period depends primarily on the value of F_{CD} . The bilinear flow period is not operative when the fracture has a high storage capacity (high ratio of fracture porosity to matrix porosity) and its conductivity is high.

For a low-conductivity fracture, the bilinear flow period is followed by a transition period towards the pseudo-radial flow period. High-conductivity fractures ($F_{cD} > 300$) also exhibit a linear-formation-flow period after a transition period (see Fig. 7.3.3c). The formation linear flow period is dominated by linear flow in the matrix towards the fracture. This flow period is characterized by a straight line of slope 0.5 in a log-log graph (see Fig. 7.3.2). After a transition period the pseudo-radial flow period starts. This period is characterized by a straight line of slope 1.15 in a semi-log graph (see Fig. 7.3.1). This is the theoretical slope for radial flow in a homogeneous formation (see Section 4.2.1).

The pressure response during the bilinear flow period may be expressed (Cinco-Ley and Samaniego 1981) as:

$$p_D = \frac{2.45}{\sqrt{F_{cD}}} t_{Df}^{1/4} \quad (7-3)$$

This equation indicates that a linear graph of p_D versus $\sqrt[4]{t_{Df}}$ produces a straight line of slope $2.45\sqrt{F_{cD}}$ intercepting the origin.

During the formation linear flow period, which only appears for high-conductivity fractures, the dimensionless pressure change at the borehole may be approximated (Raghavan 1976) as:

$$p_D = \sqrt{\pi t_{Df}} \quad (7-4)$$

This equation indicates that a linear graph of p_D versus $\sqrt{t_{Df}}$ produces a straight line of slope $\sqrt{\pi}$ intercepting the origin. Eqn. (7-4) is a special case of the short time solution in the model by Karasaki et al (1985) (see Section 7.2).

During the pseudo-radial flow period the dimensionless pressure change using the logarithmic approximation may be expressed (Barker and Ramey 1978) as:

$$p_D = 1.151 (\log t_{Df} + 0.351) + 2.30 \log \frac{x_f}{r_w} + \zeta_f \quad (7-5)$$

Eqn. (7-5) indicates that p_D versus $\log t$ should yield a straight line in a semi-log graph. In this equation ζ_f denotes the fracture pseudo-skin factor, which represents the reduction in the pressure change at the borehole due to the fracture. This pseudo-skin factor should be negative. During the pseudo-radial flow period, a fractured borehole behaves like an unfractured borehole with an increased effective radius (Cinco-Ley and Samaniego 1981).

The test interpretation may be made by combined analysis in the log-log, semi-log and linear graphs. In the log-log graph the head change H is plotted versus time, t . The analysis is performed by matching to the type curves shown in Fig. 7.3.2. The hydraulic conductivity of the formation is calculated from Eqn. (4-12) and the fracture half-length from Eqn. (7-1). The fracture conductivity, K_{fe} , is then calculated from Eqn. (7-2).

During the pseudo-radial flow period a conventional analysis may be made on a semi-log graph with H versus $\log t$, as described in Section 4.2.1. The hydraulic conductivity of the formation is determined using Eqn. (4-8) and the (total) skin factor using Eqn. (4-9).

During the bilinear flow period the change in head, H , is plotted versus $t^{1/4}$ in a linear graph. The slope, m , of the straight line intercepting the origin is then determined. Effects of skin damage (e.g. clogging) and borehole storage may cause the straight line to deviate from the origin (Cinco-Ley and Samaniego 1981). The fracture conductivity, K_{fe} , is calculated from Eqn. (7-3):

$$(K_{fe})^{0.5} = \frac{2.45 Q}{2\pi m L (KS_s)^{1/4}} \quad (7-6)$$

The value of K_{fe} obtained can then be used as a control in the type-curve matching procedure in the log-log graph.

Constant-pressure tests

The theoretical flow rate behaviour was investigated for the case of a constant pressure being maintained in a borehole intersected by a vertical fracture by Agarwal et al (1979) and Guppy et al (1981). The same basic model and assumptions were used as in the constant flow rate case investigated by Cinco-Ley et al (1978). The dimensionless reciprocal flow rate at the borehole, defined by Eqn. (4-20), may be expressed as a function of dimensionless time and dimensionless fracture conductivity. These parameters are defined as earlier by Eqns. (7-1) and (7-2) respectively.

The logarithmic type curves for short times for the constant-pressure case exhibit an early straight line with a slope of 0.25, indicating bilinear flow, as in the constant-rate-of-flow case. These type curves are similar in shape to the constant-rate-of-flow type curves shown in Fig. 7.3.2. The same flow periods as described for the constant-rate-of-flow case, i.e. the fracture linear, bilinear, formation linear and pseudo-radial flow periods, may also be identified for the constant-pressure case.

The approximate short-time solution for the constant-pressure case may be expressed (Guppy et al 1981) as:

$$1/Q_D = \frac{2.72}{\sqrt{F_{cD}}} t_{Df}^{1/4} \quad (7-7)$$

Eqn. (7-7) represents the bilinear flow period for a low or medium-conductivity fracture. This equation indicates that a linear graph of $1/Q$ versus $t^{1/4}$ should yield a straight line passing through the origin if no skin damage has occurred. The fracture conductivity, K_{fe} , may be determined

from the slope of the straight line, which is proportional to $2.72/\sqrt{F_{CD}}$. The approximate solution for high-conductivity fractures ($F_{CD} > 300$), representing the formation-linear flow period, may be expressed (Guppy et al 1981) as:

$$1/Q_D = \frac{\pi^{3/2}}{2} t_{Df}^{1/2} \quad (7-8)$$

Eqn. (7-8) indicates that a linear plot of $1/Q$ versus $t^{1/2}$ will yield a straight line through the origin. As can be seen from Eqns. (7-7) and (7-8), a log-log plot of $1/Q$ versus t will have an early slope of 0.25 during the bilinear flow period and 0.5 during the formation-linear flow period as in the constant-rate-of-flow case.

The interpretation of constant-pressure tests is analogous to that of constant-rate-of-flow tests, i.e. a combined of analysis in log-log, semi-log and linear graphs. The reciprocal flow-rate $1/Q$, plotted versus time, t , can be matched to the type curves for the constant-pressure case. The hydraulic conductivity of the formation is calculated from Eqn. (4-21).

During the pseudo-radial flow period the hydraulic conductivity of the formation is calculated from semi-log analysis using Eqn. (4-23) and the (total) skin factor from Eqn. (4-24). During the bilinear flow-period the reciprocal flow rate is plotted versus $t^{1/4}$ in a linear graph. The fracture conductivity, K_{fe} , is calculated from Eqn. (7-7):

$$(K_{fe})^{0.5} = \frac{2.72}{2\pi m L H_o (K S_s)^{1/4}} \quad (7-9)$$

As in the constant-rate-of-flow case effects of skin damage may distort the bilinear flow analysis.

7.3.2 Build-up (Fall-off) tests

The build-up or fall-off behaviour is strongly influenced by the preceding production or injection time. To account for this, the equivalent time method proposed by Agarwal (1980) may be used (see Section 5.2). The applicability of this method to boreholes intersected by a single vertical fracture was investigated by Rosato et al (1982). The equivalent time is defined by Eqn. (5-8). The dimensionless form of this equation can for (vertically) fractured boreholes be expressed in analogy with Eqn. (4-4) as

$$dt_{eD} = \frac{dt_{Df} \times t_{pD}}{t_{pD} + dt_{Df}} = \frac{K}{S_s \times f^2} \left(\frac{dt \times t_p}{t_p + dt} \right) \quad (7-10)$$

In this equation, t_p denotes the production (or injection) time and dt is the ^p recovery time.

Tests after a constant-rate-of-flow period

Rosato et al (1982) found that the build-up (or fall-off) curve will follow the constant-rate-of-flow drawdown solution both at early and late times when data are plotted on the equivalent-time scale. This observation applies equally well to the linear, bilinear and pseudo-radial flow periods. This means that the same analysis as described for constant-rate-of-flow tests may be applied for build-up and fall-off tests provided the changes in head are plotted versus the equivalent time. At intermediate recovery times, the agreement between the build-up curve and fall-off curve is not perfect, particularly for high-conductivity fractures. This is due to the fact that the equivalent-time method assumes that the semi-log approximation of P_D in Eqn. (4-6) for radial flow is valid. The response of a low-conductivity fracture should be better approximated by radial flow solutions than a high-conductivity fracture (Rosato et al 1982).

Tests after a constant-pressure period

The build-up or fall-off curves after production (or injection) at constant pressure may also be analysed using the constant-rate-of-flow drawdown solution when the equivalent-time method is used. To do this, a pseudo-production time, t_{pp} , must be used to calculate dt_e instead of the actual production time. According to Rosato et al (1982) the pseudo-production time may be determined as follows:

$$t_{pp} = \frac{V_{tot}}{Q_p} \quad (7-11)$$

In this equation, V_{tot} is the cumulative fluid volume produced or injected and Q_p is the flow rate at the end of the test. It follows that the pseudo-production time is always greater than the actual production time, t_p , since the flow rate declines during a constant-pressure test. To conclude, the constant-rate-of-flow drawdown curves may be used to analyse buildup-data from the linear, bilinear and pseudo-radial flow periods, both for constant-rate-of-flow and constant-pressure tests, with the equivalent-time method. The test interpretation is performed using the equations presented in Section 7.3.1.

8. PULSE RESPONSE TESTS

8.1 General

In pulse response tests, the decay of an instantaneous (pressure) pulse applied to a borehole (section) is monitored as a function of time. Depending on the test conditions, these tests may be divided into slug tests, pressure pulse tests and drill stem tests. The pressure variations during different pulse response tests are shown in Fig. 8.1.1. The aim of such tests is mainly to determine the hydraulic properties of relatively lowconductive to virtually impermeable formations. In general, the main advantage of pulse response tests is the relatively short test time required. But a consequence, the radius of investigation during the tests is limited.

Pulse response tests may thus be an alternative to water injection tests and pumping tests in tight formations (Forster and Gale 1982). With the pressure pulse test it is also possible to get information about the extent of minor fissures intersecting the borehole section (Wang et al, 1977). Drill stem tests permit determination of the hydraulic conductivity and skin factor as well as the natural static pressure in different test sections of the borehole provided the permeability is not too low.

8.2 Slug tests

A slug test is performed under open borehole conditions, i.e. the section being tested is exposed to atmospheric pressure and the change in water level in a standpipe is monitored over a period. The response curves are interpreted according to the theory of transient, radial flow in a porous medium.

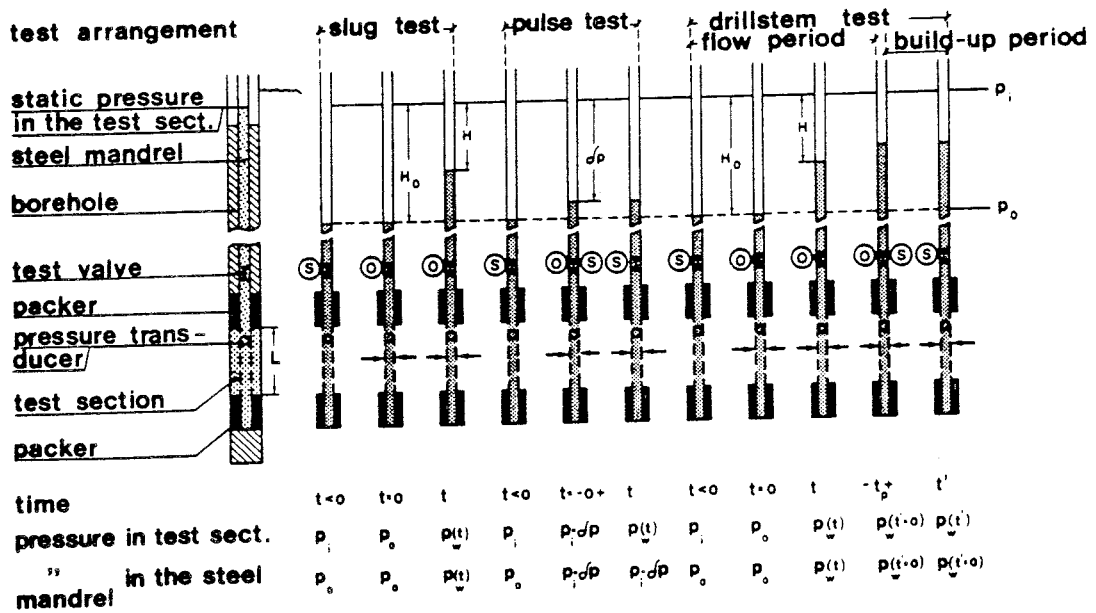


Figure 8.1.1 Pressure conditions and test conditions in various response tests.

To derive the theory for interpretation of slug tests, the diffusivity equation, Eqn. (4-1) is normally used with appropriate boundary conditions. An interpretation technique for slug tests was presented by Cooper et al (1967) which was later extended by Papadopoulos et al (1973). In this theory, the skin effect in the borehole section was not taken into account.

The flow boundary condition for slug tests may be expressed (Cooper et al 1967) as follows:

$$2 \pi r_w KL \frac{\partial h(r_w, t)}{\partial r} = \pi r_c^2 \frac{\partial H(t)}{\partial t} \quad (8-1)$$

Eqn. (8-1) states that the flow to or from the formation equals the change of volume of water per unit time in the borehole section (according to Darcy's Law). In Eqn. (8-1), r_w and r_c denote the (nominal) radius of the borehole and the inside radius of the standpipe respectively.

Ramey et al (1975) presented a method for interpreting slug tests which also took the skin effect into account. The skin was regarded as being concentrated to an infinitesimally thin skin-zone at the borehole walls (see Section 3.2). The theoretical head decline, H , during a slug test, expressed as a fraction of the total head change, H_0 , (Ramey et al 1975) takes the following form:

$$H/H_0 = F(\zeta, 1/C_D, t_D) \quad (8-2)$$

In Eqn. (8-2), F is a function of the skin factor, dimensionless borehole storage coefficient C_D and dimensionless time t_D . Ramey et al (1975) showed that the solution may be represented graphically in a single graph with H/H_0 versus t_D/C_D , with the expression $C_D e^{2\zeta}$ as a parameter. The solution may thus be plotted as a set of type curves in a log-log or semi-log graph. Fig. 8.2.1 shows slug test type curves in a semi-log graph.

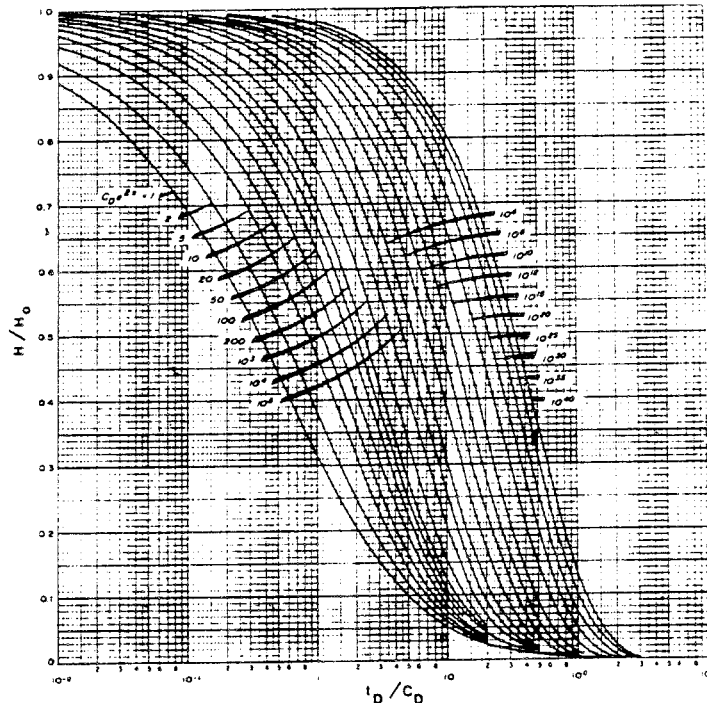


Figure 8.2.1 Type-curves in a semi-log graph for analysing slug test data. After Earlougher (1977).

The normalized head change H/H_0 is plotted versus the test time, t , in a semi-and/or log-log graph. Also $(1-H/H_0)$ may be plotted as a function of time in a log-log graph. These data curves are then matched to respective type curves in the usual manner. The hydraulic conductivity may in all cases be calculated using the following expression in metric units in analogy with Ramey et al (1975):

$$K = \frac{C \rho g}{2\pi L t_m} \left(\frac{t_D}{C_D}\right)_m \quad (8-3)$$

In Eqn. (8-3), C is the borehole storage coefficient for an open borehole system and t_m and $(t_D/C_D)_m$ are the time value on the data curve and type curve respectively. Since for an open borehole system $C = \pi r_c^2 / \rho g$ (according to Eqn. (3-5)), Eqn. (8-3) may be expressed as:

$$K = \frac{r_c^2}{2 L t_m} \left(\frac{t_D}{C_D}\right)_m \quad (8-4)$$

The skin factor is determined from the parameter value $(C_D e^{2s})_m$ according to Eqn. (4-17).

The effect on slug tests of a skin-zone with a finite radius around the borehole and a hydraulic conductivity that is different from that of the formation has been investigated by Faust and Mercer (1984). They found that when the hydraulic conductivity of the skin-zone is lower than that of the formation (positive skin effect), the estimates of hydraulic conductivity from slug tests may be more representative of the skin-zone itself than of the formation, particularly if the transmissivity of the skin-zone is much lower than that of the formation.

On the other hand, when the hydraulic conductivity is higher in the skin-zone (negative skin effect), the effect of the skinzone should not significantly affect evaluation of the hydraulic conductivity of the formation. Moench and Hsieh

(1985) found that the method of Ramey et al (1975) may be used for interpreting (open-borehole) slug tests in most cases.

8.3 Pressure pulse tests

Pressure pulse tests are normally used in very low-permeability formations. In this kind of test the section being tested has no contact with atmospheric pressure during the test. Instead, the pressure pulse decay is monitored as a function of time in a confined test section. Thus, in this case the confined borehole storage coefficient dominates the pulse decay. Since this coefficient is several orders of magnitude less than the borehole storage coefficient under open borehole conditions, the test times required for pressure pulse tests are usually much shorter than for slug tests.

The boundary flow condition in Eqn. (8-1) for slug tests corresponds (Bredehoeft and Papadopoulos 1980) to the following condition for pressure pulse tests :

$$2\pi r_w K L \frac{\partial h(r_w, t)}{\partial t} = V_w c_w \rho g \frac{\partial H(t)}{\partial t} \quad (8-5)$$

Eqn. (8-5) states that (for a test on a section subject to over-pressure) the flow rate from the borehole into the formation equals the expansion of the volume of water contained in the test section per unit time during the pulse decay. It is assumed that no changes in the volume of the test equipment take place.

The principal difference between slug tests and pressure pulse tests may be seen by comparing Eqns. (8-1) and (8-5). The right-hand sides of these two equations describe the change in the volume of water per unit time. This change in volume may be expressed using the general definition of the borehole storage coefficient in Eqn. (3-4):

$$\Delta V = C \Delta p = C \rho g H \quad (8-6)$$

In Eqn. (8-6), ΔV is the change in the volume of water in the section being tested. Δp and ΔH is the change in pressure and head respectively. From Eqn. (8-6) the change in volume per unit time may be expressed in differential form as:

$$\frac{\partial V}{\partial t} = C \rho g \frac{\partial H(t)}{\partial t} \quad (8-7)$$

By inserting the expressions for open and confined borehole conditions into Eqn. (8-7), the right-hand sides of Eqns. (2-1) and (8-5) respectively are obtained. All other boundary conditions are identical for slug tests and pressure pulse tests. This implies that the theory and interpretation are equivalent for slug tests and pressure pulse tests.

Bredehoeft and Papadopoulos (1980) derived a method for interpreting pressure pulse tests analogous to the theory for slug tests by Cooper et al (1967). Skin effects were not considered. Neuzil (1982) pointed out the importance of an approximate equilibrium pressure in the section being tested before the test to eliminate natural pressure trends during the pressure pulse test. He also recommended the use of an effective compressibility in the calculations, rather than the water compressibility, to account for compliance effects of the test equipment during pressure pulse tests (see Section 2.3.5).

The solution by Ramey et al (1975) in Eqn. (8-2) may thus also be used for interpreting pressure pulse tests provided the confined borehole storage coefficient is used in the calculations. This solution considers an infinitesimally thin skin-zone. The same interpretation techniques are used for pressure pulse tests as for slug tests, as described in the previous section. The hydraulic conductivity is calculated using Eqn. (8-3). Using an effective compressibility, c_{eff} instead of c_w , and C , calculated from Eqn. (8-3), may be approximated by the following expression:

$$K = \frac{r_w^2 c_{eff} \rho g}{2 t_m} \left(\frac{t_D}{C} \right)_m \quad (8-8)$$

However, Moench and Hsieh (1985) pointed out that the pressure pulse test may only yield information on the hydraulic properties of the skin-zone since only a small quantity of water needs to leave (or enter) the test section for the hydraulic head to change in the section. This amount of water may be dissipated in the skin-zone itself and thus the test data will represent only the skin-zone.

As pointed out by Bredehoeft and Papadopoulos (1980) the time required for a complete pulse decay to the original pressure in the test interval is generally very long both for pressure pulse tests and slug tests. Usually the first 50 % of the pulse decay ($H/H_0 = 0.5$) or maximum 80 % ($H/H_0 = 0.2$) is sufficient to analyse both types of test. The real test time required for an actual test depends on the hydraulic properties of the section being tested.

A special theory for pressure pulse tests in a confined section of a tight formation with minor, horizontal fractures has been developed by Wang et al (1977). With this theory, the fracture aperture and hydraulic conductivity of a single, horizontal fracture can be determined. If long-term data are available, the fracture geometry can also be investigated using this method. It is assumed that the aperture and hydraulic conductivity of the fracture are constant and independent of pressure. No skin effects are considered.

The theory is based on the diffusivity equation, Eqn. (4-1), for transient, radial flow in a discrete fracture. The hydraulic properties of the fracture are based on intrinsic fracture properties. The hydraulic conductivity, K_e , in a discrete fracture is represented by the parallel-plate-model for laminar flow in a smooth fracture according to Eqn. (2-3).

The solution of Eqn. (4-1) for a fracture of infinite extent is identical to the one obtained for slug tests and for pressure pulse tests. Wang et al (1977) presented solutions for a fracture with both infinite and finite extents. For the interpreting of pressure pulse tests a linear relationship can be constructed between the aperture and the time for a certain

pulse decay. Using this relationship the fracture aperture can be estimated from the actual pulse decay time. The hydraulic conductivity of the fracture is then calculated from Eqn. (2-3). This value can then be transformed into an equivalent rock mass hydraulic conductivity for the section being tested (see Section 10.7.1).

8.4 Drill stem tests (DST)

A drill stem test is generally performed with two flow periods with two intervening recovery periods (see Fig. 8.4.1). During the flow periods the change in the water level in a standpipe is monitored as in a slug test. During the recovery periods the pressure change is monitored under confined borehole conditions.

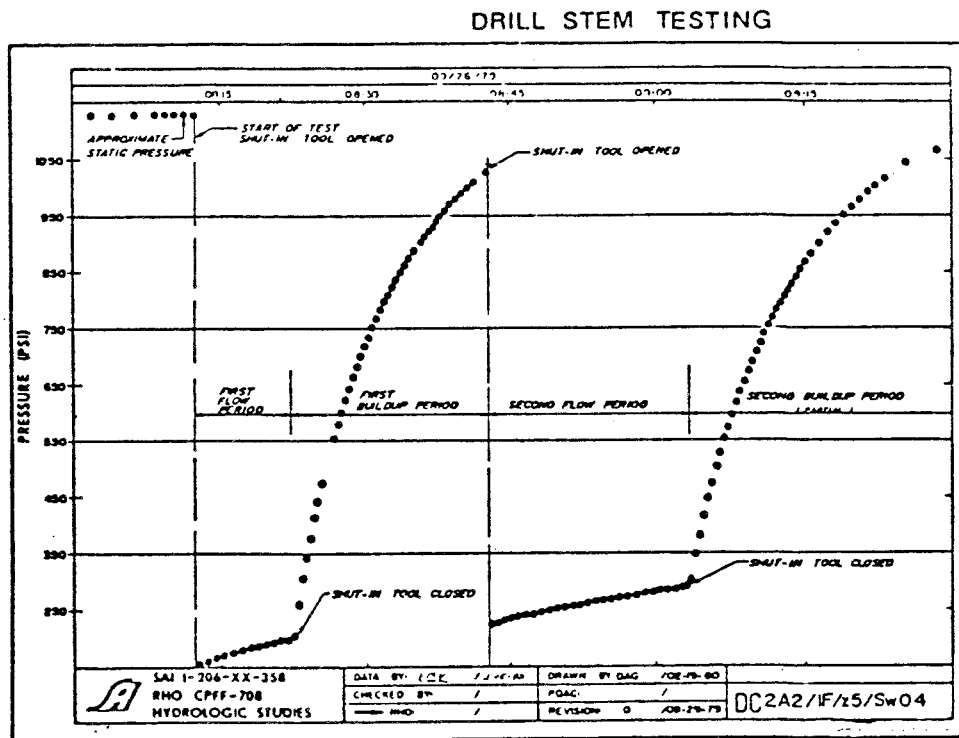


Figure 8.4.1 Pressure behaviour during drill stem testing. After Updegraff et al (1980).

The interpretation of the flow periods during a DST is identical to the interpretation of the slug tests described in Section 8.2. The hydraulic conductivity is estimated from Eqn. (8-4) and the skin factor from Eqn. (4-17). If the water level rises above the top of the standpipe during the flow period of a DST, the test data from these periods cannot be evaluated using the slug test theory presented.

During the recovery periods of a DST, the residual pressure change may be expressed by the Horner Eqn. (5-2). The flow rate during a DST is normally defined as the average flow rate during the previous flow period by dividing the cumulative volume of water produced in the standpipe by the duration of the flow period. The duration of the previous flow period is generally used as t_p in Eqn. (5-2). Although it is possible to calculate the actual flow rate at a certain time during the flow periods from the pressure change, the flow rate is generally considered as being constant during the flow periods in analysis of the build-up periods in a DST.

The data from the recovery periods are generally plotted in a Horner graph (see Section 5.2.1). The first recovery period is usually short so the most reliable interpretation is obtained from the second recovery period. The hydraulic conductivity is calculated from the slope of the straight line in the Horner graph from Eqn. (4-8). If borehole storage affects the recovery data, the time criterion in Eqn. (5-4) must be satisfied. The skin factor for the recovery period is determined in analogy with Eqn. (4-9) according to Earlougher (1977):

$$\zeta = 1.151 \left[\frac{(p_{1 \text{ min}} - p_p)/\rho g}{\Delta H} + \log \left(\frac{t_p + 60}{60} \right) - \log \left(\frac{K}{r_w^2 S_s} \right) - 2.13 \right] \quad (8-9)$$

In Eqn. (8-9), t_p is expressed in minutes and $p_{1 \text{ min}}$ is the extrapolated pressure at $dt = 1$ minute. The second term may be neglected if t_p is much longer than 60 minutes. The recovery period(s) during a DST may also be analysed using the equivalent-time method (see Section 5.2.1) as a multiple rate test.

The Horner graph may also be used to estimate the natural static pressure or head in the section being tested by extrapolating the straight line (see Section 5.2.1). The static head determined should be approximately the same for both the first and second recovery periods. The radius of influence during a DST can for practical purposes be estimated from Eqn. (4-11).

9. TESTS PERFORMED

9.1 General

The project test programme involved performance of the following methods of hydraulic testing: transient injection tests at constant pressure or constant rate of flow, pressure fall-off tests after transient injection tests, water loss measurements, slug tests, pressure pulse tests and drill stem tests. The work was carried out during the spring of 1981. All tests were performed in two different intervals of borehole Fi 6 of the Finnsjön field research area (see Table 9.1). The aim of the tests was to study the applicability of the various methods in crystalline bedrock. The results of measurements made using the various methods were compared, and equipment and measurement procedures tested and adjusted. The experience gained from the tests was the basis for selection of a standard hydraulic testing method being used in study site investigations since 1981.

Table 9.1 Tests performed and sections used in borehole Fi 6 at Finnsjön test site.

Borehole section (m)	TRANSIENT TESTS				water-loss tests	slug-tests	pressure pulse tests	drill-stem tests
	const. flow-rate injection	flow-rate fall-off	const. pressure injection	pressure fall-off				
61-64					X			
64-67					X			
67-70	X	X	X		X	X	X	X
70-73	X	X			X			
73-76					X			
76-79	X		X		X		X	
79-82	X	X	X	X	X	X	X	X
82-85					X			
85-88	X				X			
88-91					X			
91-94					X			
163-166					X			
166-169	X		X		X		X	
169-172					X			
172-175			X	X	X			
175-178					X			
178-181	X		X		X	X	X	X
181-184	X		X	X	X	X	X	X
184-187					X			
187-190					X			
190-193	X		X	X	X	X	X	X
193-196					X	X	X	X
196-199					X			

9.2 Description of the test site

9.2.1 Finnsjön field research area

The Finnsjön field research area is situated to the east of Finnsjön lake in northern Uppland (140 km north of Stockholm) and consists of a runoff area covering approximately 25 km² (see Fig. 9.2.1). The average annual precipitation is about 670 mm and the evaporation has been estimated at approximately 475 mm. The topography is relatively flat, with levels ranging between 20 and 44 metres above sea level. The soil cover, of which glacial deposits (till) constitute the main part, are mostly shallow. About 20% of the area consists of exposed rock. The bedrock consists of granite and granodiorite in the central part of the area. Leptite is found in the northern and southern parts of the area, and greenstones were also found in the northern part.

The geology, hydrology and groundwater conditions of the field research area have been described by several authors, including Almén et al (1979) and Olkiewicz et al (1979). Since 1984 extensive investigations of a fracture zone is going on in the Finnsjön area (Ahlbom et al 1986).

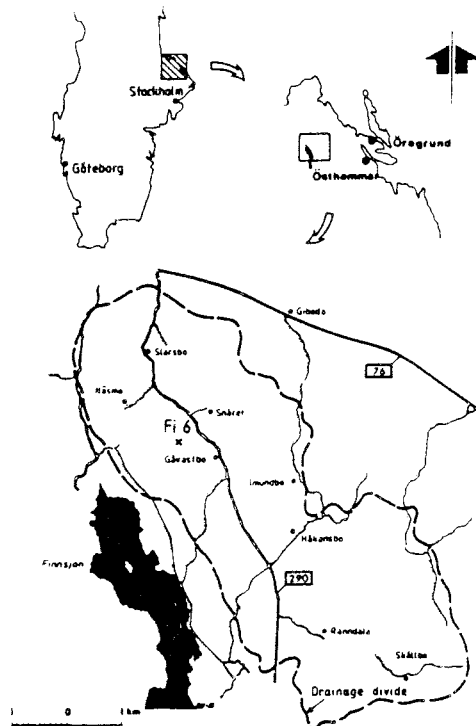


Figure 9.2.1 Map showing the location of borehole Fi 6 at the Finnsjön test site.

9.2.2 Borehole Fi 6

Borehole Fi 6 is 691 m deep and was drilled vertically from an elevated plateau in the western part of the Finnsjön area. The plateau consists of a relatively well exposed area of bedrock which is composed mainly of granodiorite. The main type of rock found in the borehole changes between a grey and a red, medium-grained to fine medium-grained schistosed granodiorite (Olkiewicz et al, 1979).

Horizons with a red medium-grained, unstratified granite occur below a depth of 330 m. Pegmatite dykes between 2 and 10 cm wide are widespread. A few metabasite horizons were also encountered. Fractures and fracture zones are relatively evenly distributed in the borehole. An average of 2.48 fractures/metre has been estimated from core logs.

Hydraulic tests have earlier been carried out in the borehole between depths 61 m and 679 m. These were performed as water loss measurements with a section length of 3 m and a number of single packer measurements. The test results indicate that the hydraulic conductivity is relatively evenly distributed between 2×10^{-10} m/s and 1×10^{-6} m/s down to a depth of 400 m, with the exception of five sections in which values of around 1×10^{-5} m/s were measured. Sections below a depth of 400 m were dominated by hydraulic conductivities of between 1×10^{-7} m/s and 1×10^{-9} m/s. On the basis of these results presented by Carlsson et al (1980), borehole sections 64-88 and 166-196 were selected for investigation of the methods presented in this report. The core logs for the uppermost 200 metres are appended to this report as Appendix 1.

The elevated plateau should constitute a local in-flow area, with only a limited hydraulic gradient near the borehole. The groundwater level in the hole throughout the duration of the test period was about 3.5 metres below ground level.

9.3 Test equipment

All tests of methods carried out were performed with a basic set of equipment that was modified to meet the special requirements of the various methods. Fig. 9.3.1 shows the equipment used in the transient injection tests. The main parts of the equipment are the measuring probe, injection equipment with flow meter, recording instrument, control equipment and hoisting rig.

It should be mentioned in this context that after the method tests had been completed (1981) with the equipment described below, the instrumentation has been improved and is subject to continual enhancement (Almén et al, 1983 and Almén et al, 1986).

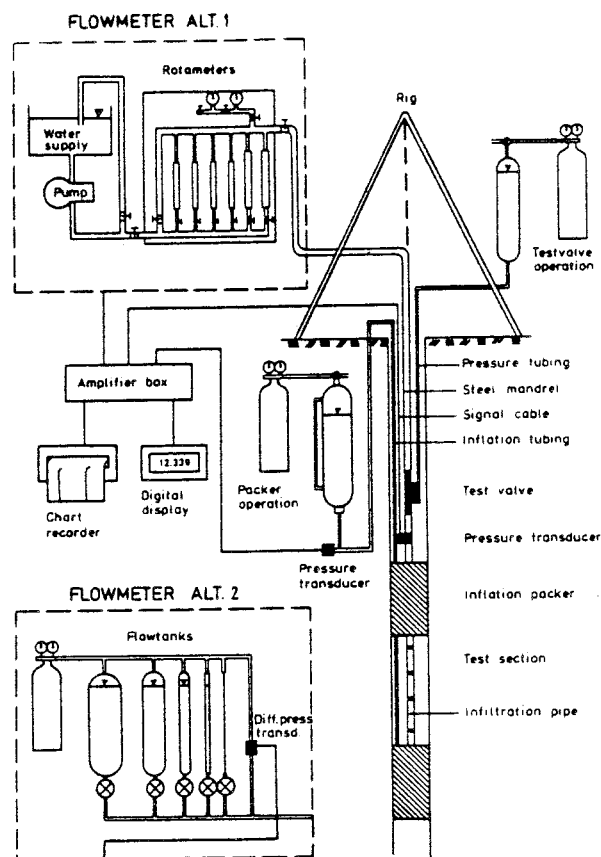


Figure 9.3.1 Configuration of equipment used to investigate different methods of testing.

9.3.1 Measuring probe

The measuring probe consists of a test valve, pressure transducer and two packers separated by an infiltration pipe. The packers, whose construction is shown in Fig. 9.3.2, were developed within the project in a special effort to minimize the elastic properties of the equipment. The 1-m long sealing elements of chloroprene rubber are expanded against the wall the borehole using water pressure and delimit a 3-m long test section from the remainder of the borehole. A hydraulically operated test valve was constructed (see Fig. 9.3.3) to permit accurate pressure measurement in a completely confined test section at the transient start and termination of some tests, e.g. pressure pulse tests.

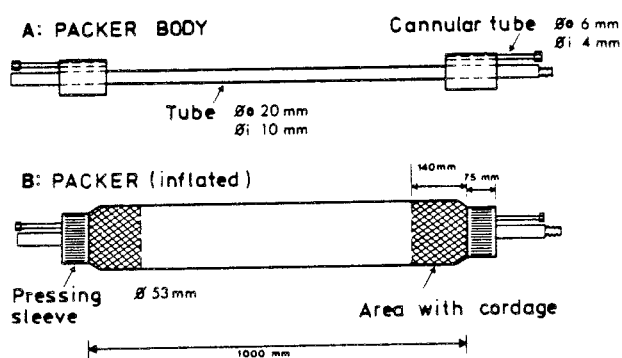
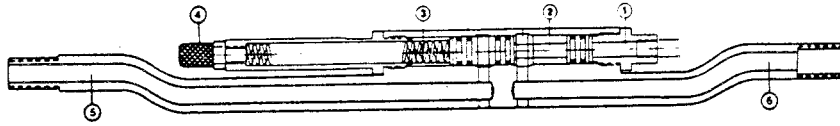


Figure 9.3.2 Drawing showing the principle of the Ux:53 packer.

The pressure transducer is located immediately above the packers and in hydraulic connection with the test section, which implies that the pressure there is measured, irrespective of whether the test valve is open or closed. The pressure in the section and the sealing pressure in the packers is read off digitally and recorded continually using an analogue chart recorder.

The measuring probe is connected to a string consisting of 2-m long steel pipes of 10 mm i.d. and 20 mm o.d., with 10 rings to seal joints. The packers and test valve are operated hydraulically through steel-reinforced hydraulic hoses.



- | | |
|----------------------------------------|-----------------------------------|
| 1. Connection for pressure supply hose | 4. Filter |
| 2. Slide | 5. Connection to the test section |
| 3. Return spring | 6. Connection to pipe string |

Figure 9.3.3 Hydraulically operated test valve.

9.3.2 Flow meters and injection system

The rate of water flow to the test section was recorded either by using rotameter type flow meters or by measuring the water head in a series of standpipes of known diameter. The rotameter flow meters were used in transient constant-rate-of-flow injection tests and water-loss measurements. The injection rate was adjusted manually using control and needle valves on a flow meter board. Rotameters with ranges that overlapped one another to provide a total range of 8.5×10^{-5} l/min to 65 l/min were used.

The second flow measurement system was used in the constant-pressure injection tests. The flow meter consisted in this case of five connected, closed graduated cylinders with inside diameters 4, 9, 18, 37.5 and 100 mm respectively, control

valves, gas regulators and a differential pressure transducer. With the gas pressure (injection pressure) suitably set, the water was pressed out of one of the graduated cylinders and down through the pipe string into the test section. The flow rate could be calculated from a recording of the differential pressure (head of water) between the upper and lower parts of the graduated cylinder. To permit performance of longer injection tests without stoppages, two parallel sets of cylinders were provided and used alternately. The range that could be measured using this configuration was from about 5×10^{-5} l/min to 1.5 l/min.

For the remaining tests, the equipment was modified as follows: Slug, pressure pulse and drill stem tests were performed without flow meters or pumping equipment. During certain pressure pulse tests, overpressure was generated in the pipe string using a pressure vessel connected to the system.

9.3.3 Performance tests on equipment

Transient hydraulic tests involve recording changes in pressure or flow rate as a function of time. These changes are dependent on the elastic properties of the water, formation and measuring equipment, as well as the water conducting properties of the formation and borehole conditions. In this case, the packers were regarded as being the component with the greatest elasticity. During tests in which the water pressure is kept constant, the equipment will only act elastically (change in the volume of the test section) during the initial stage. But during pulse response and constant-rate-of-flow injection tests and recovery tests, in which the pressure in the section varies, the entire test sequence may be affected by the elasticity of the packers. This will affect evaluation of the tests, particularly in test sections with low hydraulic conductivity.

Against this background, the elastic properties of a number of packers were tested (see Table 9.2). The selection of packer

equipment for the hydraulic tests was decided on the basis of the results. A method for correcting the influence of the elasticity on pulse response tests was also developed.

Table 9.2 Change in volume and effective compressibility on 0.1 MPa change in pressure in a 0.7-m test section in a brass pipe, and in a 3-m measurement section in a borehole. The various components of the change in volume have been separated. The values shown are for the selected type of packer.

		0.7-m test section with packers	0.6-m test section with welded ends	3-m measurement section
Total volume	(m ³)	1.3·10 ⁻³	1.5·10 ⁻³	6.4·10 ⁻³
Compressibility of water	(m ³)	6.0·10 ⁻⁸	6.9·10 ⁻⁸	2.9·10 ⁻⁷
Change in volume of brass pipe	(m ³)	7.4·10 ⁻⁸	7.4·10 ⁻⁸	-
Change in volume of packers	(m ³)	7.3·10 ⁻⁷	-	7.3·10 ⁻⁷
Total change in volume	(m ³)	8.6·10 ⁻⁷	1.4·10 ⁻⁷	1.0·10 ⁻⁶
Effective compressibility	(Pa ⁻¹)	6.6·10 ⁻⁹	9.3·10 ⁻¹⁰	1.6·10 ⁻⁹

9.3.4 Elastic properties of the test equipment

Testing of the elastic properties of the various items of measuring equipment (packers) was performed in a test pipe lowered into water, to simulate conditions in a borehole as well as possible. Changes in volume and pressure in a 0.6 - 0.8 m long test section were recorded in the following tests (Fig. 9.3.4).

In Test 1, the sealing phase of the packer was tested by recording continually the quantity of water displaced. The total time required for sealing was also determined. In Test 2, a 0.4 MPa pressure pulse was applied to the test section. The longer the applied pressure was retained, the better the implied result.

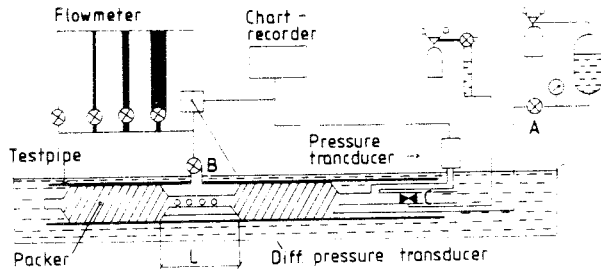
The aim of Test 3 was to determine the elasticity of the packer rubber by pressurizing the test section in stages. The volume of water pumped in and the stabilization of the pressure in the section between each pressure stage were recorded. Test 4 was similar to Test 2, but in this case a thin cannular tube, which corresponded to a transmissivity of about $3 \times 10^{-9} \text{ m}^2/\text{s}$, was connected to the section. The duration of the pressure pulse tests or its deviation from the pressure-curve of the cannular tube provided an indication of the elasticity of the system (principally the packers).

As mentioned earlier, the packer selected was the one that exhibited the least elasticity and shortest time to achieve a seal.

9.3.5 Correction for the elasticity of the equipment

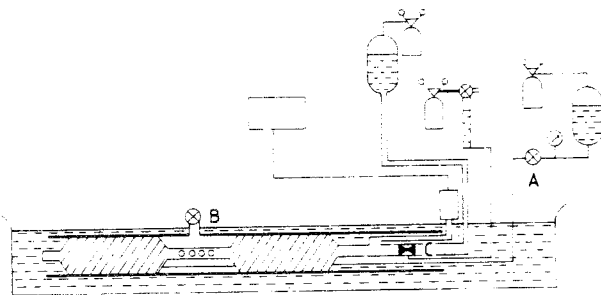
During a pressure pulse test, the water pressure is changed momentarily in a test section, after which the decline in pressure is recorded as a function of time. In theory it is assumed that the test section is incompressible and that all pressure changes are due to the compressibility of the water and the hydraulic conductivity and compressibility of the formation.

The tests on packers, above all Test 4 described in the previous section, however, indicated elastic changes in volume. As a complementary study, therefore, the change in volume of the test pipe was determined in a separate test using fixed end pieces. The relationship between the volume of water pressed in and the pressure in the test section was then analysed with



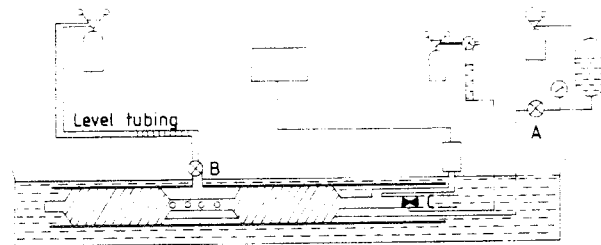
Test 1

- A: Manually operated valve, open
- B: Manually operated valve, open
- C: Hydraulically operated test valve, closed
- l: Length of the test section



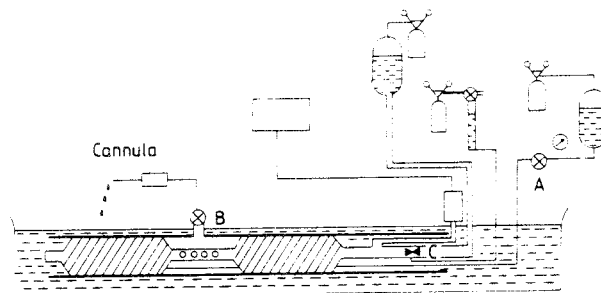
Test 2

- A: Open
- B: Closed
- C: Opened for 3 seconds



Test 3

- A: Open
- B: Alternately open and closed
- C: Closed



Test 4

- A: Open
- B: Closed
- C: Opened for 3 seconds

Figure 9.3.4 Equipment configuration by the packer tests.

respect to the compressibility of the water and the change in volume of the packers and the test pipe, in accordance with the relationship:

$$\Delta V = \Delta p \cdot V \cdot c_w + \Delta V_r + \Delta V_m \quad (9-1)$$

where V = volume of the test section
 ΔV = total change in volume
 ΔV_r = change in volume of the test pipe
 ΔV_m = change in volume of the packers
 Δp = pressure increase that caused the changes
 c_w = compressibility of water

It was thereby possible to calculate the change in volume of the packers, while the effective compressibility, c_{eff} , was determined (see also Table 9.2) in accordance with:

$$c_{eff} = \frac{\Delta V}{\Delta p} \cdot \frac{1}{V} \quad (9-2)$$

For the 3-m test section length used in the field tests described in this report, the effective compressibility used was $1.6 \times 10^{-9} \text{ Pa}^{-1}$. The reliability of this value was checked in the field by calculating c_{eff} from pressure pulse tests through the cannular tube. The tests was conducted in the tight casing of borehole Fi 6 with the cannular tube connected to the pipe between the down-hole valve and the test section. Data from Test 4 was also used. The known transmissivity of the cannular tube, $3 \times 10^{-9} \text{ m}^2/\text{s}$, was used when calculating c_{eff} from the type-curve method (Eqn 8-8) and the Wang method described in section 10.7.1. The results show good agreement with the c_{eff} -value determined from the elasticity tests (Table 9.3). The use of c_{eff} instead of c_w is thus justified for a 3-m long test section. With longer section lengths, the influence of the packers on the c_{eff} -value diminishes in significance, i.e. c_{eff} approaches c_w .

Table 9.3 Effective compressibility of test sections determined from pressure pulse tests through a cannular tube.

Test	Compressibility, c_w		Compressibility, c_{eff}	
	Type-curve method (Pa ⁻¹)	Wang method (Pa ⁻¹)	Type-curve method (Pa ⁻¹)	Wang method (Pa ⁻¹)
Laboratory, without packer 0.6-m section	0.6-1.5·10 ⁻⁹	-	1.3-3.0·10 ⁻⁹	-
Laboratory, with packer, 0.7-m section	1.6-5.8·10 ⁻¹⁰	-	2.3-7.9·10 ⁻⁹	-
Field $\Delta p = +40$ kPa	7.8·10 ⁻¹⁰	5.5·10 ⁻¹⁰	2.7·10 ⁻⁹	1.9·10 ⁻⁹
Field $\Delta p = -69$ kPa	4.2·10 ⁻¹⁰	3.3·10 ⁻¹⁰	1.5·10 ⁻⁹	1.1·10 ⁻⁹
Field $\Delta p = 270$ kPa	1.0·10 ⁻⁹	1.0·10 ⁻⁹	3.6·10 ⁻⁹	2.5·10 ⁻⁹

9.4 Test methods

9.4.1 Constant-rate-of-flow injection tests

In conjunction with the expansion of the packers and sealing off a given test section, the enclosed water was pressed up in the pipe string to a maximum height of 1.4 m and overpressure was generated in the test section. In high-conductivity sections, this head of water quickly drained into the surrounding formation, but it took a long time in low-conductivity zones. To speed up this process, this column of water was removed manually from the pipe string immediately after sealing the packers.

After completion of packer sealing, (for about 30 minutes, determined from tests on the equipment) the down hole test valve was closed, the pipe string was filled with water and

connected to the injection equipment above ground level. Using a special shunt valve, all the injection equipment could be completely bled of air and a preselected water flow adjusted. Injection into the section was then started instantaneously with the correct rate of flow, by closing the shunt line and opening the test valve. Injection at a constant rate of flow was normally carried out for 180 minutes, during which the transient build-up in the section was recorded continually on a chart recorder.

The rate of water flow was selected on the basis of earlier water loss measurements (see Section 9.4.5). If earlier measurements had not been made it would have been difficult to select the correct rate of flow, as too low rate of flow results in insufficient or nonexistent pressure build-up. Excessive rate of flow, on the other hand, causes the pressure to increase too quickly, which may result in the test having to be broken off too early.

A momentary deviation from complete transient build-up from reference pressure occurred at the start of all injection test. As the test valve was opened, the pressure increased by about 0.05 MPa, corresponding to the height of the water column from the pressure head of the section to the injection equipment at ground level. This means that evaluation of the initial part of the pressure curve may be affected.

9.4.2 Pressure fall-off tests after injection at a constant-rate-of-flow

These tests formed the continuation of the transient constant-flow injection tests. The pressure achieved at the end of a transient constant-flow test was confined into the test section, using the down hole test valve. The decline in pressure in the section was then recorded continuously by the chart recorder.

9.4.3 Constant-pressure injection tests

After the expansion of the packers was completely finished and the resulting squeeze pressure in the section had been reduced, the test valve was closed, the pipe string filled with water and connected to the injection equipment at ground level. When the system had been completely bled of air, the required injection pressure was applied in the pipe string down to the test valve in the borehole. This was permitted to stand for a while, to check that the rate of flow was zero, i.e. no leakage in the test valve, pipe joints or other parts of the injection system. Injection of water into the measurement section was then started instantaneously by opening the test valve. The flow meter was checked to ensure that a suitable graduated measuring cylinder was connected. The injection pressure (usually 0.2 MPa) and the declining rate of flow was recorded by the chart recorder for about 180 minutes.

9.4.4 Pressure fall-off tests after injection at constant pressure

These tests formed the continuation of the transient constant-pressure injection tests. Basically, they were performed in the same manner as those described in Section 9.4.2. The test section was confined and the pressure fall-off was recorded.

9.4.5 Water loss measurements

Packer sealing was allowed to continue until the packers were regarded as being completely expanded. As the tests were carried out before the performance tests on the packers described earlier, the time to achieve a complete seal was not known. Afterwards, it may be said, for these tests, that the time allowed to achieve a seal was too short, which may have affected measurements in zones of low-conductivity close to the lower limit of measurement. After sealing of the packers, the pipe string was filled with water and connected to the already bled injection equipment above ground level.

Water injection was started by increasing the pressure in the section to 0.2 MPa as quickly as possible. This pressure was then kept constant by regulating the rate of flow. Initially, the flow rate dropped relatively quickly, but the curve gradually became flatter. The rate of flow was read off when it had become "stable" for about 3 minutes. The pressure was then increased momentarily to 0.4 MPa, and a new rate of flow value was determined in a corresponding manner. The total injection time was normally 10 - 15 minutes.

9.4.6 Slug tests

The water column pressed up into the pipe string in conjunction with the expansion of the packers was removed as quickly as possible. After the recommended packer sealing period, the down hole test valve was closed. A hose was lowered about 10 m into the pipe string through which pressurized gas was led to force an approximately 5-m high column of water out of the pipe string. The test section was then subjected to a momentary change in pressure (pressure drop) by opening the test valve. The pressure recovery was then recorded continuously by the chart recorder.

9.4.7 Pressure pulse tests

The squeeze pressure obtained in the test section in conjunction with sealing of the packers was released, the test valve closed, and various types of pulse (pressure above or below the original water pressure in the test section) were tested as follows:

- a) The pipe string was filled with water (from the groundwater table up to the top of the pipe string, about 3.5 m). The down hole test valve was then opened for 1 - 2 seconds.

- b) The pipe string was filled with water to the top. To this was applied a pressure corresponding to water column of about 10 m, using pressurized gas, and the test valve was opened for 1 - 2 seconds.
- c) A hose was lowered about 10 m into the pipe string in order to force approximately 5 m of water column out of the pipe string by gas pressure. The test valve was then opened for 1 - 2 seconds.

The short (1 - 2 second) pulses caused a momentary pressure change in the test section. The subsequent pressure recovery was recorded continuously by the analogue chart recorder.

9.4.8 Drill stem tests

The principle for a drill stem test is that the response of a momentary change in pressure is recorded under alternating open and closed test conditions. The various parts of the test are called flow and recovery periods respectively.

After completion of packer sealing, including removal of the water column pressed up, the test valve was closed. As in slug tests and pressure pulse tests, a water column of approximately 5 m was forced out of the pipe string by the gas pressure. The first flow period of the drill stem test was started instantaneously by opening the test valve (see Fig. 8.4.1). The various phases of the drill stem tests were performed in accordance with the schedule in Table 9.3 by opening and closing the test valve alternately (the pressure recovery is related to the initial, momentary pressure change).

Table 9.4 Schedule used for the drill stem tests performed.

Test phase	Pressure recovery
1st flow period	10 - 15%
1st recovery period	approx. 80%
2nd flow period	20 - 30%
2nd recovery period	90 - 100%

10. RESULTS AND COMMENTS

10.1 Constant-rate-of-flow injection tests

10.1.1 Evaluation

The transient test theories shown in Chapter 4 were originally derived for drawdown tests. But they may also be used for injection tests as the theory behind both types of test is identical, with the exception of the direction of water flow.

In evaluating constant-flow injection tests, the transient pressure change dp (or H) was plotted as a function of the time t in both semi-log and log-log graphs (see Section 4.2.1). As a complement to this, dp was also plotted as a function of $\sqrt[4]{t}$ in linear graphs. This latter type of graph was used primarily to facilitate identification of various flow regimes, specially linear flow, and thereby provide more reliable evaluation.

The (equivalent) hydraulic conductivity and skin factor of the rock was normally determined from the semi-log graph in accordance with Eqns. (4-8) and (4-9), whereas the hydraulic and physical properties of any fractures were evaluated from the log-log graph in combination with the linear one. The apparent fracture length and conductivity were calculated from the log-log graph in accordance with Eqns. (7-2) and (7-3) and the fracture conductivity from the linear one in accordance with Eqn. (7-4).

The effective borehole radius and specific storage coefficient cannot be determined simultaneously from transient single-hole tests as they are related to one another (see Eqn. 4-13). In this investigation, it was decided to calculate the effective borehole radius using the skin factor (Eqn. 3-2). Determination of the skin factor is conditional on the specific storage coefficient being known or possible to estimate (in accordance with Eqn. 4-9).

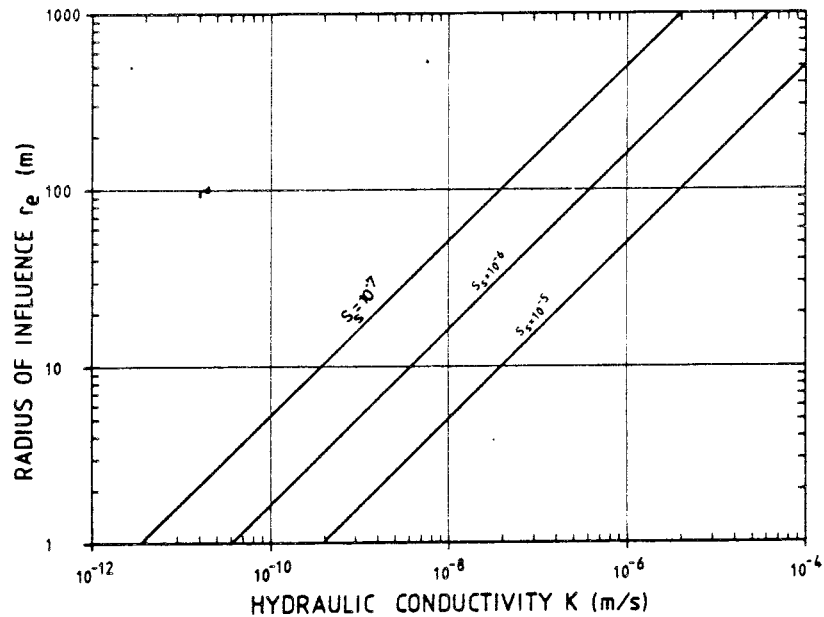


Fig. 10.1.1 Theoretical relationship between the radius of influence and the hydraulic conductivity of a section under homogeneous conditions and a 3-h test duration.

In this study of methods, the specific storage coefficient has been estimated on the basis of experience from other investigations in crystalline rock. Thus, the specific storage coefficient for the rock was taken as $S_s = 10^{-5} \text{ m}^{-1}$ for sections with a hydraulic conductivity S above 10^{-7} m/s , and $S_s = 10^{-6} \text{ m}^{-1}$ for sections in which K is below 10^{-7} m/s .

The radius of influence, i.e. the radius of the rock influenced by the test, was calculated approximately in accordance with Eqn. (4-11). This equation, which applies to homogeneous and isotropic conditions, should provide an apparent minimum value for the radius of influence in fractured formations. If one or more fractures are present in a section, the actual radius of influence should be larger than that obtained from Eqn. (4-11).

The radius of influence calculated in accordance with Eqn. (4-11) as a function of the hydraulic conductivity of the rock for various values of specific storage coefficient is shown graphically in Fig. 10.1.1. The graph is based on a test duration of 3 hours.

It should be pointed out that certain sections were found to be almost impermeable, i.e. a very small flow into the section causes such a large rise in pressure that, in certain cases, the test had to be discontinued. In such sections the result is very sensitive to any deformation of the equipment. The validity of the theory used may also be questioned in such cases. This results in that the calculated values of the hydraulic parameters for these sections should be regarded as being approximate.

10.1.2 Results

The results of the transient constant-flow injection tests are shown in Table 10.1 and are commented on section by section below. In the first instance, the equivalent hydraulic conductivity of the rock (section conductivity), K , was calculated for each section. Where possible, the fracture conductivity, $K_f e$, and apparent fracture length, $2 x_f$, were determined. It should be noted that the fracture conductivity is the hydraulic conductivity, K_f , of a vertical fracture multiplied by the fracture aperture, e . The fracture conductivity may therefore be compared to the transmissivity concept. The ratio $K_f e/L$, in which L is the length of the section, was also determined. The resulting skin factor and effective borehole radius, r_{wf} , determined from it, and, in appropriate cases pseudo-skin-factor, ζ_f , for the fracture, were determined. An apparent value for the radius of influence, r_e , is also stated, and the test duration, t , for each section. Test responses and interpretation are presented for most sections.

Table 10.1 Results of transient injection tests with constant flow-rate.

Section (m)	t_p (min)	K (m/s)	ζ	r_{wf} (m)	r_e (m)
67-70 ¹⁾	180	$1.9 \cdot 10^{-7}$	-3.4	0.84	21
70-73	180	($9.0 \cdot 10^{-13}$)	-	-	(0.15)
76-79	180	($7.5 \cdot 10^{-13}$)	-	-	(0.14)
79-82 ²⁾	180	$1.5 \cdot 10^{-9}$	-3.2	0.65	6.0
85-88	180	($4.4 \cdot 10^{-13}$)	-	-	(0.10)
166-169	180	($6.6 \cdot 10^{-13}$)	-	-	(0.13)
178-181	180	$1.2 \cdot 10^{-6}$	4.8	$2.3 \cdot 10^{-4}$	53
181-184	180	$4.1 \cdot 10^{-10}$	-2.7	0.40	3.2
190-193 ³⁾	180	$2.2 \cdot 10^{-9}$	-3.9	1.33	7.3

Note: Values within brackets denote approximative evaluation of parameter.

- 1) $K_{fe} = 8.4 \cdot 10^{-7} \text{ m}^2/\text{s}$ $2x_f = 5.6 \text{ m}$
 $K_{fe}/L = 2.8 \cdot 10^{-7} \text{ m/s}$ $\zeta_f = -3.3$
- 2) $K_{fe} = \text{infinite}$ $2x_f = 7.3 \text{ m}$
- 3) $K_{fe} = 2.5 \cdot 10^{-8} \text{ m}^2/\text{s}$ $2x_f = 14.2 \text{ m}$
 $K_{fe}/L = 8.2 \cdot 10^{-9} \text{ m/s}$

Section 67 - 70 m

The pressure build-up during transient constant-flow injection tests is shown in semi-log, log-log and $\sqrt[4]{t}$ graphs in Fig. 10.1.2a-c. The pressure change curves obtained indicate that evaluation should be performed in accordance with the model for a vertical fracture with finite fracture conductivity. In the log-log graph, a straight line with a slope of 1:4, indicating bilinear flow, can be identified up to a time of 6 minutes. This flow regime is represented by a straight line in the linear graph. As this line passes through the origin, it indicates that little or no clogging appears to occur in the fracture. The deviation from a straight line in the beginning is probably due to a failure to build up a constant flow for about the first 0.3 minutes. The fracture conductivity was calculated from the linear graph (see Fig. 10.1.2c). The theory is described in Chapter 7.

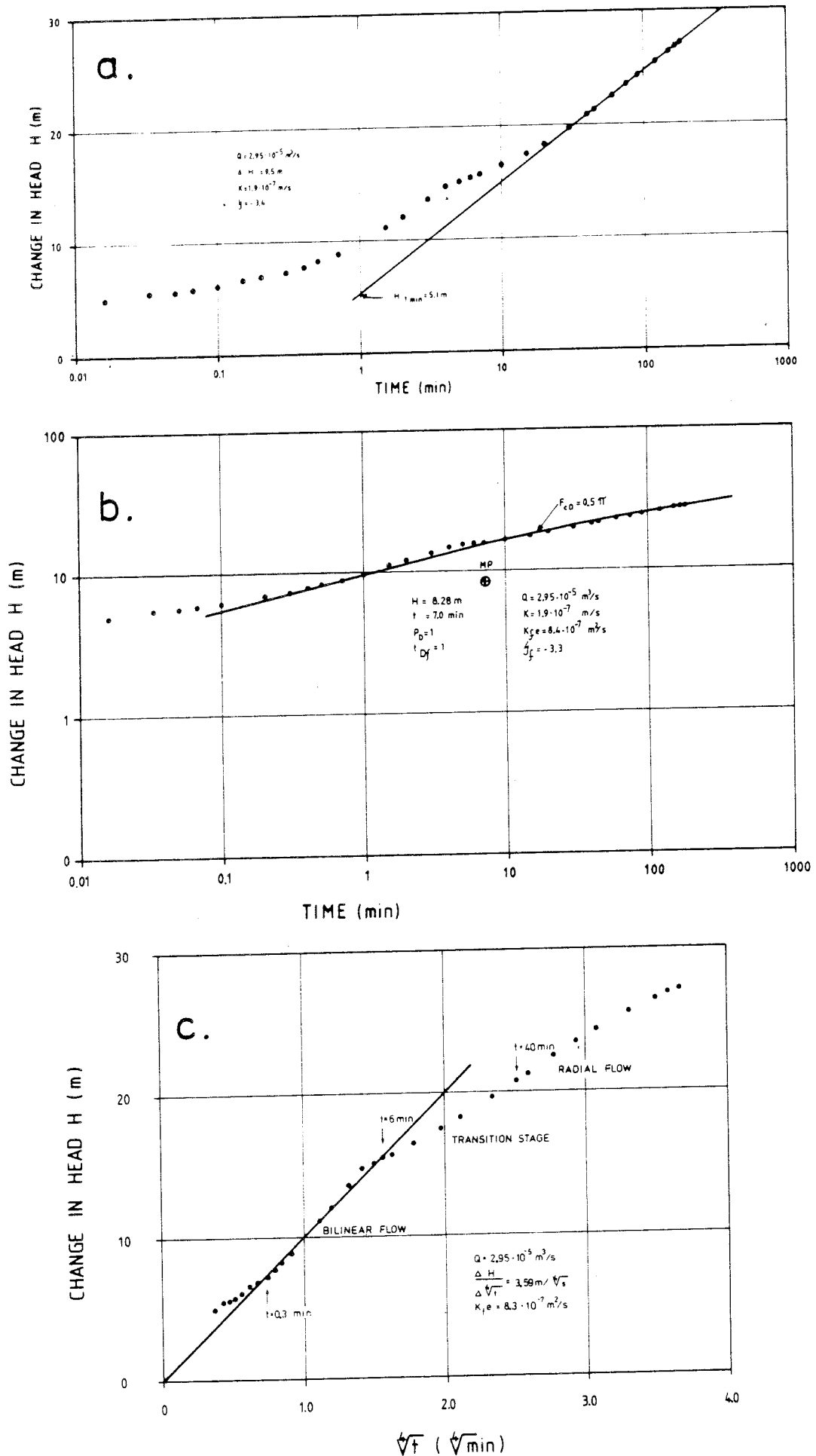


Figure 10.1.2 Transient injection test with constant flow rate. Section 67-70 m a) semi-log graph b) log-log graph c) linear graph

After the bilinear flow regime, follows a transition period of up to about 40 minutes, after which radial flow takes place in the rock. This stage corresponds to a straight line in the semi-log graph, from which the hydraulic conductivity and skin factor of the rock were determined.

The interpretation may be summarized as one (equivalent) 5.6-m long vertical fracture with finite conductivity that intersects the test section. Little or no clogging was present in the fracture.

Sections 70 - 73, 76 - 79, 85 - 88 and 166 - 169 m

The transient pressure build-up in the semi-log graph for section 70 - 73 is shown together with the interpretation line in Fig. 10.1.3. This section has been interpreted as being almost impermeable. The delay in pressure build-up that occurred is assumed to be associated with deformation of the test equipment. The response in the log-log graph is dominated by borehole storage effects, so that it not possible to make a quantitative evaluation of the hydraulic conductivity or skin factor in this case. The radius of influence probably only extends in the order of a few centimetres outside the borehole.

The calculated value of K must be regarded as an apparent measurement value. In addition to deformation of the equipment, variations in temperature may also have affected the evaluation. A correction was applied for packer deformation during the pressure build-up stage. The test responses in sections 76 - 79, 85 - 88 and 166 - 169 are similar.

Section 79 - 82 m

The pressure build-up in the log-log graph (Fig. 10.1.4) follows a straight line with a slope of 1:2 at an early stage. The straight line stops after about 20 minutes. The pressure response may be interpreted as linear flow in one (vertical)

fracture that intersects the section. This interpretation is supported by the pressure build-up plotted in linear graphs.

Data points after about 20 minutes represent a transition period to pseudo-radial flow. If the data points are matched to a type curve for a vertical fracture, pseudo-radial flow would however not appear to have been achieved during the test (180 minutes). So evaluation formulas applicable to radial flow cannot be used in this case. But an approximate evaluation may be made in the log-log graph by matching a type curve for a vertical fracture. This evaluation provides approximate values for the hydraulic conductivity of the rock and an apparent fracture length, using Eqns. (4-12) and (7-1) respectively.

Section 178 - 181 m

The pressure build-up curve is relatively flat, apart from the first half minute, when the most of the total increase in pressure took place (Fig. 10.1.5). The relatively high rate of flow used in the injection test ($Q = 2.75 \times 10^{-5} \text{ m}^3/\text{s}$) implies that the section is intersected by one or more fractures. The fast fall-off in pressure at the beginning of the tests indicates clogging effects in the fracture or fracture system. Radial flow occurs after about 40 minutes. The flat part of the curve before this time may mask a linear flow regime. This prevents unambiguous evaluation of any fracture parameters. The hydraulic conductivity of the rock and the section's skin factor were calculated from the semi-log graph. It should be pointed out that the skin factor calculated is a relatively high and positive, which implies partial clogging of fractures.

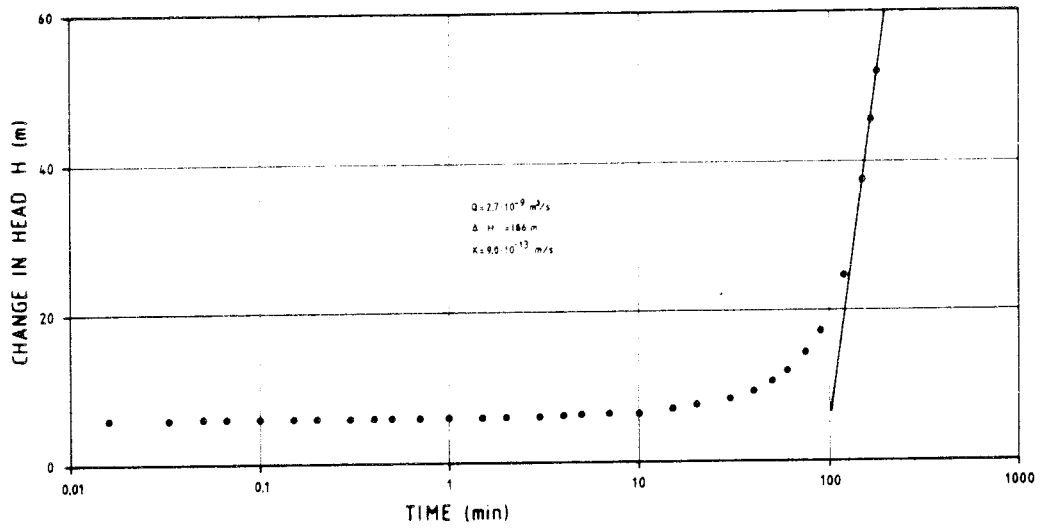


Fig. 10.1.3 Transient injection test with constant flow rate. Section 70 - 73 m.

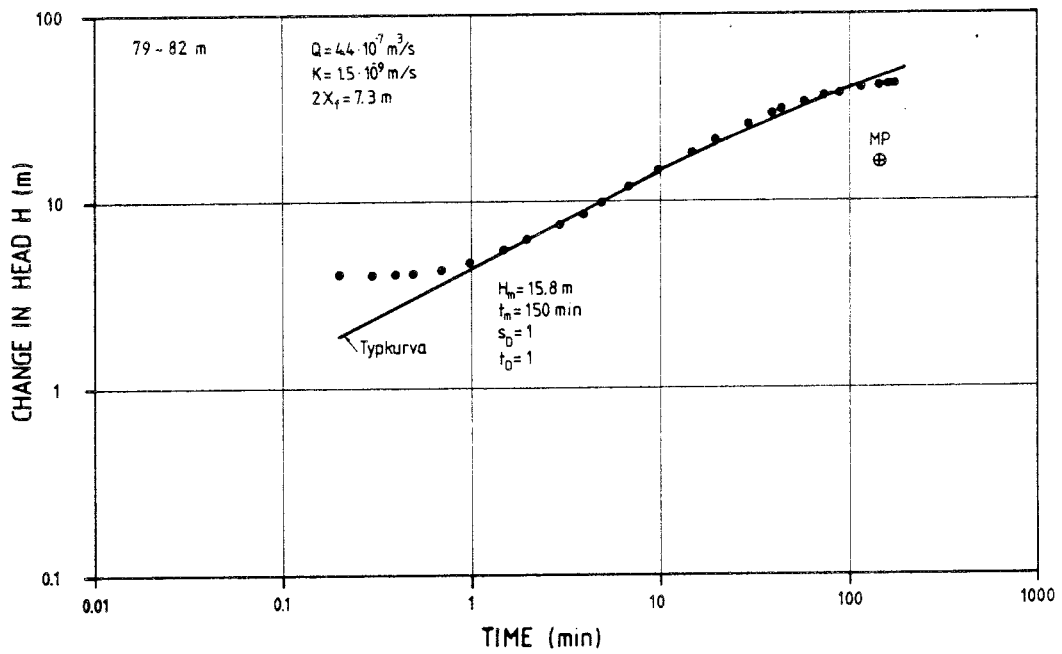


Fig. 10.1.4 Transient injection test with constant flow rate. Section 79 - 82 m.

Section 181 - 184 m

The pressure build-up in this section is shown together with the plotted interpretation lines in a semi-log graph in Fig. 10.1.6. The shape of pressure build-up curve obtained indicates that the evaluation should be made in accordance with the model for dual-porosity formations (see Chapter 6).

The section has been interpreted as being a medium with dual-porosity, consisting of a system of minor fractures in an otherwise relatively impervious rock mass. The hydraulic conductivity of the fracture system was calculated from the slope of the two parallel lines. The skin factor was calculated from the later straight line.

Section 190 - 193 m

Two tests, separated by an interval of about 14 hours, were performed in this section. However, the tests show a somewhat different pressure build-up behaviour.

The pressure response in the first test is relatively flat up to a time of about 15 minutes. The curve then rises steeply before levelling off by the end of the test. The response may be interpreted as injection into a partly clogged fracture. In the second test (Fig. 10.1.7), the pressure rise is relatively large during the first minute, after which the curve levels off and only starts to rise again after about 30 minutes to approach a straight line with a slope of 1:4 in the log-log graph. The earlier response may have been caused by borehole storage effects in combination with clogging. The pressure response may be interpreted as linear flow in a vertical fracture with finite conductivity. Pseudo-radial flow was not achieved during the test (180 minutes). This implies that the hydraulic conductivity and apparent fracture length must be estimated from the log-log graph.

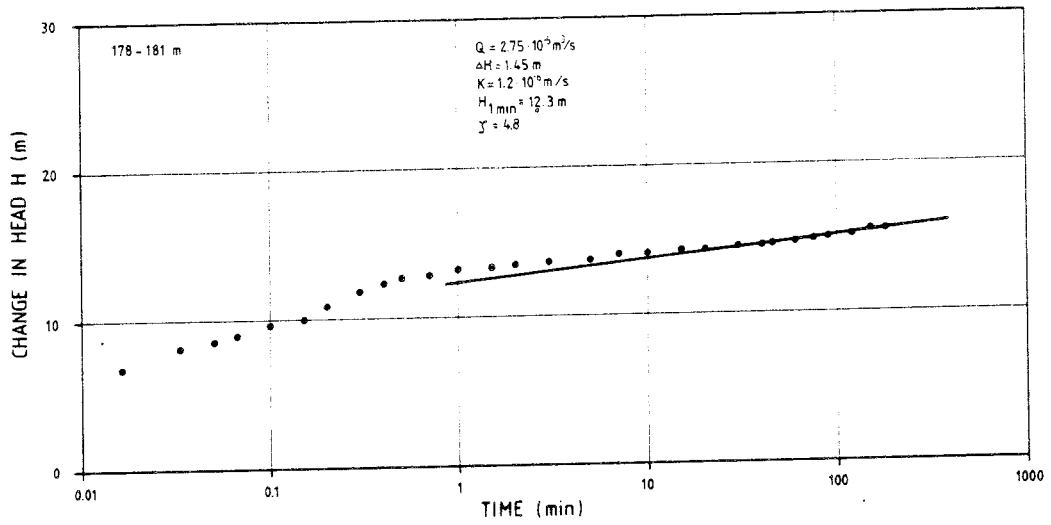


Figure 10.1.5 Transient injection test with constant flow rate. Section 178 - 181 m.

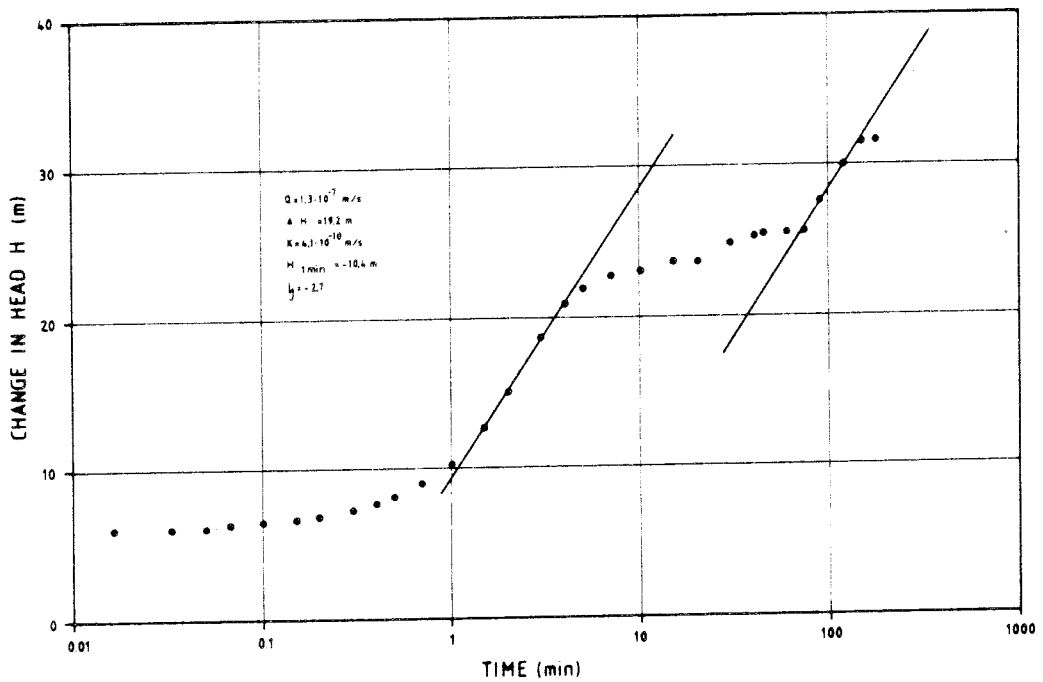


Figure 10.1.6 Transient injection test with constant flow rate. Section 181 - 184 m.

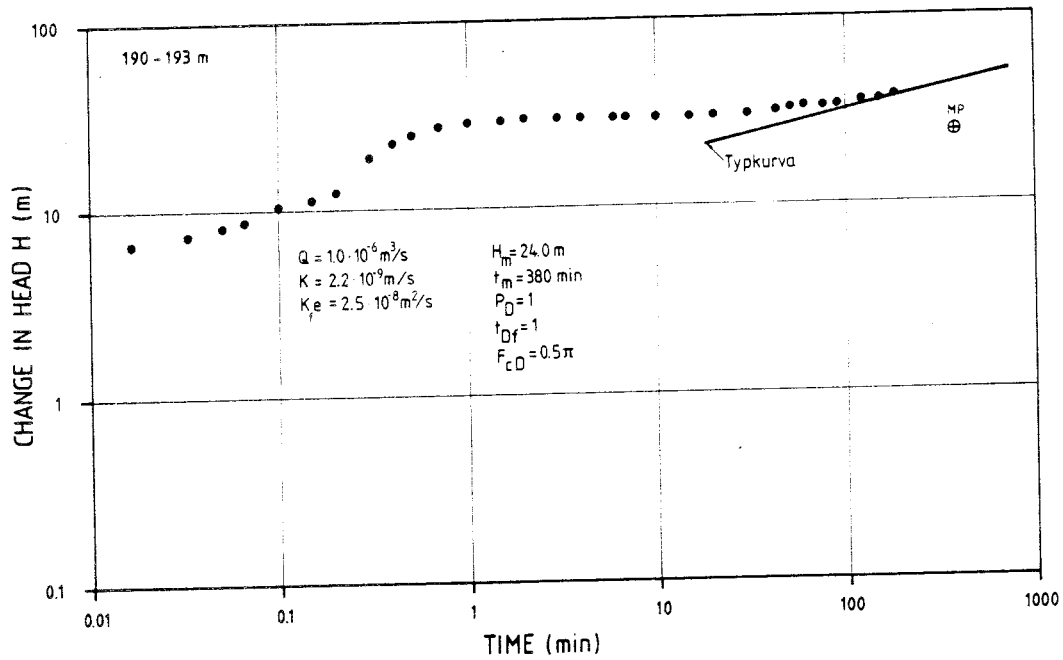


Figure 10.1.7 Transient injection test with constant flow rate. Section 190 - 193 m.

10.2 Pressure fall-off tests after injection at a constant rate of flow

10.2.1 Evaluation

The pressure fall-off data was plotted on both Horner graphs and as a function of the equivalent time on semi-log and log-log graphs. The residual pressure change was plotted on semi-log graphs, while the pressure change related to the pressure at the stop of injection was plotted on log-log graphs. The pressure fall-off data was also plotted on linear graphs.

Both the Horner method and the method employing equivalent time were used in analysis of the pressure fall-off data. If borehole storage and skin effects occur during a test, the conditions contained in Eqns (5-3) and (5-4) must be satisfied for correct evaluation from Horner graphs, as discussed in Section 5.2.1. As stated in Section 4.2.1, the hydraulic conductivity is calculated from semi-log graphs in accordance with Eqn. (4-8) and the skin factor in accordance with Eqn.

(4-9). In log-log graphs, the hydraulic conductivity is calculated in accordance with Eqn. (4-12) and the effective borehole radius in accordance with Eqn. (4-13). In evaluation, the same specific storage coefficient as stated in Section 10.1.1 was assumed.

10.2.2 Results

The results from pressure fall-off tests after constant-flow injection are shown in Table 10.2 and are commented on, section by section, below. The designations used are the same as those in the injection tests described in the previous section.

In section 70 - 73, pressure fall-off takes place considerably more slowly than the pressure build-up in the injection stage. At the end of the test (130 minutes), only about 30% of the maximum pressure rise at the cessation of injection had dissipated, which confirms the assumption that the section was virtually impervious. As pointed out in Section 10.1.2 (section 70 - 73), tests in almost impervious sections are more sensitive to deformation of and leakage in equipment and changes in the packer pressure as a result of small changes in temperature. The results should therefore be regarded as apparent and approximate.

Table 10.2 Results of transient pressure fall-off tests after injection with constant flow rate.

Section (m)	dt (min)	K (m/s)	ζ	r_{wf} (m)
67 - 70	55	1.8×10^{-7}	-4.1	1.63
70 - 73 *	130	$< 9.2 \times 10^{-12}$	< -1.5	> 0.13
79 - 82 *	42	7.9×10^{-10}	-3.2	0.69

* Approximative evaluation

Section 67 - 70 m

The pressure fall-off is presented in a semi-log graph as a function of the equivalent time, together with the interpretation line, in Fig. 10.2.1. The pressure fall-off behaviour is similar to the pressure build-up during the injection phase, but is somewhat slower. The pressure fall-off time is also shorter. The calculated hydraulic conductivity and skin factor values are in good agreement with the results from the injection test. The static pressure in the section was found to be -0.2 m, i.e. 0.2 m below the actual pressure before the injection test.

Section 79 - 82 m

The pressure fall-off test was discontinued after 42 minutes, at which point about 60 % of the pressure build-up during the injection test had dissipated. The pressure fall-off data were plotted on both a Horner graph and as a function of equivalent time. As true radial flow does not occur during the injection test, the radial flow theory is not applicable during the pressure fall-off test. Test data are shown in a linear graph in Fig. 10.2.2. The points approximate closely to a straight line in this graph, which indicates linear flow, even during the pressure fall-off test. The hydraulic conductivity evaluation is approximate due to the absence of the radial flow period.

10.3 Constant-pressure injection tests

10.3.1 Evaluation

In evaluating transient constant-pressure injection tests, the flow rate $Q(t)$ was plotted as a function of the time, t , on a log-log graph and $1/Q(t)$ as a function of t on semi-log and log-log graphs. In certain cases, $1/Q(t)$ was also plotted as a function of $\sqrt[4]{t}$ on a linear graph in a manner analogous to constant-flow rate tests. From this graph the fracture conductivity was determined in accordance with Eqn. (7-8).

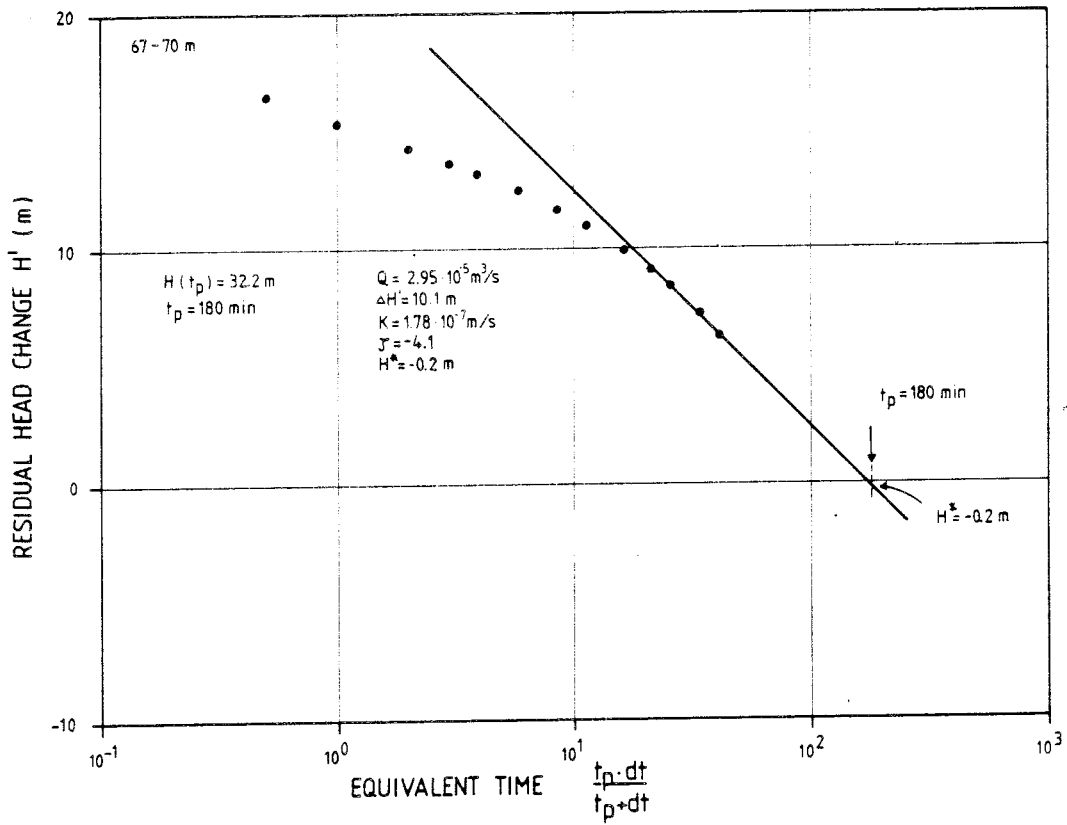


Figure 10.2.1 Pressure fall-off test after injection with constant flow rate. Section 67 - 70 m.

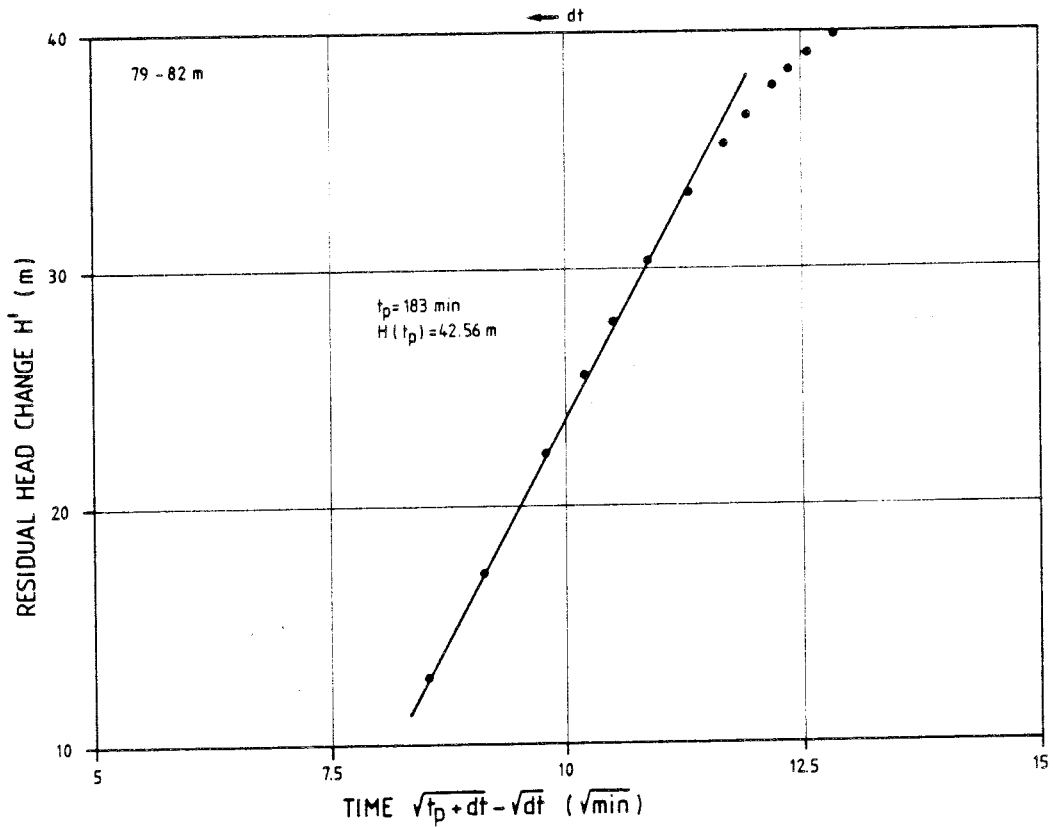


Figure 10.2.2 Pressure fall-off test after injection with constant flow rate. Section 79 - 82 m.

The hydraulic conductivity of the test sections was preferably evaluated from the semi-log graphs in accordance with Eqn. (4-24) and the skin factor in accordance with Eqn. (4-25). In evaluation, the same specific storage coefficient as that stated in Section 10.1.1 was assumed. In evaluation in accordance with the dual-porosity model, the hydraulic conductivity was calculated in accordance with Eqn. (4-24) and the skin factor from the later straight line in accordance with Eqn. (4-25).

The data curves for the constant-pressure injection tests on semi-log graphs are very similar to those obtained for corresponding constant-flow rate tests. This implies that practically the same information is obtained from the two types of test.

The effective borehole radius was calculated in accordance with Eqn. (3-2). As the radius of influence is assumed to be independent of the injection pressure, it was calculated approximately in accordance with Eqn. (4-11), in a manner analogous to that used in the constant-flow rate injection tests.

10.3.2 Results

The results from the transient constant-pressure injection test are shown in Table 10.3 and are commented on, section by section in the text below. The designations used are the same as those used in the injection tests described in earlier presentations of results.

Sections 76 - 79 and 166 - 169 are low-conductivity sections, so that equipment deformations and variations in temperature may strongly influence the pressure changes. The interpretation curves are also based on only a few measured values. The evaluation is therefore approximate.

In testing sections 172 - 175 and 178 - 181, maintenance of a constant injection pressure proved to be a problem. In the former section, the flow rate curve rises sharply and becomes a straight line (radial flow - semi-log graph) after a very flat start. The latter test developed into a constant-flow rate test (cf. Section 10.1.2). Radial flow occurred after about 10 minutes and the pressure response implies a partially clogged fracture or fracture system.

Table 10.3 Results of transient injection tests with constant pressure.

Section (m)	t_p (min)	K (m/s)	ζ	r_{wf} (m)	r_e (m)
67-70	180	$1.7 \cdot 10^{-7}$	-3.4	0.84	20
76-79	70	($6.0 \cdot 10^{-14}$)	-	-	(0.08)
79-82	180	$1.3 \cdot 10^{-9}$	-2.3	0.28	5.6
166-169	180	($2.8 \cdot 10^{-14}$)	-	-	(0.03)
172-175	180	($1.8 \cdot 10^{-9}$)	-2.3	0.25	6.6
178-181	90	$2.3 \cdot 10^{-6*}$	-	-	53
181-184	180	$4.1 \cdot 10^{-10}$	-1.0	0.08	3.2
190-193	180	$2.6 \cdot 10^{-9}$	-3.2	0.69	7.9

* evaluated as constant flow-rate test

() values within brackets are approximative

Section 67 - 70 m

The transient change in flow rate coincides after about 10 minutes with a straight line in a semi-log graph (see Fig. 10.3.1). After 60 minutes, this line is moved laterally, parallel to the original one, probably caused by a flow meter change. Calculated values of the hydraulic conductivity, skin factor and fracture conductivity are in good agreement with the values of corresponding parameters from the constant-flow rate test.

Section 79 - 82 m

The transient test response on this section, together with the interpretation line on a semi-log graph, are shown in Fig. 10.3.2.

The flow rate values are relatively scattered, but the position selected for the interpretation line is quite clear. Radial flow occurs after about 15 minutes. After about 100 minutes of injection time, a positive hydraulic boundary is implied. The hydraulic conductivity and skin factor were calculated from the semi-log graph.

Section 181 - 184 m

The transient test response on this section, together with the interpretation line on a semi-log graph, are shown in Fig. 10.3.3.

The test response was evaluated in accordance with the dual-porosity model in a manner analogous to corresponding theory for constant-flow rate injection tests (see Chapter 6). The hydraulic conductivity and skin factor were calculated in accordance with Eqns. (4-24) and (4-25) respectively. The section was interpreted as a medium with dual-porosity, consisting of a system of minor fractures in an otherwise relatively impervious rock mass (cf. corresponding constant-flow rate injection test).

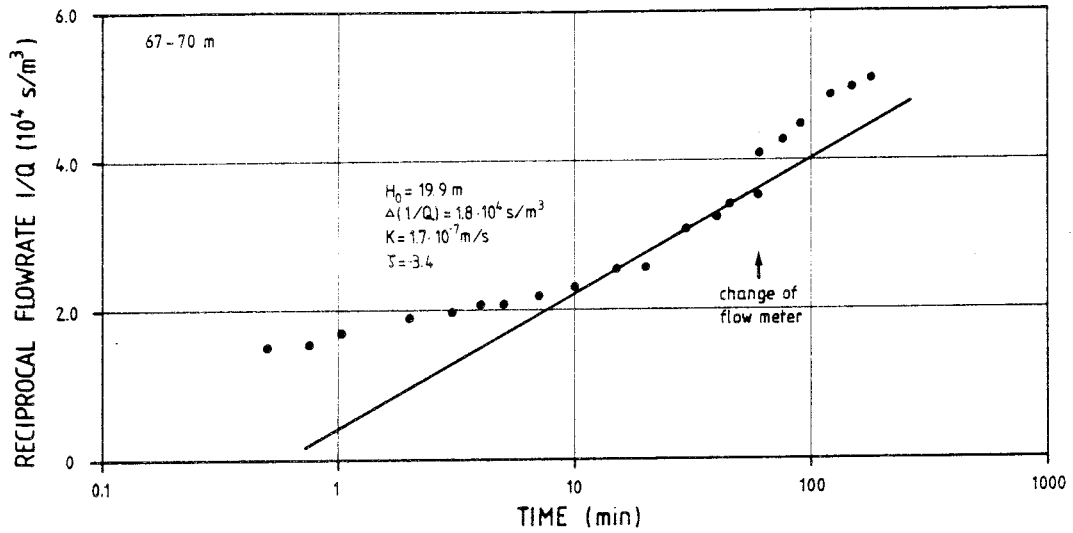


Figure 10.3.1 Transient injection test with constant pressure. Section 67 - 70 m.

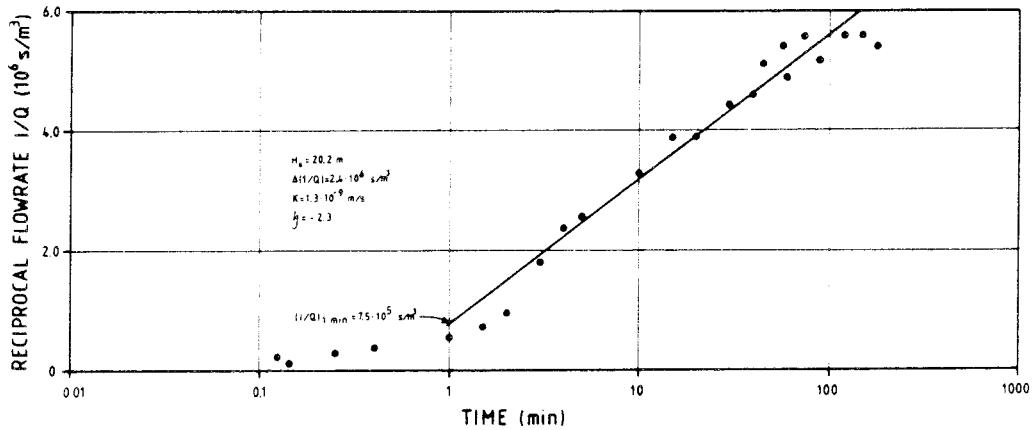


Figure 10.3.2 Transient injection test with constant pressure. Section 79 - 82 m.

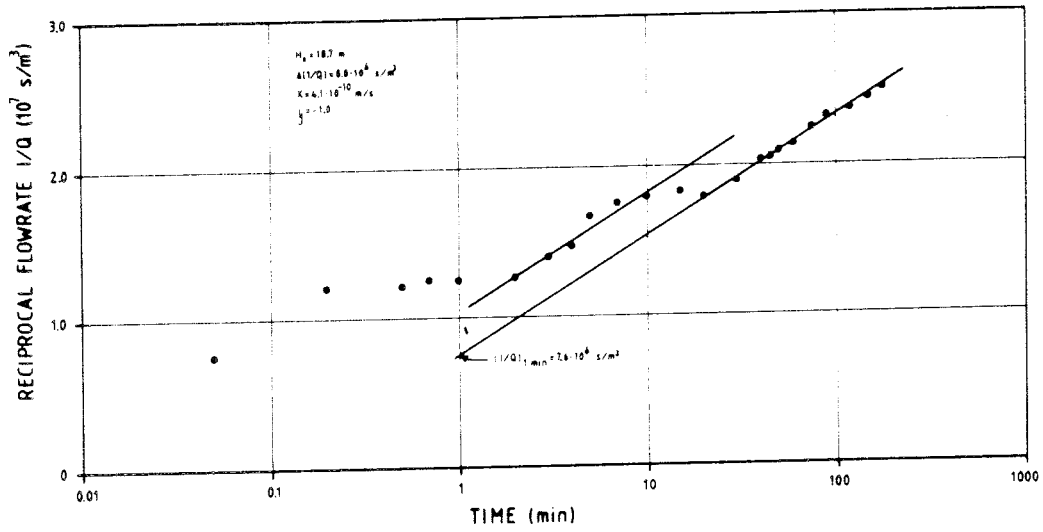


Figure 10.3.3 Transient injection test with constant pressure. Section 181 - 184 m.

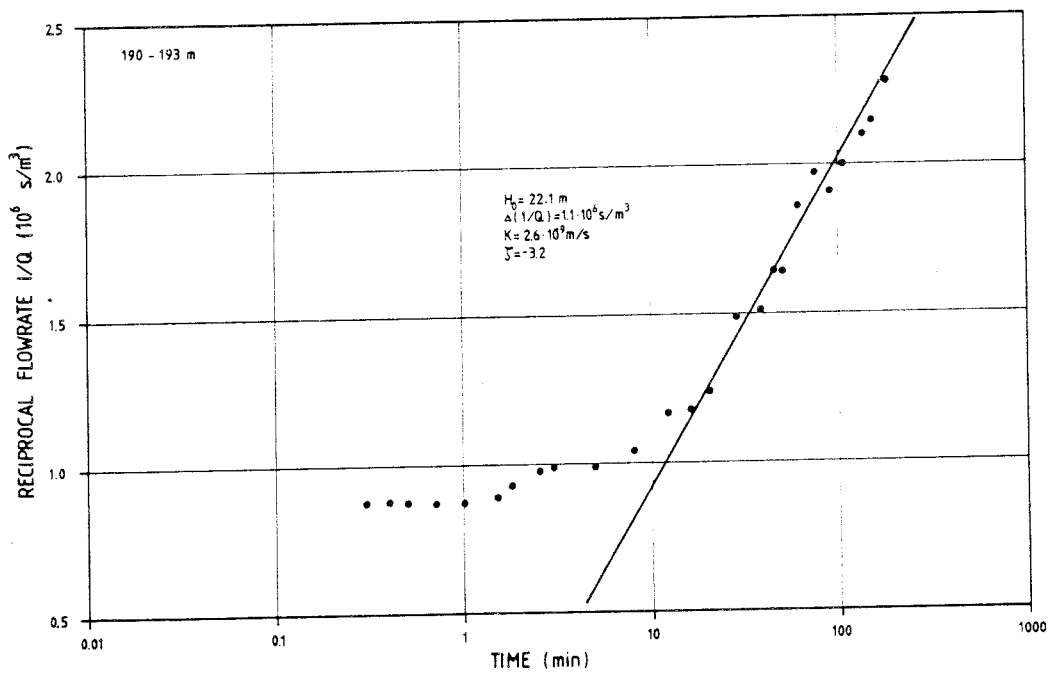


Figure 10.3.4 Transient injection test with constant pressure. Section 190 - 193 m.

Section 190 - 193 m

After about 15 minutes of injection time, the transient flow rate curve coincides well with a straight line on the semi-log graph (Fig. 10.3.4). The hydraulic conductivity and skin factor were evaluated on the basis of this straight line and the values exhibit good agreement with corresponding values from the constant-flow rate test.

10.4 Pressure fall-off tests after injection at constant-pressure

10.4.1 Evaluation

In evaluating the transient pressure fall-off tests after constant-pressure injection, the residual pressure change, H , was plotted on Horner graphs and as a function of the equivalent time on semi-log graphs. The pressure change in relation to the pressure at the stop of injection was plotted as a function of the equivalent time on log-log graphs. The pressure change was also plotted on linear graphs.

The hydraulic conductivity was calculated in accordance with Eqn. (5-11) and the skin factor in accordance with Eqn. (5-5). The flow rate value used was the momentary flow rate at the stop of injection. Very fast pressure fall-off was obtained in some tests. This may possibly be due to the shortness of the (dimensionless) injection time. In this case, the actual pressure approaches the static pressure in the section asymptotically (see Section 5.2.1). Equipment faults cannot either be ruled out for these tests. The specific storage coefficient value stated earlier was assumed (see Section 10.1.1).

10.4.2 Results

The results from the pressure fall-off tests after constant-pressure injection are shown in Table 10.4 and are commented on, section by section in the text below. The designations used are the same as those in earlier presentations of results.

In section 79 - 82, the pressure fall-off test was discontinued after 40 minutes, at which time 60% of the applied injection pressure had dissipated. The graphs show that radial flow was not achieved during the test. The linear graph implies instead that linear flow existed (cf. corresponding test in Section 10.2.2). The evaluation of the hydraulic conductivity is approximate because of the short duration of the test. It was not possible to determine reliably the static pressure in this section.

Sections 172 - 175, 181 - 184 and 190 - 193 exhibit similar behaviour. In all cases the pressure fall-off was largely complete after a very short time (about 1 minute). Because of the short duration of the test, the results must be regarded as being uncertain. In sections 172 - 175 and 190 - 193, the pressure change curve levels off towards zero, i.e. the actual pressure acting in the section before the injection test. In section 181 - 184, the pressure change curve levels off towards a value of +0.25 m, i.e. 0.25 m above the pressure prevailing before the injection test.

Table 10.4 Results of pressure fall-off tests after injection with constant pressure.

Section (m)	dt (min)	K (m/s)	ζ	r_{wf} (m)
79 - 82	40	7.5×10^{-10}	-3.1	0.62
172 - 175	0.85	9.4×10^{-10}	-0.4	0.04
181 - 184	0.7	1.6×10^{-10}	-0.3	0.04
190 - 193	1.7	1.3×10^{-9}	-0.3	0.04

10.5 Water loss measurements

10.5.1 Evaluation

The water loss measurements were evaluated using equations valid for steady-state conditions. Thus, Eqn. (4-41) was used, and as data values, the flow measured under the latter part of each test and the actual injection pressure were used. In no test were real steady-state conditions measured under which the formulas used become strictly valid. But in all cases, the change in flow rate with time was considered to be so small during the latter part of the test that steady-state conditions were assumed in the evaluation.

10.5.2 Results

The (equivalent) hydraulic conductivity values calculated for the rock at a constant injection pressure of 0.2 MPa are presented in Table 10.5.

10.6 Slug tests

10.6.1 Evaluation

In evaluating the slug tests, the normalized pressure change, H/H_0 , was plotted on semi-log and log-log graphs as a function of the time (see Section 8.2). The equivalent hydraulic conductivity of the section was preferably calculated from the semi-log graph by matching the data curve to the type curve in accordance with Ramey et al (1975) and entering the match point coordinates into Eqn. (8-4). As a complement, corresponding evaluation was carried out from log-log graphs in certain cases.

Table 10.5 Results from water loss tests performed with an injection pressure of 0.2 MPa.

Section (m)	Hydraulic conductivity (m/s)	Section (m)	Hydraulic conductivity (m/s)
61 - 64	3.9×10^{-9}	163 - 166	$<1.8 \times 10^{-11}$ *
64 - 67	7.5×10^{-10}	166 - 169	$<1.8 \times 10^{-11}$ *
67 - 70	5.3×10^{-7}	169 - 172	$<1.8 \times 10^{-11}$ *
70 - 73	2.2×10^{-11}	172 - 175	5.4×10^{-9}
73 - 76	$<1.8 \times 10^{-11}$ *	175 - 178	1.6×10^{-8}
76 - 79	2.4×10^{-11}	178 - 181	5.7×10^{-7}
79 - 82	7.5×10^{-9}	181 - 184	2.1×10^{-9}
82 - 85	$<1.8 \times 10^{-11}$ *	184 - 187	1.5×10^{-7}
85 - 88	$<1.8 \times 10^{-11}$ *	187 - 190	3.6×10^{-9}
88 - 91	$<1.8 \times 10^{-11}$ *	190 - 193	2.1×10^{-8}
91 - 94	$<1.8 \times 10^{-11}$ *	193 - 196	1.2×10^{-7}
		196 - 199	6.0×10^{-9}

* The value 1.8×10^{-11} m/s constitutes the lower measurement limit for all sections.

Table 10.6 Results from the slug tests.

Section (m)	Number of tests*	Test duration (min)	H/Ho at end of test	K, K mean (m/s)	Comments
64-67	1	930	40%	$3.9 \cdot 10^{-10}$	Good match to the type curve.
67-70	1	2	7.5-46	$7.6 \cdot 10^{-7}$ **	Good match apart from the first part of the curve.
79-82	2	955-1000	0%	$3.5 \cdot 10^{-9}$	Identical curves but difficult to interpret. Match carried out on final part.
178-181	1	5.5	0%	$1.2 \cdot 10^{-6}$	Very good match.
181-184	1	188	39%	$5.5 \cdot 10^{-9}$	Good match.
190-193	1	70	0%	$1.7 \cdot 10^{-7}$	The data curve may be divided into two parts, each of which may be matched to its type curve and give the same value of K.
193-196	1	20	0%	$1.3 \cdot 10^{-6}$	Relatively good curve match.

* 0 = with overpressure applied
 U = with underpressure applied
 ** K range: $6.0 \cdot 10^{-7}$ to $9.3 \cdot 10^{-7}$ m/s

10.6.2 Results

The results from the slug tests are presented in Table 10.6. The following designations are used:

- K The equivalent hydraulic conductivity of the rock (conductivity in the section)
- K-range the range in the value of K from several tests in the same section
- K-mean the logarithmic average value of K in a section
- H/H_0 the pressure change in relation to the momentary pressure change

Examples of response curves for slug tests are given for sections 181 - 184 and 190 - 193 in Figs. 10.6.1 and 10.6.2.

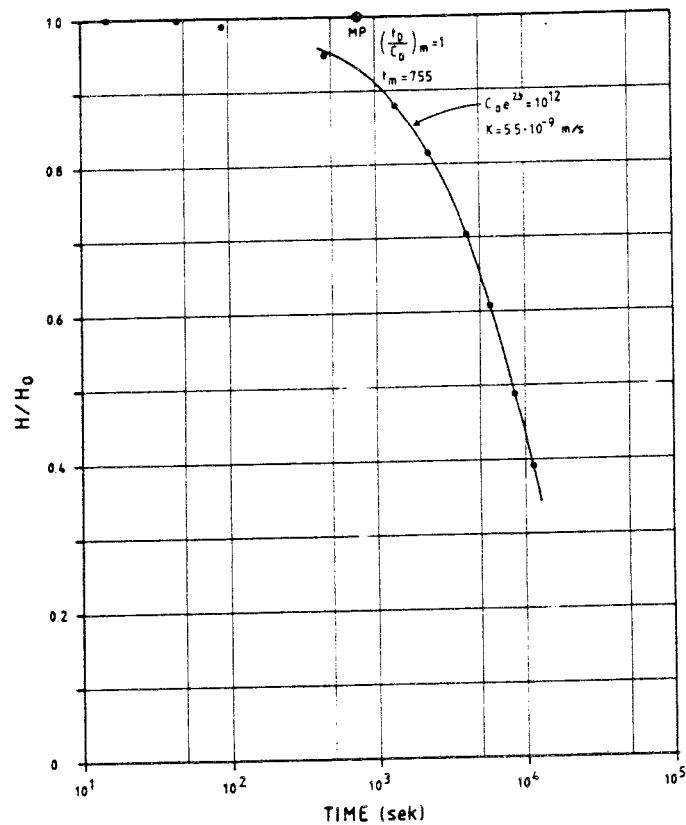


Fig. 10.6.1 Slug test. Section 181 - 184 m.

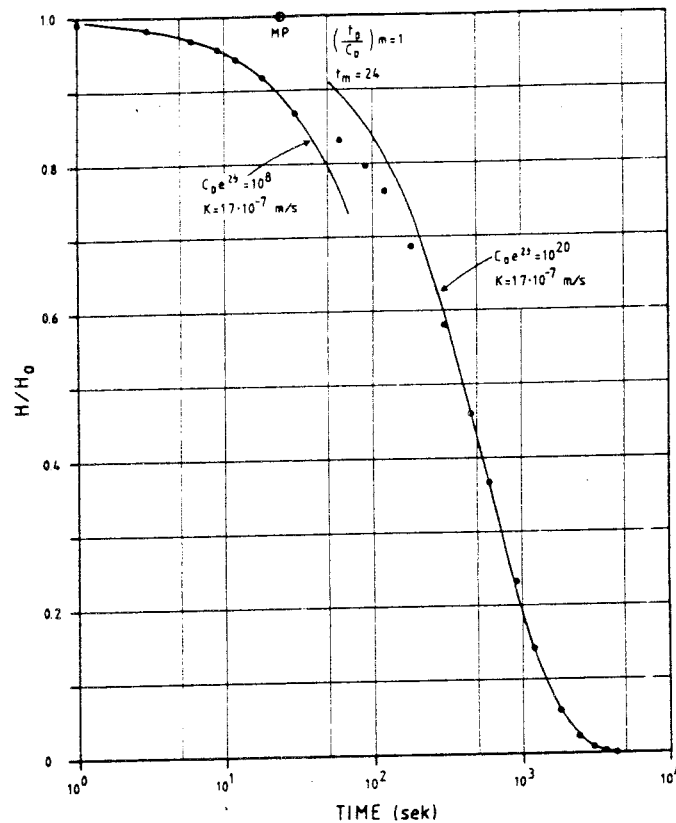


Fig. 10.6.2 Slug test. Section 190 - 193 m.

10.7 Pressure pulse tests

10.7.1 Evaluation

As in the case of the slug tests, the normalized pressure change during pressure pulse tests was plotted on semi-log and log-log graphs. Evaluation was then carried out using two methods: by matching the field curves to type curves, in accordance with Ramey et al (1975) - the type-curve method, and by evaluation in accordance with Wang et al (1977) - here referred to as the Wang method.

The type-curve method is employed in the same manner as in evaluating slug tests (see Sections 8.2 and 8.3). In pressure

pulse tests, evaluation is preferably carried out from a semi-log graph plot. But Eqn. (8-8) is used instead of Eqn. (8-4). As the compressibility of water is of decisive importance for the decay of the pressure pulse, its value was corrected for deformation of the equipment. The compressibility of water was replaced by an effective compressibility of $1.6 \times 10^{-9} \text{ Pa}^{-1}$ (see Section 9.3.5).

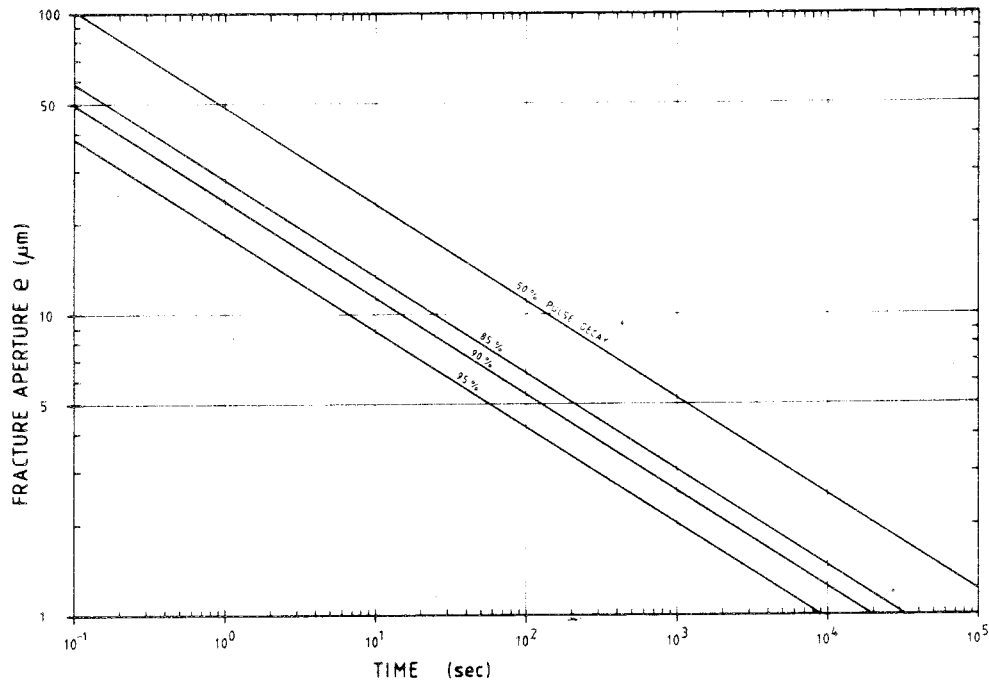


Figure 10.7.1 Theoretical relationship between fracture aperture and test time at pulse decays of 50, 85, 90 and 95 %. After Wang et al (1977).

The Wang method is based on consideration of the section as an impervious mass of rock penetrated by minor fractures (see Section 8.3). From the semi-log plot of H/H_0 as a function of time, the time at which 90, 85 or 50% of the applied pressure pulse remains, i.e. $H/H_0 = 0.9, 0.85$ or 0.5 respectively. The aperture, e , of the assumed fracture may then be obtained, using a special graph in which the fracture aperture is plotted as a function of this time (see Fig. 10.7.1). (In using this method of evaluation, it was assumed that there is only one plane, parallel fracture per section.) The hydraulic

conductivity in the fracture, K_e , may then be calculated, using Eqn. (2-2). If this conductivity is spread out over the whole length of the section in accordance with Eqn. (2-4), a conductivity value is obtained that is comparable with the equivalent hydraulic conductivity of the rock obtained from other types of test. In the preparation of the graph mentioned above, as in the type-curve method, the compressibility of water was replaced by the effective compressibility. The dynamic viscosity was set at 1.4×10^{-3} Pa . s.

10.7.2 Results

The results from the pressure pulse tests are presented in Table 10.7. In most cases, the applied pressure had dissipated completely by the end of the test. In addition to the designations used in presentation of the results of slug tests, the following were used:

- e fracture aperture
- K_e hydraulic conductivity in the fracture

Examples of results from the pressure pulse tests performed in sections 166 - 169 and 181 - 184 are shown in Fig. 10.7.2 and Fig. 10.7.3 respectively. The type curves used for interpretation are also shown in the figures.

Table 10.7 Results from pressure pulse tests evaluated using the type-curve method and the Wang method.

Section (m)	Number of tests*		Test duration (min)	H/Ho at end of test	Type-curve method K range (m/s)	Wang method K, K mean (m/s)	Wang method	
	O	U					H/Ho	e (μm)
64-67	4	4	5-35	0-3%	$2.9 \cdot 10^{-10} - 6.0 \cdot 10^{-9}$	$2.5 \cdot 10^{-9}$	50, 85, 90%	13.5-21
67-70	6	1	2-5	0-1%	$3.0 \cdot 10^{-9} - 3.2 \cdot 10^{-8}$	$8.0 \cdot 10^{-9}$	50%	29-58
76-79	1		50	92%		$5.4 \cdot 10^{-14}$	95%	2.7
79-82	5	1	10-45	0-7%	$3.7 \cdot 10^{-8} - 6.0 \cdot 10^{-8}$	$4.7 \cdot 10^{-8}$	50%	44-59
166-169	1		120	72%		$1.8 \cdot 10^{-13}$	85%	2.3
178-181	2	1	0.8-1.5	0%	$1.5 \cdot 10^{-8} - 2.3 \cdot 10^{-8}$	$1.8 \cdot 10^{-8}$	50%	24
181-184	2	1	0.8-2	0-1%	$1.3 \cdot 10^{-8} - 2.3 \cdot 10^{-8}$	$1.7 \cdot 10^{-8}$	50, 85, 90%	25-28
190-193	4	3	0.2-0.4	0%	$1.3 \cdot 10^{-7} - 1.7 \cdot 10^{-7}$	$1.5 \cdot 10^{-7}$	50%	46-64
193-196	2	1	0.2-0.3	0%	$1.1 \cdot 10^{-7} - 1.5 \cdot 10^{-7}$	$1.2 \cdot 10^{-7}$	50%	55-62

cont. Wang method				
Section (m)	K _f (m/s)	K range (m/s)	K, K mean (m/s)	Comments
64-67	$1.1 \cdot 10^{-4} - 2.6 \cdot 10^{-4}$	$4.8 \cdot 10^{-10} - 1.8 \cdot 10^{-9}$	$8.8 \cdot 10^{-10}$	Good type-curve match throughout the curve. The results using the Wang method for various H/Ho levels are similar. Good agreement between the two methods.
67-70	$4.9 \cdot 10^{-4} - 1.9 \cdot 10^{-3}$	$4.8 \cdot 10^{-9} - 3.7 \cdot 10^{-8}$	$1.8 \cdot 10^{-8}$	Unreliable values from the type-curve method because of poor matching despite the similarity of the data curves.
76-79	$4.3 \cdot 10^{-6}$		$3.8 \cdot 10^{-12}$	Curve match unreliable (required extrapolation of the upper part of the data curve). The results must be regarded as apparent values.
79-82	$1.2 \cdot 10^{-3} - 2.0 \cdot 10^{-3}$	$1.7 \cdot 10^{-8} - 4.0 \cdot 10^{-8}$	$2.2 \cdot 10^{-8}$	Similar data curves, but very difficult to match data curves.
166-169	$3.1 \cdot 10^{-6}$		$2.4 \cdot 10^{-12}$	Comments as for section 76-79.
178-181	$3.2 \cdot 10^{-4}$		$2.5 \cdot 10^{-9}$	Data curves very difficult to interpret. Only one test evaluated using the Wang method.
181-184	$3.7 \cdot 10^{-4} - 4.4 \cdot 10^{-4}$	$3.0 \cdot 10^{-9} - 4.1 \cdot 10^{-9}$	$3.5 \cdot 10^{-9}$	Good type curve match. Mean value from three tests. Wang method results from three tests are well collected.
190-193	$1.2 \cdot 10^{-3} - 2.4 \cdot 10^{-3}$	$1.8 \cdot 10^{-8} - 5.0 \cdot 10^{-8}$	$3.8 \cdot 10^{-8}$	Poor curve matching.
193-196	$1.8 \cdot 10^{-3} - 2.2 \cdot 10^{-3}$	$3.2 \cdot 10^{-8} - 4.6 \cdot 10^{-8}$	$3.8 \cdot 10^{-8}$	Similar data curves, but very poor match to the type curves.

* O = overpressure pulse applied
 U = underpressure pulse applied

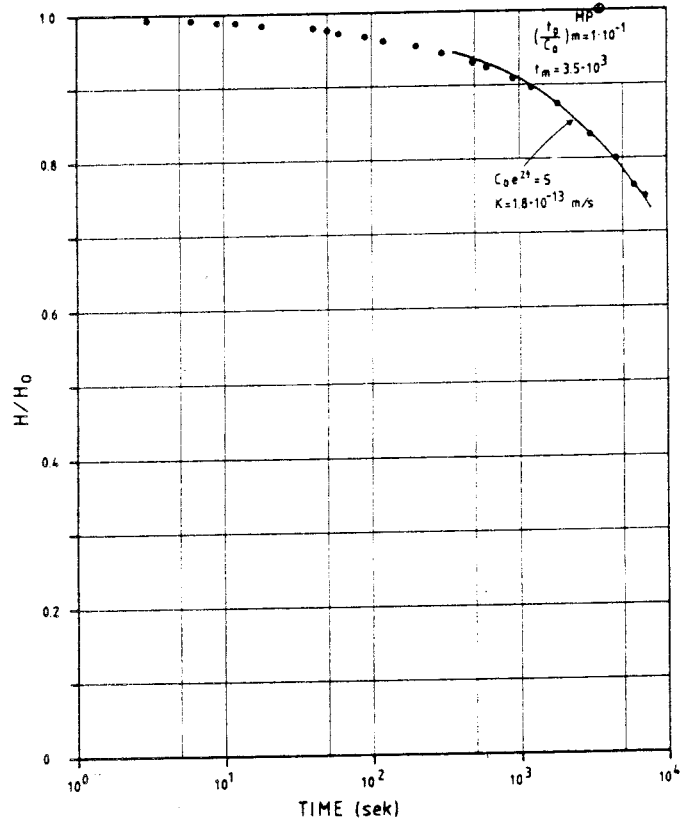


Fig. 10.7.2 Pressure pulse test; section 166 - 169 m.

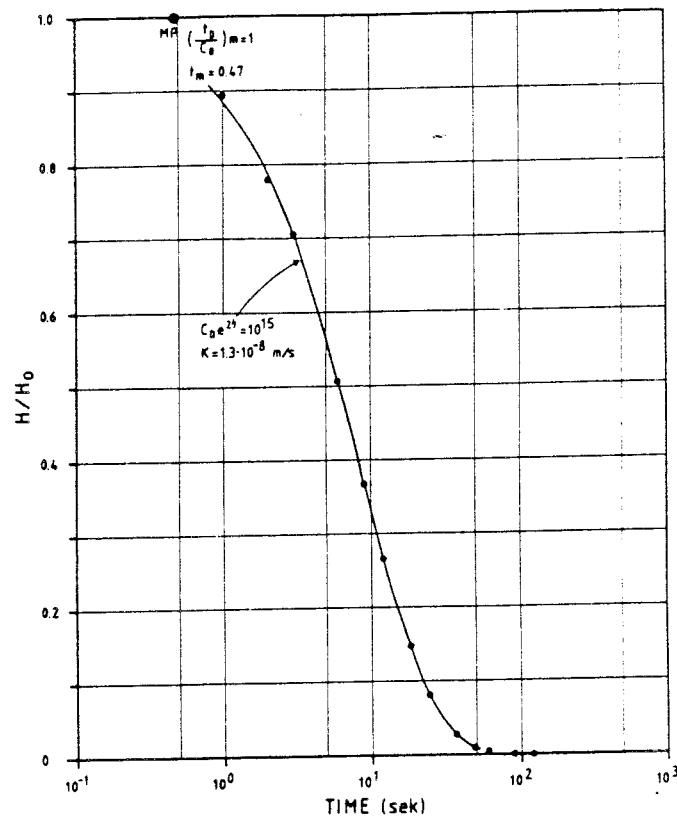


Fig. 10.7.3 Pressure pulse test; section 181 - 184 m.

10.8 Drill stem tests

10.8.1 Evaluation

In evaluating the drill stem tests, the flow and recovery periods were dealt with separately. The flow periods were evaluated in the same manner as the slug tests (see Section 10.6.1). The recovery (pressure fall-off) periods were evaluated in accordance with the Horner method (see Sections 8.4 and 5.2). As the data points follow a straight line, the hydraulic conductivity of the rock may be calculated in accordance with Eqn. (4-8) and the skin factor in accordance with Eqn. (8-9). The piezometric pressure in the section was also determined by extrapolating this line.

10.8.2 Results

The results from the tests are presented in Table 10.8. The greatest emphasis has been placed on the results from the second recovery period as this usually provides a more reliable evaluation than other periods.

The designations used are the same as in the presentation of the slug and pressure pulse tests, with the addition of:

H* deviation from the piezometric head existing in the section before sealing by the packers.

Data plots from the first flow period and second recovery period of the drill stem test in section 67 - 70 are presented, together with the type curve used and interpretation line, in Figs. 10.8.1a and b, respectively.

Table 10.8 Results from drill stem tests.

Section (m)	Flow period	Recovery period		H* (m)	Comments
	K (m/s)	K (m/s)	Skin factor ζ		
64-67	$6.0 \cdot 10^{-10}$	$3.7 \cdot 10^{-10}$	-0.6	0.24	
67-70	$2.0 \cdot 10^{-6**}$	$4.9 \cdot 10^{-7}$	-3.0	0.14	Two tests performed. Results from the flow periods are an average. The recovery periods during one test were too short to permit interpretation.
79-82	$3.2 \cdot 10^{-9}$	$>3.6 \cdot 10^{-10}$	-1.9	≈ 0	H* \pm 0.1, because of the flat intercept between the straight line and the time axis.
178-181	$2.8 \cdot 10^{-7}$	$5.1 \cdot 10^{-7}$	-1.2		Unreliable result because of too short periods. The straight line was extrapolated to H* = 0 for the recovery period.
181-184	$5.0 \cdot 10^{-9}$				It was only possible to interpret one of the flow periods. The recovery period was excessively affected by borehole storage and skin effects.
190-193	$6.5 \cdot 10^{-8}$	$>2.0 \cdot 10^{-8}$	<0.3	3.9	The recovery period was affected by borehole storage effects.
193-196	$7.9 \cdot 10^{-7}$	$3.7 \cdot 10^{-7}$	+8.0	0.47	

** Range of values of K: $1.3 \cdot 10^{-6}$ to $3.2 \cdot 10^{-6}$ m/s

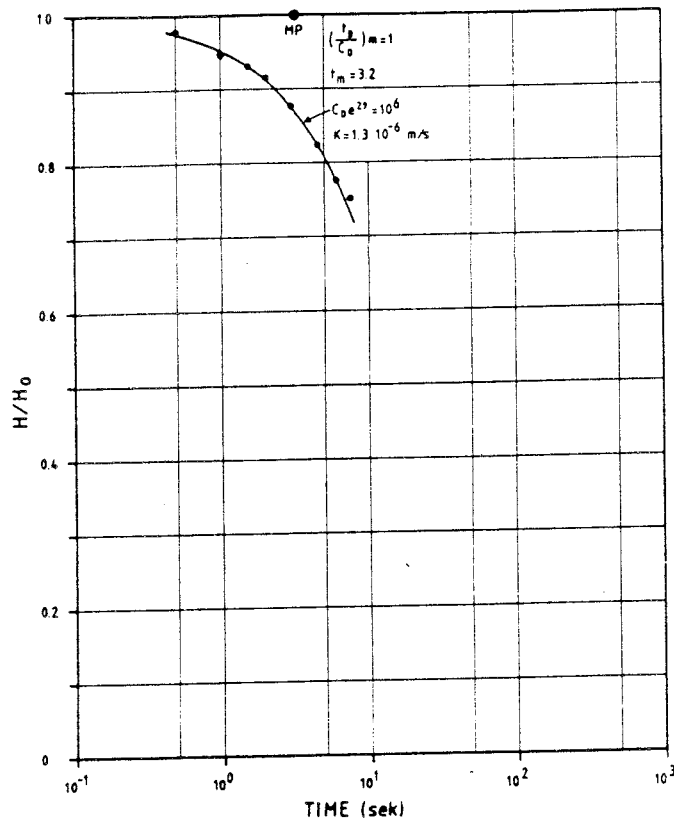


Fig. 10.8.1a Drill stem test, flow period; section 67 - 70 m.

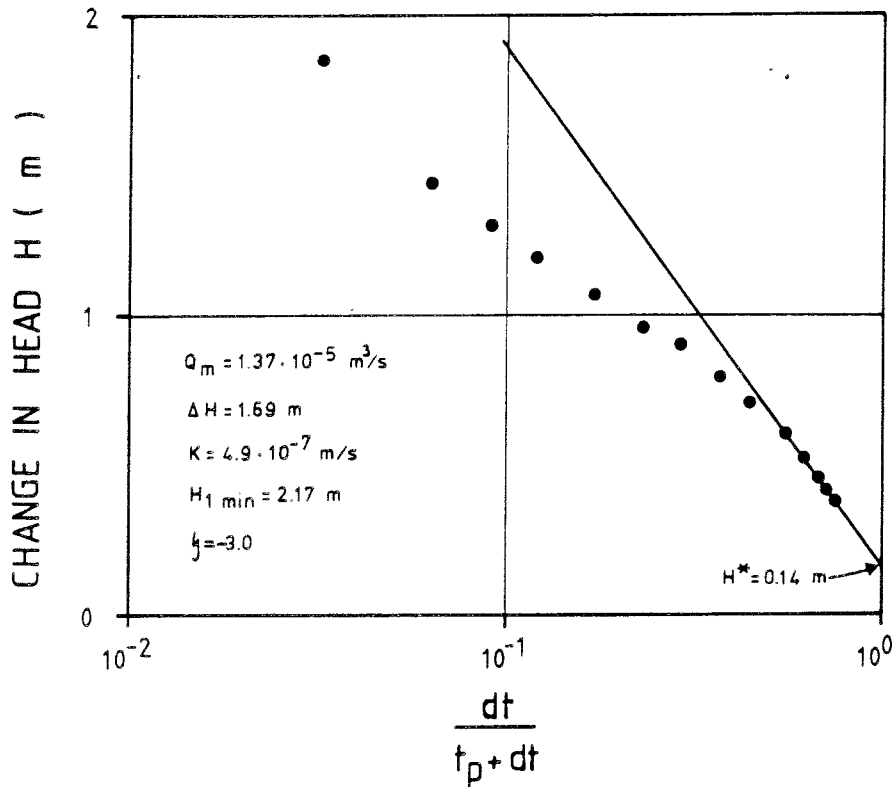


Fig. 10.8.1b Drill stem test, recovery period.
Section 67 - 70 m.

The applicability of the method of testing used is dependent on the magnitude of the hydraulic conductivity. As the test may be divided into two flow and recovery periods, the pressure range and test duration within each period may be too short in relation to the hydraulic conductivity of the test section. With only one flow period (to about 25% pressure dissipation) and a subsequent recovery period (to, if possible, 100% pressure dissipation) it should be possible to achieve more reliable evaluation, especially from the recovery period. It should be noted that data, particularly from the flow periods, are usually affected by borehole storage effects.

11. COMPARISONS OF DIFFERENT METHODS

This chapter deals with and compares the results obtained from all the injection, pressure fall-off and pulse response tests. The tests are first summarized and compared section by section, after which the methods are compared in relation to different ranges of conductivity. Finally, the applicability of the methods is reported and the selection of a method discussed.

11.1 Summary of results

The calculated hydraulic conductivity values are presented in Table 11.1. A varying number of methods for determining conductivity were used in the different sections. The time available and the limited applicability of individual methods to certain ranges of conductivity restricted the number of tests. If the method permitted it, the skin factor was also determined and is shown in Table 11.2.

Table 11.1 Summary of hydraulic conductivity values calculated from hydraulic tests in borehole Fi 6 at Finnsjön test site.

Section	Transient tests				Water loss measurements	Slug tests	Pressure pulse tests		Drill stem flow period	tests recovery period
	Constant flow-rate injectn.	fall-off	Constant pressure injectn.	fall-off			Type-curve method	Wang method		
64-67					$7.5 \cdot 10^{-10}$	$3.9 \cdot 10^{-10}$	$2.5 \cdot 10^{-9}$	$8.8 \cdot 10^{-10}$	$6.0 \cdot 10^{-10}$	$3.7 \cdot 10^{-10}$
67-70	$1.9 \cdot 10^{-7*}$	$1.8 \cdot 10^{-7}$	$1.7 \cdot 10^{-7}$		$5.3 \cdot 10^{-7}$	$7.6 \cdot 10^{-7}$	$8.0 \cdot 10^{-9}$	$1.8 \cdot 10^{-8}$	$2.0 \cdot 10^{-6}$	$4.9 \cdot 10^{-7}$
70-73	$9.0 \cdot 10^{-13}$	$< 9.2 \cdot 10^{-12}$			$2.2 \cdot 10^{-11}$					
76-79	$7.5 \cdot 10^{-13}$		$6.0 \cdot 10^{-14}$		$2.4 \cdot 10^{-11}$		$5.4 \cdot 10^{-14}$	$3.8 \cdot 10^{-12}$		
79-82	$1.5 \cdot 10^{-9}$	$7.9 \cdot 10^{-10}$	$1.3 \cdot 10^{-9}$	$7.5 \cdot 10^{-9}$	$7.5 \cdot 10^{-9}$	$3.5 \cdot 10^{-9}$	$4.7 \cdot 10^{-8}$	$2.2 \cdot 10^{-8}$	$3.2 \cdot 10^{-9}$	$> 3.6 \cdot 10^{-10}$
85-88	$4.4 \cdot 10^{-13}$				$< 1.8 \cdot 10^{-11}$					
166-169	$6.6 \cdot 10^{-13}$		$2.8 \cdot 10^{-14}$		$< 1.8 \cdot 10^{-11}$		$1.8 \cdot 10^{-13}$	$2.4 \cdot 10^{-12}$		
172-175			$1.8 \cdot 10^{-9}$	$9.4 \cdot 10^{-10}$	$5.4 \cdot 10^{-9}$					
178-181	$1.2 \cdot 10^{-6***}$		$2.3 \cdot 10^{-6}$		$5.7 \cdot 10^{-7}$	$1.2 \cdot 10^{-6}$	$1.8 \cdot 10^{-8}$	$2.5 \cdot 10^{-9}$	$2.8 \cdot 10^{-7}$	$5.1 \cdot 10^{-7}$
181-184	$4.1 \cdot 10^{-10}$		$4.1 \cdot 10^{-10}$	$1.6 \cdot 10^{-10}$	$2.1 \cdot 10^{-9}$	$5.5 \cdot 10^{-9}$	$1.7 \cdot 10^{-8}$	$3.5 \cdot 10^{-9}$	$5.0 \cdot 10^{-9}$	
190-193	$2.2 \cdot 10^{-9***}$		$2.6 \cdot 10^{-9}$	$1.3 \cdot 10^{-9}$	$2.1 \cdot 10^{-8}$	$1.7 \cdot 10^{-7}$	$1.5 \cdot 10^{-7}$	$3.8 \cdot 10^{-8}$	$6.5 \cdot 10^{-8}$	$> 2.0 \cdot 10^{-8}$
193-196					$1.2 \cdot 10^{-7}$	$1.3 \cdot 10^{-6}$	$1.2 \cdot 10^{-7}$	$3.8 \cdot 10^{-8}$	$7.9 \cdot 10^{-7}$	$3.7 \cdot 10^{-7}$

* $K_{fe} = 8.4 \times 10^{-7} \text{ m}^2/\text{s}$ *** $K_{fe} = 2.5 \times 10^{-8} \text{ m}^2/\text{s}$

** $K_f = \text{infinite}$

Table 11.2 Summary of values on the skin factor calculated from hydraulic tests in borehole Fi 6 at Finnsjön test site.

Section	T r a n s i e n t t e s t s				
	Constant injectn.	Flow-rate fall-off	Constant injectn.	Pressure fall-off	Drill-stem tests recovery
64-67					-0.6
67-70	-3.4	-4.1	-3.4		-3.0
70-73	---	<-1.5			
76-79	---		---		
79-82	-3.2	-3.2	-2.3	-3.1	-1.9
85-88	---				
166-169	---		---		
172-175			-2.3	-0.4	
178-181	4.8		---		-1.2
181-184	-2.7		-1.0	-0.3	---
190-193	-3.9		-3.2	-0.3	<0.3
193-196					8.0

--- not possible to determine the skin factor

Section 64 - 67 m

11.2 Section-by-section comparison

The calculated hydraulic conductivity values are dealt with section by section below and in Figs. 11.2.1 to 11.2.12. The value of K obtained using each method of testing is presented in the figures, where relevant, as ranges of the value of K calculated from the logarithmic average value.

The following tests were performed: water loss measurement, pressure pulse tests, slug tests and drill stem tests. The results from the tests are uniformly spread between 3.7×10^{-10} m/s (drill stem and pressure fall-off) and 2.5×10^{-9} m/s (pressure pulse test).

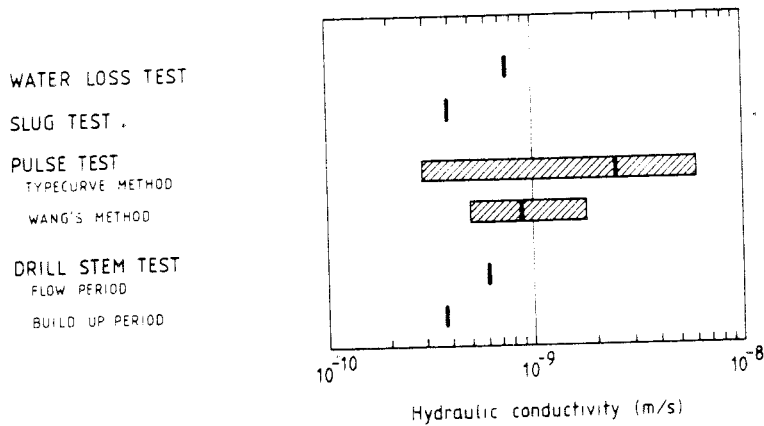


Fig 11.2.1 Summary of Results from Section 64 - 67 m

Section 67 - 70 m

All methods were performed in this section, except pressure fall-off after constant-pressure injection. The values for the hydraulic conductivity of the rock calculated from the transient injection tests and pressure fall-off after constant-flow injection were well collected between 1.7×10^{-7} and 1.9×10^{-7} m/s. The values for water loss measurements, slug tests and drill stem tests are in the range 4.9×10^{-7} to 2.0×10^{-6} m/s. The results from pressure pulse tests deviate. They range from 8.0×10^{-9} to 1.8×10^{-8} m/s, which is probably due to the conductivity in this section being above the proper measuring range of the method.

Section 70 - 73 m

The results obtained from water loss measurement (2.2×10^{-11} m/s), transient constant-flow injection tests (9.0×10^{-13} m/s) and subsequent pressure fall-off tests ($<9.2 \times 10^{-12}$) must be regarded as unreliable. Changes in temperature during the course of measurement, for example, may have affected the transient tests and the steady-state tests are close to the lower measurement limit.

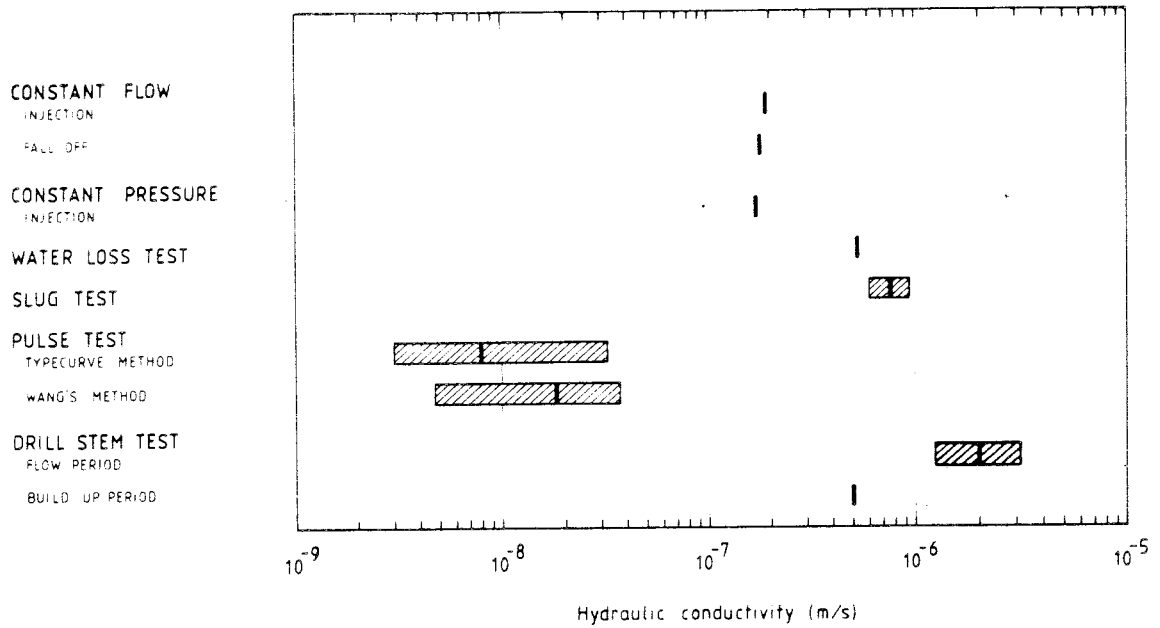


Fig 11.2.2 Summary of results from section 67 - 70 m.

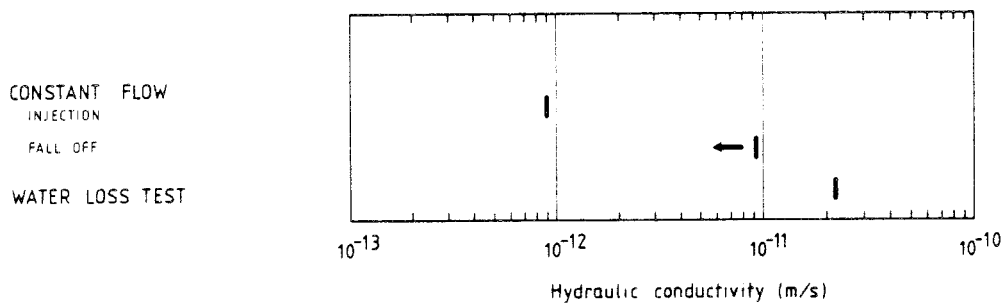


Fig 11.2.3 Summary of results from section 70-73 m.

Section 76 - 79 m

The results from the tests are between 5.4×10^{-14} and 2.4×10^{-11} m/s. The methods used were the two types of transient injection test, pressure pulse tests and steady-state tests. The comments to section 70 - 73 apply in other respects.

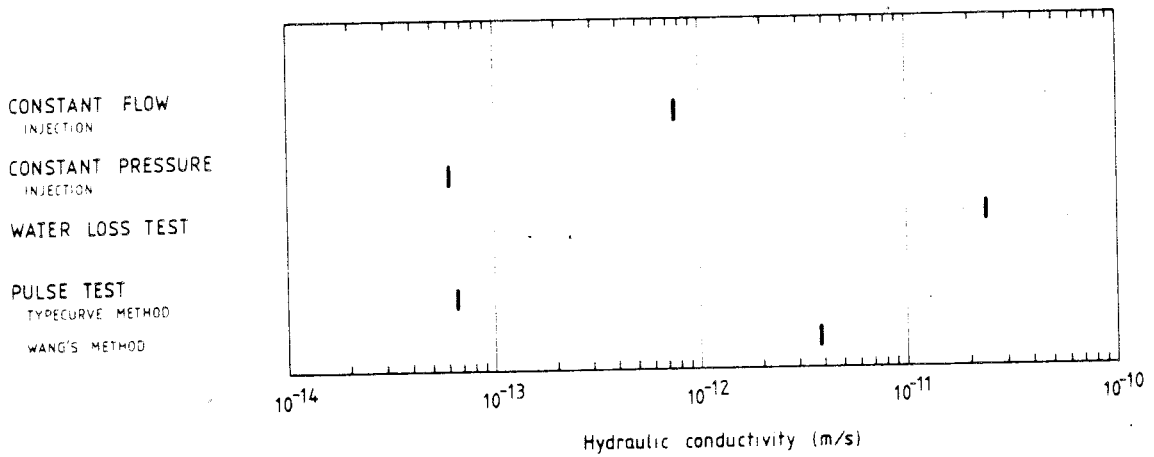


Fig 11.2.4 Summary of results from section 76-79 m.

Section 79 - 82 m

This is the only section in which all methods were performed. The transient injection tests and pressure fall-off tests provide results that were close, 7.5×10^{-10} to 1.5×10^{-9} m/s. The pressure fall-off period of the drill stem test provided the result $K > 3.6 \times 10^{-10}$ m/s, while the results from the remaining tests ranged from 3.2×10^{-9} to 4.7×10^{-8} m/s.

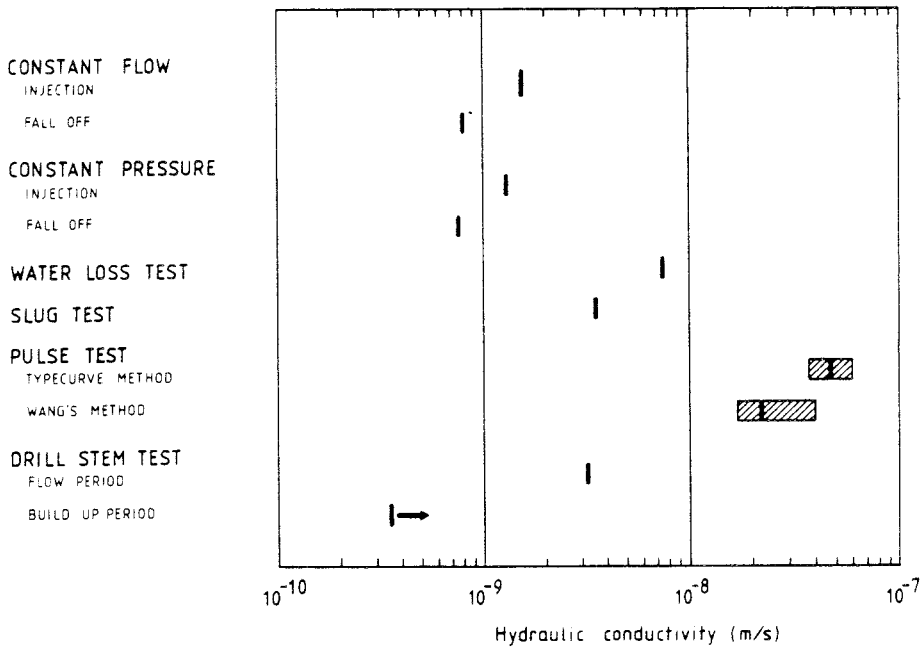


Fig. 11.2.5 Summary of results from section 79 - 82 m.

Section 85 - 88 m

Only water loss measurement and a transient constant-flow injection test were performed in this section. The water loss measurement gave a value of $K < 1.8 \times 10^{-11}$ m/s (lower measurement limit), while the transient test, which gave a value of K of 4.4×10^{-13} m/s, is very sensitive to small changes in temperature of the measuring system.

Section 166 - 169 m

The results from the methods used, water loss measurement, the transient injection tests and pulse response tests, range from 2.8×10^{-14} to 1.8×10^{-11} m/s, of which the latter value represents the lower measurement limit for water loss measurement. The results for this section may also be more or less affected by variations in temperature.

Section 172 - 175 m

In this section, a transient constant-pressure injection test, with subsequent pressure fall-off, and water loss measurement were performed. The values obtained range between 9.4×10^{-10} and 5.4×10^{-9} m/s.

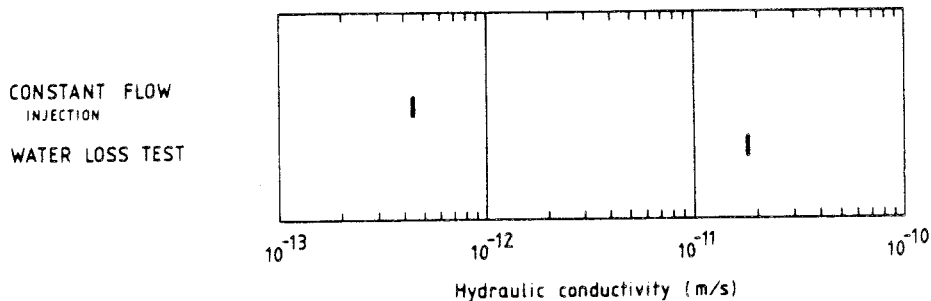


Fig. 11.2.6 Summary of results from section 85 - 88 m.

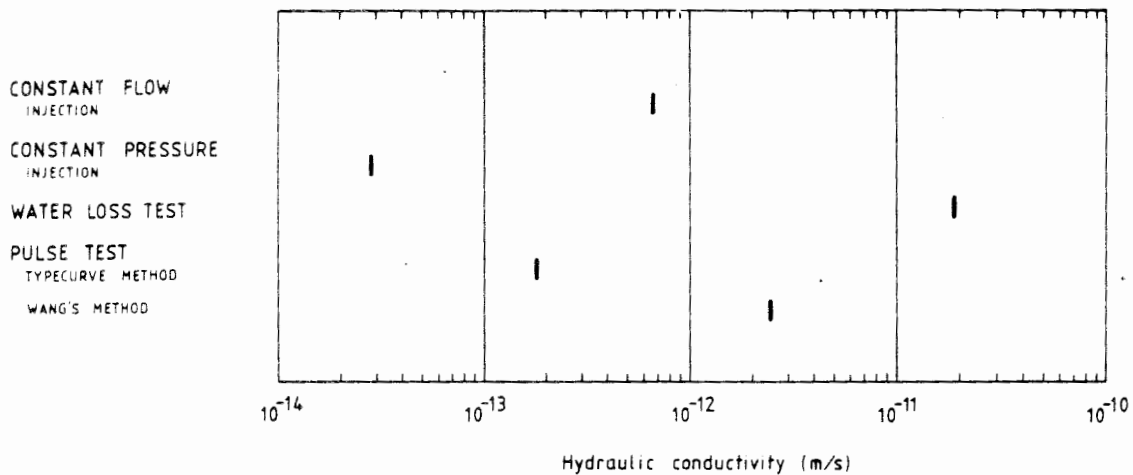


Fig. 11.2.7 Summary of results from section 166 - 169 m.

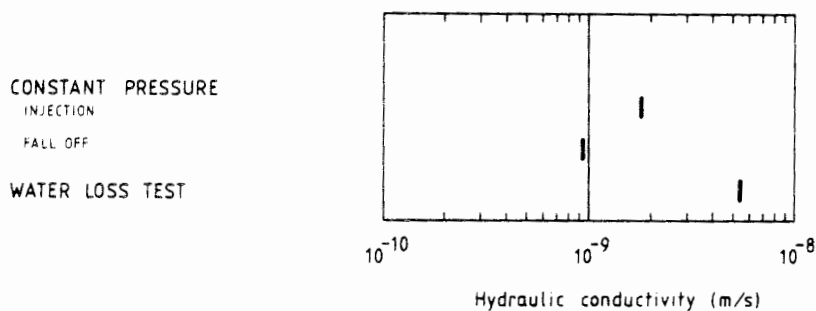


Fig. 11.2.8 Summary of results from section 172 - 175 m.

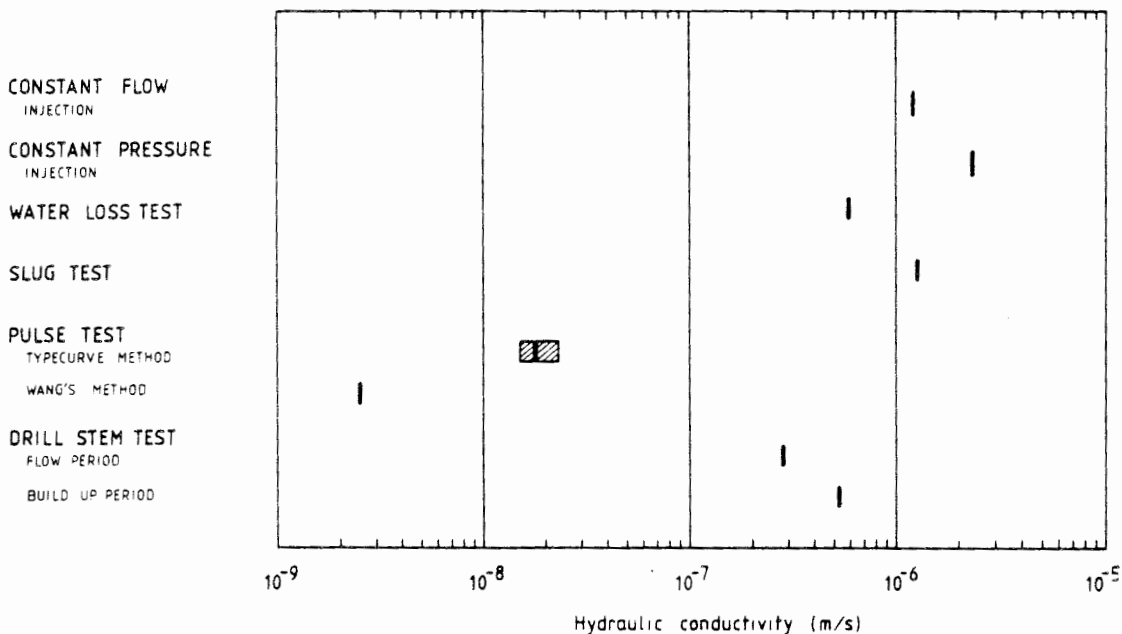


Fig. 11.2.9 Summary of results from section 178 - 181 m.

Section 178 - 181 m

All methods were performed in this section, with the exception of the pressure fall-off tests (the transient constant-pressure injection test was evaluated as a constant-flow test (see Section 10.3.2)). The results from the tests, except for the pressure pulse test, are relatively close, within the range from 2.8×10^{-7} to 2.3×10^{-6} m/s. The values of K obtained from the pressure pulse test were 1.8×10^{-8} m/s (type-curve method) and 2.5×10^{-9} m/s (Wang method).

Section 181 - 184 m

Only the pressure fall-off after injection with constant flow is missing from this section. The values of K for the two transient injection tests were the same, 4.1×10^{-10} m/s. The pressure fall-off test after injection at constant pressure was evaluated at 1.6×10^{-10} m/s, whereas the results from the remaining tests ranged from 2.1×10^{-9} to 1.7×10^{-8} m/s.

Section 190 - 193 m

All the tests were also performed in this section, with the exception of the pressure fall-off test after injection at constant pressure. The values obtained from pressure fall-off and transient injection tests range between 1.3×10^{-9} and 2.6×10^{-9} m/s. The results from the other tests range from 2.0×10^{-8} to 1.7×10^{-7} m/s.

Section 193 - 196 m

Only pulse response tests and water loss measurement were performed in this section. The results range between 3.8×10^{-8} m/s (Wang method) and 1.3×10^{-6} m/s (slug test).

11.3 Method comparisons

The results obtained from this work permit no statistical analyses, but certain conclusions may be drawn in conjunction with comparisons of the methods. The comparison applies to the special methods of testing, instruments and external conditions applicable during this work (see sections dealing with each method, Section 9.4).

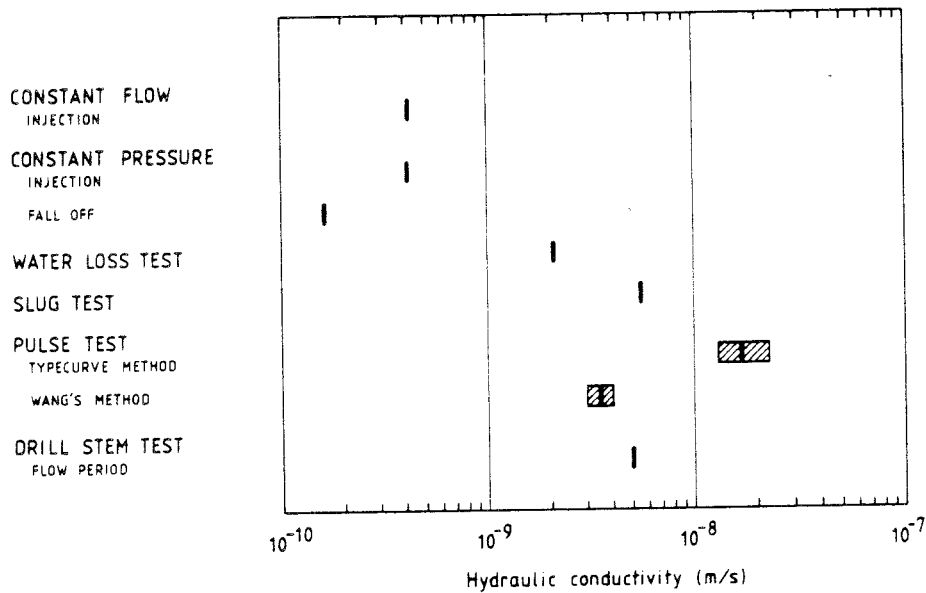


Fig. 11.2.10 Summary of results from section 181 - 184 m.

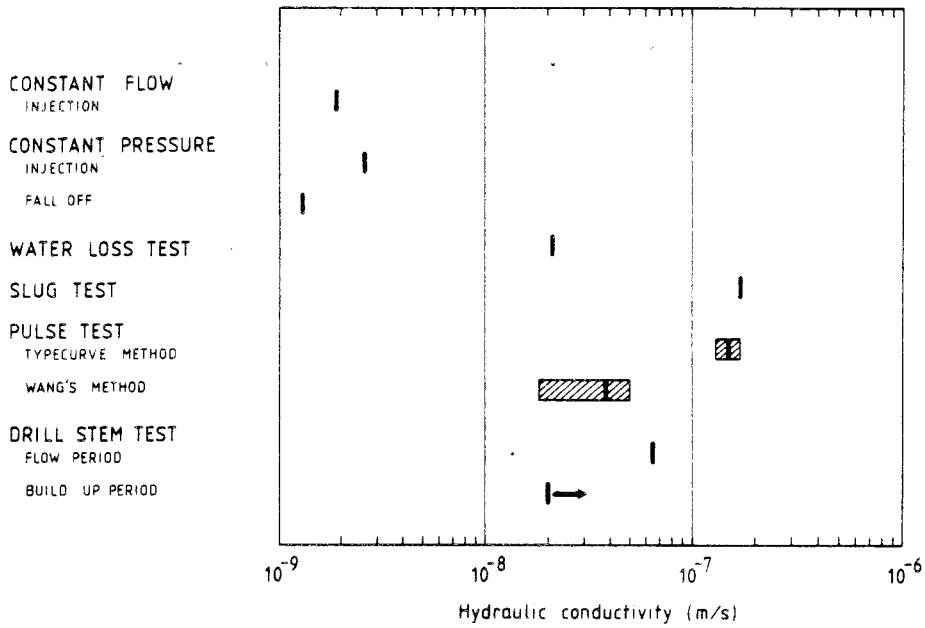


Fig. 11.2.11 Summary of results from section 190 - 193 m.

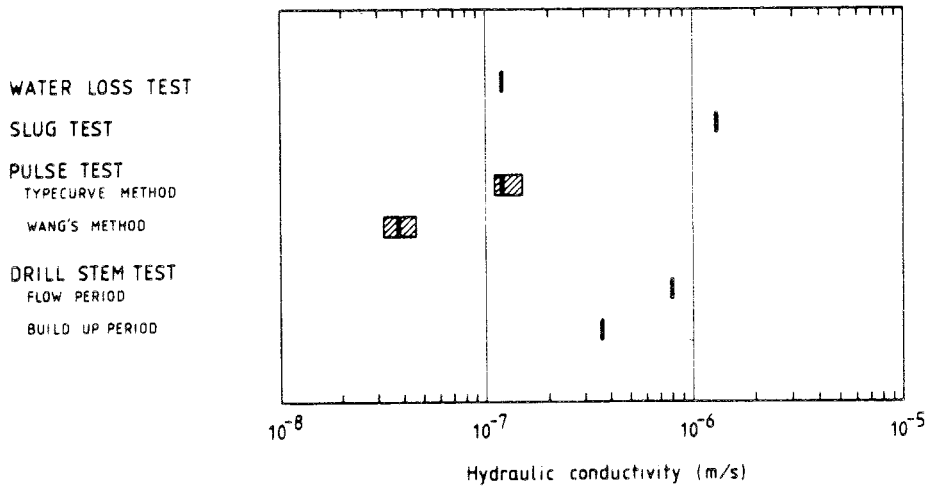


Fig. 11.2.12 Summary of results from section 193 - 196 m.

Transient constant-flow and constant-pressure injection tests

In this comparison the test at constant-pressure in section 178 - 181 is excluded since, as a result of the problem of maintaining the pressure constant, the test was evaluated as a constant-flow test.

If the conductivity values above 1×10^{-12} m/s are compared, which may be regarded as the lower measurement limit of the methods, the agreement is very good between the two methods. The greatest difference between the methods corresponds to a factor of 1.7, whereas the same result was obtained for one test section. The skin factor also shows good agreement.

Pressure fall-off - transient injection tests

Seven pressure fall-off tests were performed. Comparison between two of them and comparison with the transient injection tests as regards hydraulic conductivity shows that the agreement is good (if section 70 - 73 is excluded, as the result from this section may be regarded as unreliable because the pressure fall-off was too short, below 30%). The greatest difference corresponds to a factor of 2.6 (section 181 - 184).

Determination of the skin factor from the pressure fall-off tests resulted, as for the transient injection tests, in similar values.

Water loss measurements - transient injection tests

Both water loss measurements and transient injection tests were performed in ten sections. The results of steady-state tests from four of them are near to the lower measurement limit, leaving six sections for comparative studies.

In all cases but one (section 178 - 181) the hydraulic conductivity calculated from the water loss measurements is greater than that from the transient injection tests. The difference varies between factors 3 and 11. Corresponding equivalent hydraulic conductivities for the rock may be determined in sections in which the fracture conductivity was calculated. This value is always between the value calculated from the transient injection test and that from the water loss measurement. As the values of K from water loss measurements are based on an injection duration of 5 - 10 minutes (not full steady-state conditions), they should naturally provide a value that is too high (Andersson & Persson, 1985). On the other hand, the values of K from the water loss measurements are affected by any clogging effects adjacent to the section being tested. Instead, the effect of this is that the value of K from water loss measurements is too small in relation to that from the transient injection tests (cf. section 178 - 181). The skin factor cannot be determined from water loss measurements.

Slug tests - transient injection tests

Material for comparison of the hydraulic conductivity obtained using slug tests and transient injection tests is available from the five measurement sections. In all cases the value from the slug test is above the value of K from the transient injection test. Deviation is greatest in the case of low conductivity values. In one case the factor is 77 for a value of K of about 10^{-9} m/s (section 190 - 193), whereas agreement is good at values of K around 10^{-6} m/s.

Slug test - water loss measurement

Agreement is good in comparisons between slug tests and water loss measurement in seven measurement sections (factor: 1.9 - 2.6) for conductivity values below 10^{-8} m/s (3 sections). The variation is greater for conductivity values above 10^{-8} m/s with a factor of 1.4 - 11.

Pressure pulse tests: Type-curve method - Wang method

Pressure pulse tests were performed in nine measurement sections and evaluated using the type-curve method and the Wang method (Section 10.7.1). Because of the basic difference between the methods, evaluations of the same data curve may provide different results. In 6 out of 7 measurement sections the type-curve method provided the highest value of K in the conductivity range above 1×10^{-9} m/s. The difference ranges between factors 2.3 and 7.2. In the range of K below 1×10^{-9} m/s (2 sections), the Wang method provided results that were higher by the factors 13 and 70 respectively.

Pressure pulse tests - transient injection tests

Comparisons between pressure pulse tests and transient injection tests may be made in seven measurement sections. In two sections in which the results from the transient injection tests and also the other methods of testing, are collected around 5×10^{-7} m/s, the results from pressure pulse tests are lower by one or two orders of magnitude. This deviation is assumed to be due to the inapplicability of pressure pulse test in such high-conductivity sections.

For values of K between 10^{-10} and 10^{-8} m/s, on the other hand, the values from pressure pulse tests are 8 - 47 times higher than those from corresponding injection tests (the smallest deviation was obtained using the Wang method). In comparison with the other methods the results from these sections are well collected within a factor of ten. In two sections in which the K value is below 10^{-11} m/s, the results obtained using the Type-curve method agree best with those from the injection tests, but the scatter is very large.

Drill stem tests - transient injection tests

Results for comparison of drill stem tests and transient injection tests are available from five sections. Agreement is good in two of these sections, with the greatest difference corresponding to a factor of 3.5. The remaining sections provided results that were between 3 and 30 times higher than those from the injection tests. In only one case has it been possible to use the flow period for evaluation. The drill stem tests gave slightly higher skin factor values than the injection tests. Compared with the other pulse response tests (pressure pulse tests, slug tests), the values obtained using the drill stem test, above all from the recovery period, appear to be closer to those from the transient injection tests. The results would probably be improved by modifying the method of measurement as described earlier (see Section 10.8.2).

In the above comparison of pairs of tests, preference has been given to comparison of the transient injection tests with the other tests. This does not imply that the injection tests are absolutely correct, but they do represent a greater radius of influence because of their longer duration and they are also performed with continuous data collection and the possibility of separating the various flow regimes. This reduces the risk of incorrect interpretation and minimizes skin and borehole storage effects on the interpretation.

As noted above, it is not possible to compare only the calculated values of K obtained using the various methods. The duration of the test must be taken into account because it is principally the duration that determines the radius of influence of the test or the flow regime that is applicable. A fast method of testing always has inherent limitations in that it only permits investigation of the immediate surroundings of the borehole.

The pulse response tests and water loss measurements normally provide higher hydraulic conductivity values than transient injection tests. This may be explained in part by the

relatively short duration of the former tests. This normally implies that only a limited volume in the immediate vicinity of the borehole is investigated. This volume of material may be affected by skin effects (positive skin effect due to clogging or negative skin effect as a result of narrow fractures around the borehole caused in conjunction with drilling). The deviation in results between short tests and longer tests may also be regarded as a problem of the scale of investigation, c.f. representative elementary volume as discussed in section 2.5.

The deviation from the results of the transient injection tests is, however, relatively small for water loss measurements, and drill stem and slug tests. The pressure pulse test, which is the fastest method, appears to be less reliable. But it may be a suitable method for testing formations with very low permeability, with values of K below 10^{-10} m/s, in which, despite everything, the radius of influence of transient injection tests is small and it is impractical to perform the test.

11.4 Conclusions

The results and experience gained from the tests performed provide valuable information on the applicability and measurement accuracy of the methods. As pointed out at the beginning, the selection of a method for determining hydraulic conductivity must be made on the basis of the range of conductivity within which determination is to be carried out. In investigations of crystalline bedrock for storage of radioactive waste, interest is centred round the possibility of determining low hydraulic conductivities with great accuracy over a relatively wide range. This range may generally be said to comprise conductivity values below 10^{-7} m/s.

11.4.1 Applicability of the various methods

The results from this investigation were used as a basis for preparing the general summary contained in Fig. 11.4.1. This figure indicates the ranges of hydraulic conductivity within which the various methods are applicable. The presentation is based on the following conditions:

- o diameter of the borehole, $r_w = 56 \text{ mm}$
- o length of the measurement section, $L = 3 \text{ m}$
- o inside diameter of the pressure pipe, $r_{st} = 10 \text{ mm}$
- o maximum available test duration, $t = 180 \text{ min}$

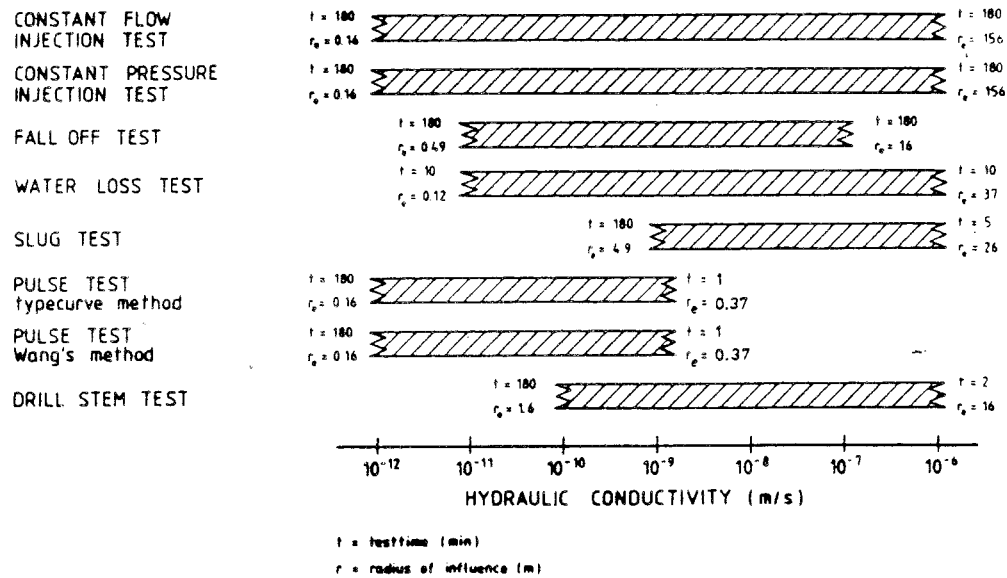


Figure 11.4.1 Ranges of hydraulic conductivity suitable for various methods of testing.

The measurement limits of the various methods are dependent on the special equipment used. For certain tests, such as the pulse response tests, the range limits are directly dependent on the duration of the test. The upper measurement limit is controlled by the minimum acceptable test duration to achieve adequate measurement accuracy, whereas the lower measurement

limit is determined by the maximum available test duration. The ranges presented may be regarded as guiding values and may be altered by, for example, the use of different equipment, different available test durations or other requirements on measurement accuracy.

Fig. 11.4.1 has been supplemented by the addition of the estimated radius of influence for the range limits of each method. This radius is dependent on the hydraulic conductivity and duration of the test. The radius of influence calculated in accordance with Eqn. (4-11) is for homogeneous conditions. The actual radius of influence for sections containing extensive fractures would probably be much larger (see Section 10.1.1).

Different methods provide different quantities of information on the properties of the bedrock and the groundwater flow conditions adjacent to the borehole. Table 11.3 gives an overall picture of the type of information provided by the various methods. An X indicates that the method is capable of providing corresponding information. (X) indicates that the information may be derived secondarily or that it is uncertain whether the information can be obtained.

11.4.2 Selection of a method

Various criteria for selecting a method are tabulated in Table 11.4, which also contains an indication of how well the various methods satisfy the stipulated conditions. Tables 11.3 and 11.4 show that transient constant-pressure injection tests and subsequent pressure fall-off tests are regarded as being the methods of hydraulic testing that best satisfy the stipulated demand criteria.

Table 11.3 Type of information obtained from the various hydraulic tests.

Type of test	K	ζ	K_{fe}	x_f	H^*	Hydr. bound.	Flow regime
A Transient injection test							
A1 constant flow-rate	X	X	X	X		X	X
A2 constant pressure	X	X	X	X		X	X
B Pressure fall-off test	X	X	X	X	X	X	(X)
C Water loss measurement	X						
D Slug test	X	(X)					
E Pressure pulse test							
E1 Type-curve method	X	(X)					
E2 Wang method		(X)	X				
F Drill stem test	X	X			X		

Table 11.4 Criteria for selecting a method, based on the results obtained. The method designations are as in Table 11.3.

Criterion	A1	A2	B	C	D	E1	E2	F
o Applicable over a large measuring range	X	X	X	X				
o Does not affect the measurement section by deformation etc.		X		X				
o Easy to evaluate	X	X	X	X				
o Large radius of influence	X	X	X	(X)				
o Provides several parameters in addition to value of K	X	X	X					X
o Short test duration					X	X	X	X

The advantages of transient constant-pressure injection tests include:

- o Possibility of measuring over a large range of hydraulic conductivities
- o The equipment used is more suitable for injection tests at constant pressure than those with constant flow. This is because the range of measurement with transient flow is larger than for a corresponding transient pressure.
- o The pressure is constant in the measurement section and in the entire system. This implies negligible borehole storage effects and small deformation of the equipment while measurements are being made.
- o Evaluation is based on a large number of measured data points.
- o Large radius of influence which should provide representative values on the hydraulic parameters.
- o Possibility of determining the skin factor and effective borehole radius and the possibility of determining approximately the apparent fracture parameters, such as fracture length (aperture) and the product, $K_f e$, in the event of any vertical fractures.
- o Certain qualitative information may be obtained, such as identification of hydraulic boundaries and different flow regimes.

For transient injection tests to provide the maximum amount of information, a minimum injection time of 2 hours is recommended. This implies that a greater volume of rock is affected by the test and not only the immediate vicinity of the borehole as is the case with shorter tests. The amount of rock affected is dictated not only by the duration of the test but principally by the hydraulic parameters of the rock. The representativeness of the calculated conductivity values should

be seen in relation to the volume of rock investigated. The greater the volume of rock, the greater the probability that the conductivity values are representative mean values for the rock tested and its inhomogeneity and that the formation may be regarded as an equivalent, homogeneous and porous medium, which is normally assumed in evaluation. If the volume of rock investigated is sufficiently large, the magnitude of its hydraulic parameters will not change significantly if the volume is further increased (see Section 2.5).

If a test duration of 2 hours is selected, it should in most cases (for sections with a hydraulic conductivity above about 10^{-11} m/s) be possible to evaluate the results from the semi-log graphs considering the temporal constraints applicable to this type of evaluation. This evaluation method is regarded as giving the most reliable determination of the hydraulic conductivity and skin factor. Evaluation from the log-log graphs and linear graphs may be used as a complement, to identify different flow regimes and determine the properties of any fractures. But correct evaluation of the subsequent pressure fall-off test also requires that the injection period be sufficiently long.

The pressure fall-off tests imply a possibility of comparing and checking corresponding values obtained from the injection tests and to determine the piezometric pressure in the section. The duration of pressure fall-off should be of the same order of magnitude as the injection time.

12. HYDRAULIC TESTING FOR SITE CHARACTERIZATION

On the basis of the literature studies and field tests described in this report a hydraulic test programme was in 1981 prepared for use in the SKB study site investigations carried out later. The aim of these site investigations was to clarify the suitability of various rock formations as final repositories for Swedish highly radioactive waste. These investigations were performed using the same methods in all areas. A certain amount of programme updating is though being carried out continuously. This 'standard programme' comprises geological and geophysical methods as well as hydrogeological ones and is reported in the SKB series of Technical Reports: Ahlbom et al (1983c) (methods) and Almén et al (1983) (equipment). A brief presentation of the hydraulic test configuration and equipment selected for site characterization investigations is given below, together with a few words about the scope of measurements and the quantity of data that is available today.

12.1 Hydraulic tests - methods and equipment

12.1.1 Test sequence

In the hydrogeological part of the standard programme, the hydraulic tests constitute the most extensive operation. As noted in the comparisons of methods (Chapter 11), the transient injection test at constant pressure and subsequent pressure fall-off test is regarded as being the most suitable one for this type of investigation.

For the transient single-hole injection tests, a double packer system was used. The standard packer spacing was 25 m. The entire length of the borehole was first tested with this spacing. Detailed tests of sections with higher hydraulic conductivities were then conducted using a packer spacing of 5 or 10 m. At some of the sites, short-duration (steady-state) tests were also performed with a packer spacing of 2 or 3 m.

The transient test sequence may be divided in three different phases with the following durations:

- * Packer sealing 0.5 hours
- * Water injection test 2 hours
- * Pressure fall-off test 2 hours

After the packer sealing has been completed a constant pressure, in general 200 kPa (20 m), is applied to the test section. In highly-conductive sections such a high injection pressure may not be achieved and a lower pressure level must be selected.

12.1.2 Test-equipment

Two different sets of test equipment were used for the single-hole injection tests, a steel pipe string system (Fig. 12.1.1) which is an improved version of the one used in Finnsjön and an umbilical hose system (Fig. 12.1.2). In the latter system the test sequence is automatically controlled while the steel pipe system is manually controlled. The two equipment systems described here was used in the site investigations between 1981-1985. During 1986 both systems have been further improved (Almén et al 1986).

Pipe string system

During the injection phase a constant head is maintained in the test section by manual regulation of the flow rate. The manually recorded flow meter covers the range in flow rate of $1.5 \times 10^{-9} \text{ m}^3/\text{s}$ - $2.5 \times 10^{-4} \text{ m}^3/\text{s}$.

Data collection and processing are schematically presented, in the block diagram in Fig. 12.1.3. The central unit of the data acquisition system is a data logger; data are stored on cassette tapes. Pressure and temperature values are assembled in the

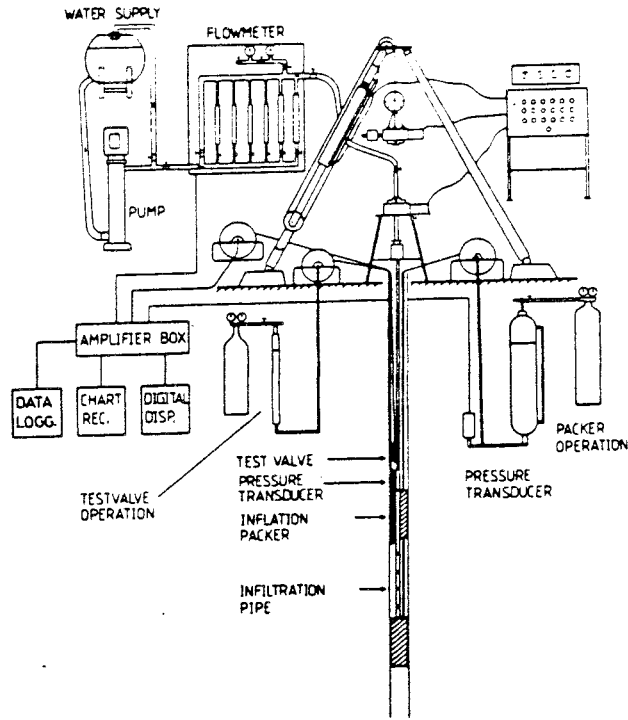


Figure 12.1.1 Schematic arrangement of steel tubing system.

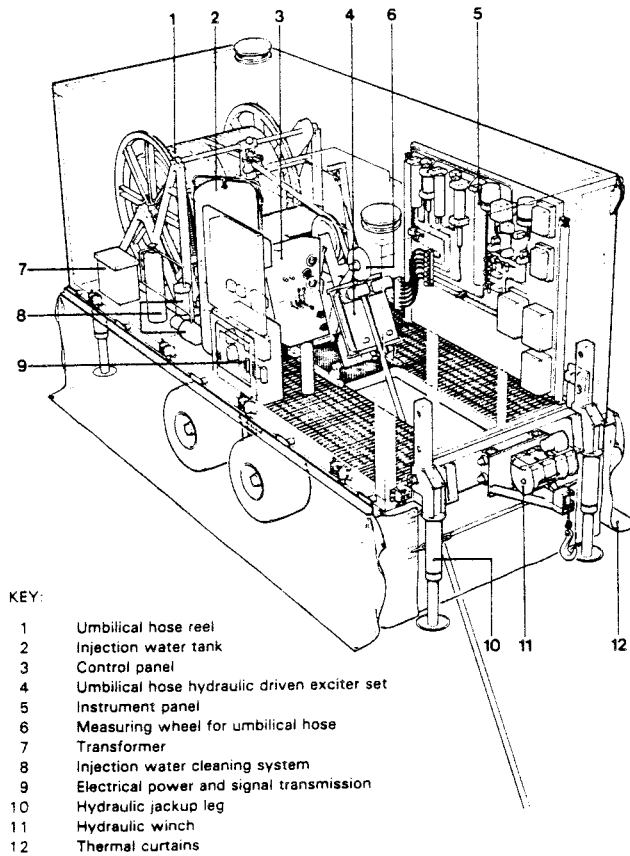


Figure 12.1.2 Instrument trailer - Umbilical hose system.

data logger with scanning at time intervals that increase in steps.

The absolute pressure in the section before injection is entered manually as digital data (multimeter value) as well as all section identification data and indications of the different phases of the test sequence. In parallel with the data logger the test data are also registered on a chart recorder, primarily for the test operator to keep control of the progress of the test.

Cassette tapes with test data are sent to the main computer centre for layback. Together with punched flow rate data, the test data are processed for plotting of the data graphs and are then stored. In addition to the injection pressure and flow rate data which are used for evaluation, the packer inflation pressure and water temperature are also plotted. Variations in these parameters may sometimes influence the tests (mainly in low-conductivity sections).

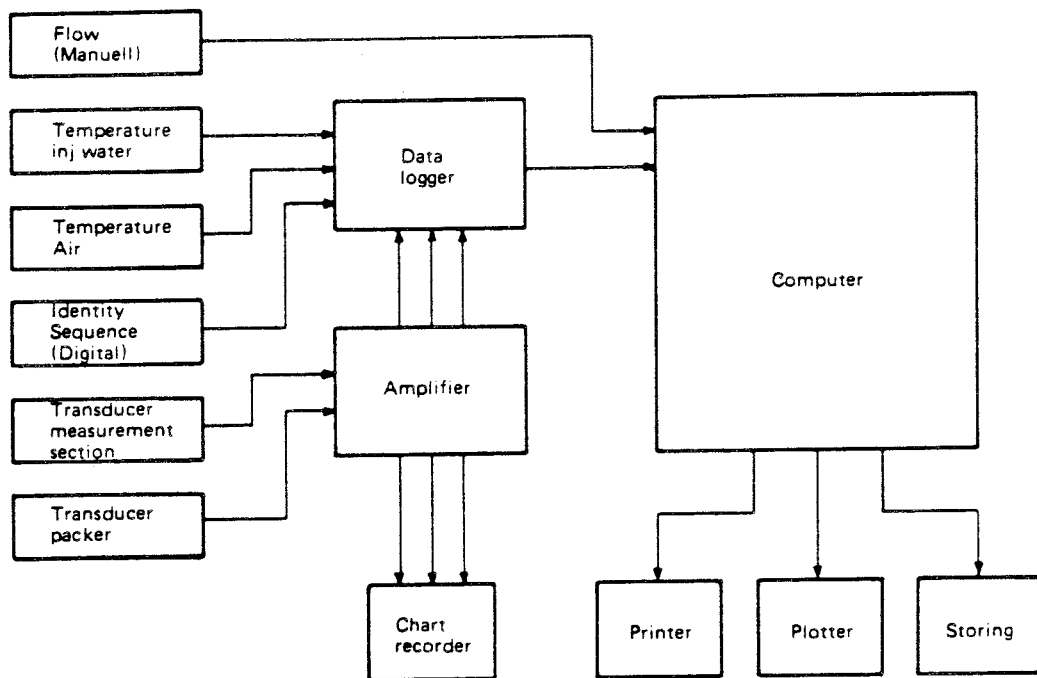


Figure 12.1.3 Data flow and handling scheme.

Umbilical hose system

This equipment consists of two units, an instrument trailer and a recording trailer. On the recording trailer the recording equipment is built around a field computer, which is connected via an expansion box to a data logger and a tape recorder. The computer also works directly on-line with a plotter. This system enables control of the test method to be used and recording and storage of information while the test is in progress. After the test has been completed, the data tape may again be read into the computer for plotting. In order to make fast evaluations in the field there is another computer which enables plotting of the test data at the same time as acquisition of new test data is carried out by the other system.

The umbilical hose system is because of its automatic test control and data acquisition a sophisticated version of the steel mandrel system. However, because of somewhat different ranges (on pressure transducers and) on the flow meters the measuring range is somewhat narrower with this equipment. There are three flow meters in the system. They represent three strictly delimited measuring ranges, together covering a range of 0.5×10^{-9} to $1.2 \times 10^{-4} \text{ m}^3/\text{s}$.

12.1.3 Description of graphs plotted

The different phases of the transient injection tests (packer sealing, injection and fall-off) are documented on several graphs (A, B and C graphs respectively). The A graphs (A1 - A5) show in linear time background information and overview of flow and section pressure during the entire test sequence. The B graphs (B1 - B4) reflect the test data from the injection phase and the C graphs (C1 - C2) from the fall-off phase.

A1: This plot shows the pressure change after lowering of the packer system to a certain level and also during the packer inflation phase. The plot also shows the flow meter calibration (cannula test).

A2 - A3: These graphs describe the changes in flow rate and pressure in the test section respectively, during the entire test sequence.

A4 - A5: These plots show the (free) groundwater level in the borehole, barometric and packer inflation pressure together with the temperature of the outdoor air, injection water at the surface and groundwater in the test section.

B1: This graph illustrates the pressure in the test section during the injection phase versus test time on a semi-log graph.

B2 - B3: These plots describe the reciprocal of the flow rate versus the fourth root of time and versus time on a log-log scale respectively.

B4: This graph shows changes in the flow rate (and reciprocal of the flow rate) versus time in a log-log graph.

C1: This plot shows the pressure fall-off in the test section after cessation of injection in a log-log graph.

C2: This plot describes the pressure fall-off in a Horner graph (semi-log).

12.2 Hydrogeological data base

Five sites in various parts of the country (Fig. 12.2.1) were investigated in accordance with the standard programme for which this report contained the basic information. On average 10 - 15 core boreholes were subjected to hydraulic testing on each site. The boreholes were 56 mm in diameter and reached a vertical depth of 300 - 900 metres. Most boreholes were drilled with an inclination of 60 - 70 degrees to the horizontal, which implies a total borehole length of some 700 - 800 metres. Thus, a total of about 30,000 borehole-metres were tested, corresponding to 1,200 hydraulic tests in 25-m sections. To which should be added detailed measurements in 5 and/or 10-m sections, of which there were some 400.

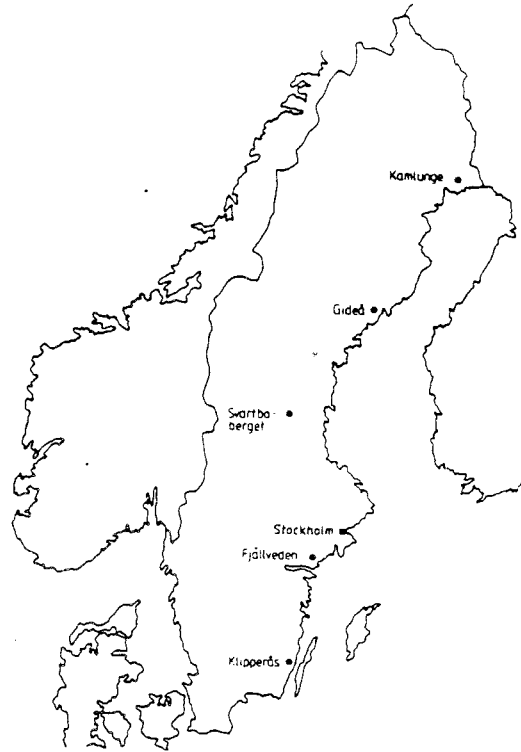


Figure 12.2.1 Location of study sites investigated 1981-1985.

Data from these investigations, together with all other hydrogeological information, is stored in a data base that is being built up (Gentzschein, 1986). The aim is that this data base will be used to store all geoscientific information from research being carried out to ensure that the highly radioactive waste can be stored in a reassuring manner in a final repository located in crystalline rock.

The hydrogeological data base contains data from the following investigation operations:

- Hydraulic tests
- Groundwater level mapping
- Piezometry
- Interference tests
- Tracer tests
- Hydraulic data classified into groups (rock mass, fracture zones, etc.)

The following information from transient single-hole injection tests is available in the data base:

- o Raw data from each section tested, as text files in a VAX 750 computer.
- o Borehole information, such as identifying code, X, Y and Z coordinates, borehole length, casing length and diameter, superficial deposits, inclination and declination of boreholes, core diameter, borehole deviation logs, and events that occurred in the borehole prior to testing (borehole history).
- o Records of the type of equipment used in each test (pipe string/umbilical hose system) and the instrumentation (types of pressure gauge, flow meter, packer, data logger, etc.).
- o Data calculated from each test, including:

hydraulic conductivity (steady state)	(KSS)
hydraulic conductivity from injection phase	(KI)
hydraulic conductivity from fall-off phase	(KT)
representative hydraulic conductivity	(K)
transmissivity ($T = K \times L$)	(T)
skin factor calculated from injection phase	(ZI)
skin factor calculated from fall-off phase	(ZT)
environmental pressure in the section tested	(PS)
- o Outer hydraulic boundary conditions (positive or negative boundary), identification of dominant flow regime(s) during the test and assessment of the quality of the test.

REFERENCES

- Agarwal, R. G., Al-Hussainy, R and Ramey, H. J., Jr., 1970: An Investigation of Wellbore Storage and Skin Effect in Unsteady Liquid Flow: I. Analytical Treatment, Soc. Pet. Eng. J., Sept. 1970, pp 279-290. Trans., AIME, 249.
- Agarwal, R.G., Carter, R.D. and Pollock, C.B., 1979: Evaluation and Prediction of Performance of Low-Permeability Gas Wells Stimulated by Massive Hydraulic Fracturing. J. Pet. Tech., March 1979, pp 362-372. Trans., AIME, 267.
- Agarwal, R.G. 1980: A new Method to Account for Producing Time Effects When Drawdown Type Curves are Used to Analyze Pressure Buildup and Other Test Data. Soc. Pet. Eng. Paper 9289.
- Ahlbom, K., Carlsson, L., Carlsten, L-E., Duran, O., Larsson, N-Å., Olsson, O., 1983 a: Evaluation of the Geological, Geophysical and Hydrogeological Conditions at Fjällveden. - KBS Technical Report TR 83-52.
- Ahlbom, K., Albino, B., Carlsson, L., Danielson, J., Nilsson, G., Olsson, O., Sehlstedt, S., Stejskal, V., Stenberg, L. 1983 b: Evaluation of the Geological, Geophysical and Hydrogeological Conditions at Kamlinge, - KBS Technical Report TR 83-54.
- Ahlbom, K., Carlsson, L. and Olsson, O. 1983c: Final disposal of spent nuclear fuel-geological, hydrogeological and geophysical methods for site characterization. SKBF/KBS Technical Report TR 83-43.
- Ahlbom, K., Andersson, P., Ekman, L., Gustafsson, E., Smellie, J. and Tullborg, E-L. 1986: Preliminary investigations of fracture zones in the Brändan area, Finnsjön study site. SKB Technical Report TR 86-05.

- Almén, K-E., Ekman, L. och Olkiewicz, A., 1979: Försöksområdet vid Finnsjön. Beskrivning till berggrunds- och jordartskartor. SKBF-KBS Teknisk rapport TR 79-02. (In Swedish)..
- Almén, K-E. et al, 1983: Final disposal of spent nuclear fuel - equipment for site characterization. SKBF/KBS Technical Report TR 83-44.
- Almén, K-E. et al, 1986: Equipment for geological, geophysical, hydrogeological and hydrochemical characterization. SKB Technical Report TR 86-16.
- Andersson, P. and Klockars, C-E., 1985: Hydrogeological investigations and tracer tests in a well-defined rock mass in the Stripa mine. SKB Technical Report TR 85-12.
- Andersson, J-E. och Carlsson, L., 1980: Hydrauliska tester i berg. Del 1: Influens av brunnsmagasin och skin vid olika transienta tester. SKBF-KBS Arbetsrapport AR 80-28. (In Swedish).
- Andersson, J-E. and Persson, O., 1985: Evaluation of single-hole hydraulic tests in fractured crystalline rock by steady-state and transient methods. SKB Technical Report TR 85-19.
- Andersson, J-E. och Hansson, K., 1986: Hydrauliska tester i berg. Del 6: Interferenstester. SKB Arbetsrapport AR 86-22. (In press).
- Barker, B.J. and Ramey, H.J., 1978: Transient Flow to Finite-Conductivity Vertical Fractures. Soc. Pet. Eng. Paper 7489.
- Black, J.H., Holmes, D.C. and Noy, D.J., 1982: Hydraulic testing in granite using the sinusoidal wave method. Rep. Inst. Geol. Sci. ENPU 82-4.

- Bredehoeft, J.D. and Papadopoulos, I.S., 1980: A Method for Determining the Hydraulic Properties of Tight Formations. *Water Resour. Res.* v 16, no 1 1980, pp 233-238.
- Brigham, W.E. et al., 1980: The Analysis of Spherical Flow with Wellbore Storage. *Soc. Pet. Eng. Paper* 9294.
- Carlsson, L., Gentschein, B., Gidlund, G., Hansson, K., Svenson, T. och Thoregren, U., 1980: Kompletterande permeabilitetsmätningar i Finnsjöområdet. KBS Teknisk Rapport TR 80-10. (In Swedish).
- Carlsson, L., Winberg, A. and Grundfelt, B., 1983: Model calculations of the groundwater flow at Finnsjön, Fjällveden, Gideå and Kamlunga. KBS Technical Report TR 83-45.
- Carlsson, L. and Olsson, T., 1985 a: Hydrogeological and Hydrogeochemical Investigations in Boreholes-/Shut-in tests. Stripa Project. Internal Report 85-08.
- Carlsson, L. and Olsson, T., 1985 b: Hydrogeological and Hydrogeochemical Investigations in Boreholes-Injection-recovery tests and interference tests. Stripa Project. Internal Report 85-09.
- Carnahan, C.L., Delany, J.M., Long, J.C.S., Silva, R.J., Watkins, D.J., White, A.F. and Wilson, C.R. 1983: Selected hydrologic and geochemical issues in site characterization for nuclear waste disposal. NUREG/CR - 2983.
- Chatas, A.T., 1966: Unsteady Spherical Flow in Petroleum Reservoirs. *Soc. Pet. Eng. J.*, June 1966, pp 102-114.
- Cinco-L., H., Samaniego, F. and Dominquez, N., 1978: Pressure Behavior for a Well with a Finite-Conductivity Vertical Fracture. *Soc. Pet. Eng. J.*, Aug 1978, pp 253-264.
- Cinco-L., and Samaniego, F., 1981: Transient Pressure Analysis for Fractured Wells. *J. Pet. Tech.*, Sept 1981, pp 1749-1766.

- Cooper, H.H., Bredehoeft, J.D. and Papadopoulos, I.S., 1967: Response of a Finite-Diameter Well to an Instantaneous Charge of Water. *Water Resour. Res.* v 3, no 1 (1967) pp 263-269.
- Culham, W.E. 1974: Pressure Buildup Equations for Spherical Flow Regime Problems. *Soc. Pet. Eng. J.*, Dec. 1974, pp 545-555.
- Doe, T. and Remer, J., 1982: Analysis of Constant-head Well Tests in Nonporous Fractured Rock. *Proceedings of the 3rd International Well-testing Symposium, Berkeley, California.*
- Earlougher, R.C., Jr., 1977: *Advances in Well Test Analysis.* - Soc. Pet. Engr. Monograph Series, Vol 5. SPE, Dallas 1977.
- Ershagi, I. and Woodbury, J.J., 1985: Examples of Pitfalls in Well Test Analysis. *J. Pet. Tech.*, Feb. 1985, pp 335-341.
- van Everdingen, A.F. and Hurst, W., 1949: The Application of the Laplace Transformation to Flow Problems in Reservoirs. *Trans., AIME* (1949) 186, pp 305-324.
- van Everdingen, A.F., 1953: The skin effect and its influence on the productive capacity of a well. *Trans., AIME* 198, pp 171-176.
- Faust, C.R. and Mercer, J.W., 1984: Evaluation of slug tests in wells containing a finite-thickness skin. *Water Resour. Res.*, 20(4), pp 504-506.
- Forster, C.B. and Gale, J.E., 1980: Injection versus pressure pulse borehole tests in fractured crystalline rocks- observations and recent experience. *Proc. 3rd Invitational Well-Testing Symposium, March 26-28, 1980, LBL-12076, Berkeley, California.*
- Gale, J., 1975: A numerical field and laboratory study of flow in rocks with deformable fractures.- Ph. D. thesis, University of California, Berkeley.

- Gale, J.E., 1982: Assessing the Permeability Characteristics of Fractured Rock. Geological Society of America, Special Paper 189.
- Gentzschein, B., 1986: Description of hydrogeological data in SKB's database. SKB Technical Report TR 86-22. (In press).
- Gringarten, A.C., Ramey, H.J., and Raghavan, R., 1974: Unsteady-State Pressure distribution created by a Well with a single Infinite-conductivity Vertical Fracture. Soc. Pet. Eng. J., Aug. 1974, pp 347-360. Trans AIME 257.
- Gringarten, A.C., Bourdet, D., Landel, P.A., and Kniazeff, V., 1979: A comparison between different skin and wellbore storage type curves for early-time transient analysis. Soc. Pet. Eng. Paper 8205.
- Gringarten, A.C., 1982: Flow Test evaluation of Fractured Reservoirs. Geological Society of America, Special Paper 189.
- Gringarten, A.C., 1984: Interpretation of Tests in Fissured and Multilayered Reservoirs with Double-Porosity Behavior: Theory and Practice. J. Pet. Tech., April 1984, pp 549-564.
- Guppy, K.H., Cinco-L., H. and Ramey, H.J., 1981: Transient Flow Behavior of a Vertically Fractured Well Producing at Constant Pressure. Soc. Pet. Eng. Paper 9963.
- Gustafsson, E. and Klockars, C-E., 1981: Studies on groundwater transport in fractured crystalline rock under controlled conditions using nonradioactive tracers. KBS Technical Report TR 81-07.
- Heimli, P., 1974: Bergarters porositet, permeabilitet, fuktutvidgelse, kapillaritet. Norges Tekniske Högskole, Rapport 12, Trondheim.
- Hsieh, P.A., Neuman, S.P., Stiles, G.K. and Simpson, E.S., 1985: Field determination of the Three-Dimensional Hydraul-

- lic Conductivity Tensor of Anisotropic Media, Part 2: Methodology and Application to Fractured Rocks. Water Resour. Res. Vol 21, No 11, Nov. 1985.
- Hurst, W., 1953: Establishment at the Skin Effect and its impediment to fluid flow into a well bore. Pet. Eng B-6-B-16. October, 1953.
- Jacob, C.E. and Lohman, S., 1952: Nonsteady flow to a well of constant drawdown in an extensive aquifer. Trans. Am. Geophys. Union, Aug. 1952 pp 559-569.
- Karasaki, K., Witherspoon, P.A. and Long, J.C.S., 1985: A New Analytical Model for Fracture-Dominated Reservoirs. Soc. Pet. Eng. Paper 14171.
- Long, J.C.S., J.S. Remer, C.R. Wilson and Witherspoon, P.A., 1982: Porous media equivalents for networks of discontinuous fractures, Water Resour. Res. 18(3), pp 1253-1265, 1982.
- Louis, D., 1969: A study of groundwater flow in jointed rock and its influence on stability of rock masses. Rock Mech. Res. Rept. No 10, Imp. Coll., London, 90pp.
- Maini, T., 1971: In situ Hydraulic parameters in Jointed Rock - Their Measurement and Interpretation. - Ph. D. Thesis, Imp. Coll. of Sci. and Technol., London 1971.
- de Marsily, G., 1985: Flow and transport in fractured rocks - Connectivity and scale effect. Proceedings of the 17th International Congress of I.A.H., Tuscon, Arizona, January 7-11, 1985.
- Mavor, M.J. and Cinco-L., H., 1979: Transient Pressure Behavior of Naturally Fractured Reservoirs. Soc. Pet. Eng. Paper 7977.
- Mc Whorter, D.B. and Sunada, D.K., 1977: Ground-water hydrology and hydraulics. Water Resources Publications, Fort Collins, Colorado.

- Moench, A.F., 1984: Double-Porosity Models for a Fissured Groundwater Reservoir With Fracture Skin. *Water Resour. Res.*, Vol. 20, No. 7, July 1984, pp 831-846.
- Moench, A.F. and Hsieh, P.A., 1985: Analysis of Slug Test Data in a well with Finite Thickness Skin. *Proceedings of the 17th International Congress of I. A. H.*, Tuscon, Arizona, January 7-11, 1985.
- Moran, J.H., and Finklea, E.E., 1962: Theoretical Analysis of Pressure Phenomena Associated with the Wireline Formation Tester. *J. Pet. Tech.*, Aug. 1962, pp 899-908. *Trans., AIME*, Vol. 225.
- Morrison, D. C., 1981: The validity of the Horner plot for tight reservoirs. Paper presented at the 32nd annual technical meeting of the Petroleum Society of CIM in Calgary, May 3-6, 1981.
- Moye, D.G., 1967: Diamond Drilling for Foundation Exploration. *Civil Eng. Trans., Inst. Eng. Australia*, Apr. 1967, pp 95-100.
- Najurieta, H.L., 1980: A Theory for Pressure Transient Analysis in Naturally Fractured Reservoirs. *J. Pet. Tech.*, July 1980, pp 1241-1250.
- Neuzil, D.E., 1982: On Conducting the Modified "Slug" Test in Tight Formations. *Water Resour. Res.* v. 18, No 2, pp. 439-441.
- Norton, D., Knapp, R. 1977: Transport Phenomena in Hydrothermal Systems: The Nature of Porosity. - *American Journal of Science*, Vol 1277, Oct 1977, pp 913-936.
- Olkiewicz, A., Scherman, S. och Kornfält, K-A., 1979: Kompletterande berggrundsundersökningar inom Finnsjö- och Karlshamnssområdena. *KBS Teknisk Rapport TR 79-05*. (In Swedish).

- Onyekonwu, M.O. and Horne, R.N. 1983: Pressure Response of a Reservoir with Spherically Discontinuous Properties. J. Pet. Tech., Nov. 1983, pp 2127-2134.
- Papadopoulos, I.S., Bredehoeft, J.D. and Cooper, H.H., 1973: On the Analysis of 'Slug Test' Data. Water Resour. Res. v 9, no 4, 1973 pp 1087-1089.
- Raghavan, R., 1976: Some Practical Considerations in the Analysis of Pressure Data. J. Pet. Tech, Oct 1976, pp 1256-1268. Trans AIME 269.
- Raghavan, R., 1980: The Effect of Producing Time on Type Curve Analysis. J. Pet. Tech., June 1980, pp 1053-1064.
- Raghavan, R. and Ohaeri, C. 1981: Unsteady Flow to a Well Produced at a Constant Pressure in a Fractured Reservoir. Soc. Pet. Eng. Paper 9902.
- Ramey, H.J., Agarwal, R.G. and Martin, I., 1975: Analysis of 'Slug Test' or DST Flow Period Data. J. Cdn. Pet. Tech., July-Sept. 1975, pp 37-42.
- Ramey, H.J., 1982: Pressure Transient Testing. J. Pet. Tech. July 1982, pp 1407-1413.
- Rasmuson, A. and Neretnieks, I., 1986: Radionuclide transport in fast channels in crystalline rock. SKB Technical Report TR 86-13.
- Rosato, N.D., Bennet, C.O., Reynolds, A.C. and Raghavan, R., 1982: Analysis of Short-Time Buildup Data for Finite-Conductivity Fractures. J.Pet. Tech., Oct. 1982, pp 2413-2422.
- Serra, K., Reynolds, A.C. and Raghavan, R. 1983: New pressure transient analysis methods of naturally fractured reservoirs. J. Pet. Tech., Dec. 1983, pp 2271-2283.

- Snow, D.T., 1968: Rock fracture spacing, openings and porosities. *J. Soil Mech. and Foundation Eng. ASCE* 94 (1968), pp 73-91.
- Streltsova, T.D., 1976: Hydrodynamics of ground-water flow in a fractured formation. *Water Resour. Res.*, vol 12, No 3, pp 405-414.
- Streltsova, T.D., 1983: Well pressure behavior of a naturally fractured aquifer. *Soc. Pet. Eng. J.*, Oct 1983, pp 769-780.
- Theis, V., 1935: The relation between the lowering of the piezometric surface and the rate and duration of discharge of a well using ground-water storage. *Trans. Am. Geophys. Union*, Vol 16, pp 519-524.
- Updegraff, C.D., Kennedy, K.G., Bakr, A.A., Culver, C.N. and Kam, J.T., 1980: Testing Low to Moderately Transmissive Zones in Basalt Rocks. Third Invitational Well Testing Symposium, March 1980, California. (Abstract).
- Uraiet, A.A. and Raghavan, R., 1980 a: Unsteady Flow to a Well Producing at constant Pressure. *J. Pet. Tech.* Oct. 1980, pp 1803-1812.
- Uraiet, A.A. and Raghavan, R., 1980 b: Pressure Buildup Analysis for a Well Produced at constant Bottomhole pressure. *J. Pet. Tech.*, Oct. 1980, pp 1813-1824.
- Wang, J.S.Y., Narasimhan, J.N., Tsang, C.F. and Witherspoon, P.A., 1977: Transient Flow in Tight Fractures. *Proceedings of Invitational Well-Testing Symposium (Oct. 1977)*, Berkeley, California.
- Öqvist, U. and Jämtlid, A., 1984: Geofysiska parametermätningar på borrhärnsprov från Finnsjön, Sternö och Stripa. KBS Arbetsrapport AR 84-16. (In Swedish).

DESIGNATIONS

2b	(m)	aperture for horizontal fracture
C	(m ³ /Pa)	borehole storage coefficient
c	(Pa ⁻¹)	compressibility
c _b	(Pa ⁻¹)	bulk vertical compressibility of the rock
c _{eff}	(Pa ⁻¹)	effective compressibility
c _w	(Pa ⁻¹)	compressibility of water
e	(m)	fracture aperture
F _{CD}	(-)	dimensionless fracture capacity
g	(m/s ²)	acceleration of gravity
H	(m)	change in head (or alternatively head) in the section tested
H ₀	(m)	injection head applied for injection tests or alt. momentary head change for pulse response tests
H'	(m)	residual head change (alt. head) in the section tested
H _s	(m)	head change due to skin effect
H*	(m)	extrapolated head difference
ΔH	(m)	change in head per logarithmic cycle
h	(m)	head change (or alt. head) some distance from the section tested
K	(m/s)	hydraulic conductivity
K _f e	(m ² /s)	fracture conductivity
L	(m)	length of test section
m		slope of straight line in linear graph
p	(Pa)	pressure
p _i	(Pa)	static pressure
p ₀	(Pa)	pressure immediately before start of injection/drawdown test
p _p	(Pa)	pressure immediately before stop of injection/drawdown test
p _{wf}	(Pa)	pressure during injection/drawdown test
p _{ws}	(Pa)	pressure during fall-off/build-up test
Δp	(Pa)	change in pressure per logarithmic cycle
Δp _s	(Pa)	pressure change due to skin effect
Q	(m ³ /s)	total flow rate
Q _f	(m ³ /s)	formation flow rate

Q_p	(m^3/s)	flow rate immediately before stop of injection/ drawdown test
$Q(t)$	(m^3/s)	transient flow rate
$\Delta(1/Q)$	(s/m^3)	change in reciprocal flow rate per logarithmic cycle
q	(m/s)	specific flow rate per unit area
r	(m)	radial distance from section tested
r_c	(m)	radius of casing or tubing
r_f	(m)	radius of inner zone with linear flow (section 7.2)
r_i	(m)	radius of influence
r_w	(m)	radius of borehole or well
r_{wf}	(m)	effective borehole radius (radial flow)
r_{ws}	(m)	effective borehole radius (spherical flow)
S	(-)	storage coefficient
S_s	(m^{-1})	specific storage coefficient
T	(m^2/s)	transmissivity
t	(s, min)	time after start of injection/drawdown test
t_p	(s, min)	duration of injection/drawdown test
t_{pp}	(s, min)	pseudo-duration of injection/drawdown test
dt	(s, min)	time after stop of injection/drawdown test
V	(m^3)	volume
V_{tot}	(m^3)	cumulative volume of water injected or produced
V_u	(m^3)	volume per unit length of borehole or tubing
V_w	(m^3)	volume of test section
x_f	(m)	half-length of vertical fracture
z	(m)	vertical coordinate
ϕ	(-)	porosity
ϕ_k	(-)	kinematic porosity
ϕ_e	(-)	effective porosity
ρ	(kg/m^3)	density
ρ_w	(kg/m^3)	density of water
μ	(Ns/m^2)	dynamic viscosity
ζ	(-)	skin factor

Subscript:	D	refers to corresponding dimensionless parameter
	e	refers to single fracture or fracture plane
	f	refers to fracture system
	m	refers to rock matrix
	m	refers to matchpoint-coordinate
	s	refers to skin zone
	t	refers to total
	w	refers to borehole or well





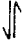
APPENDIX, CORE LOGS

Core logs for the upper 216 m of borehole Fi 6 (from Olkiewicz et al 1979).

List of symbolsFractures

- 30 Coated fractures, the figures denote the angle against the borehole direction.
- Fractures with fresh irregular surfaces.

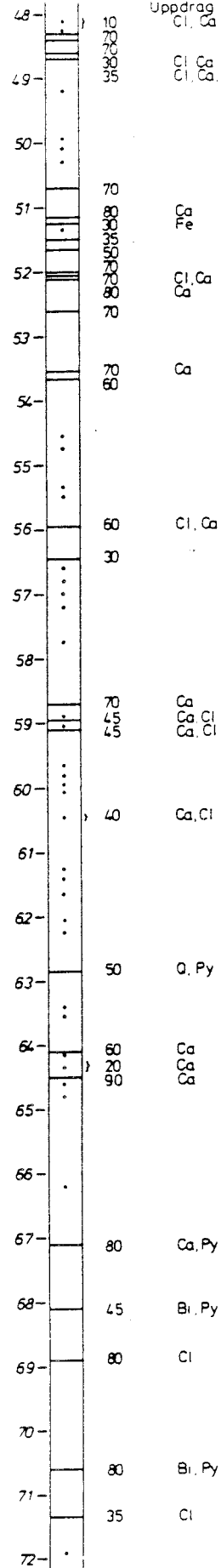
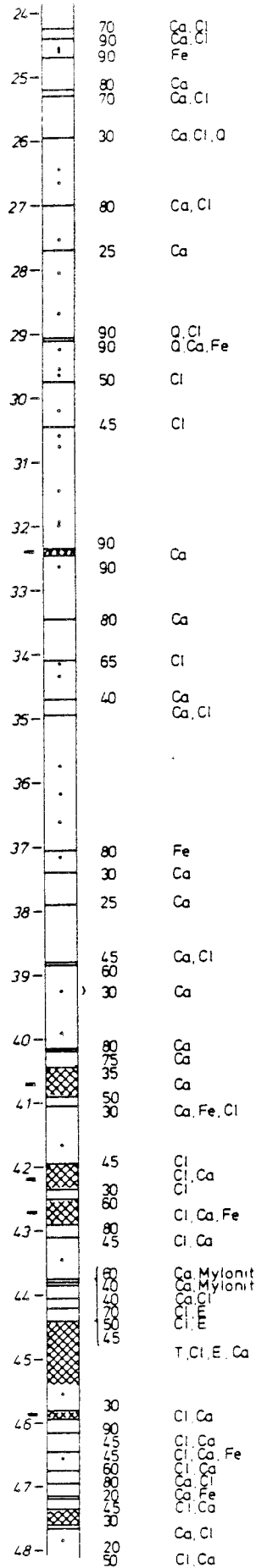
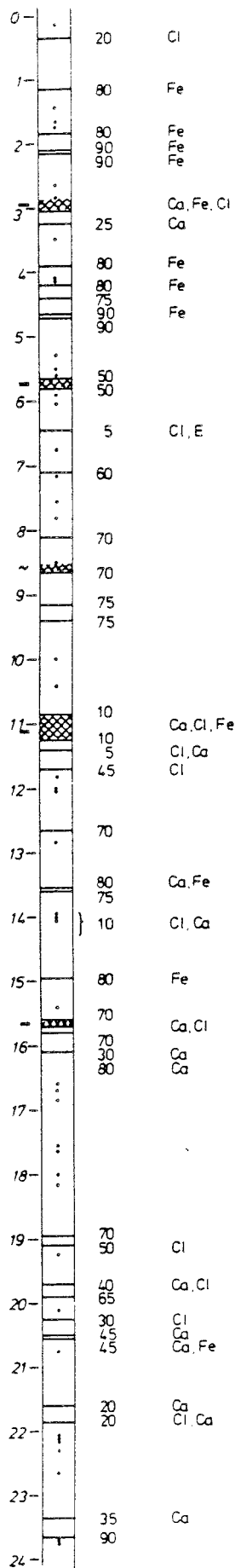
Zones of weakness

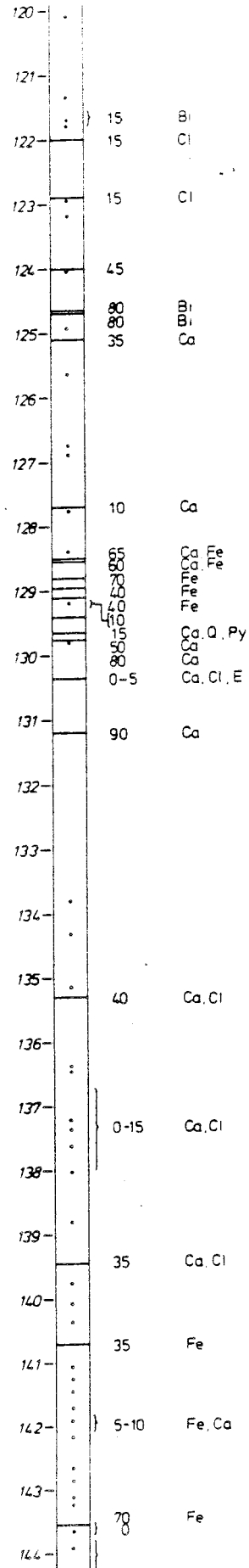
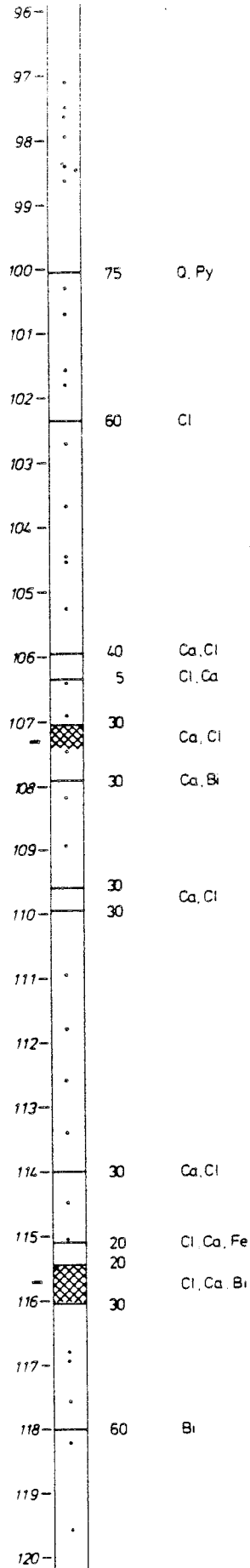
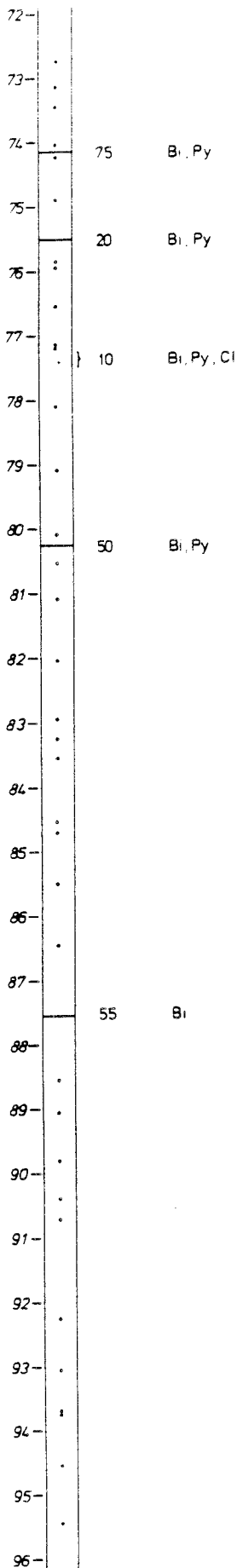
-  Crushed zone
- =  Fracture zone with mainly coated fractures with a separation of fracture core intersections less than 10 cm.
-  Fracture zone with fresh irregular fractures with a separation of fracture core intersections less than 10 cm.
-  Shear zone
-  Slickenside

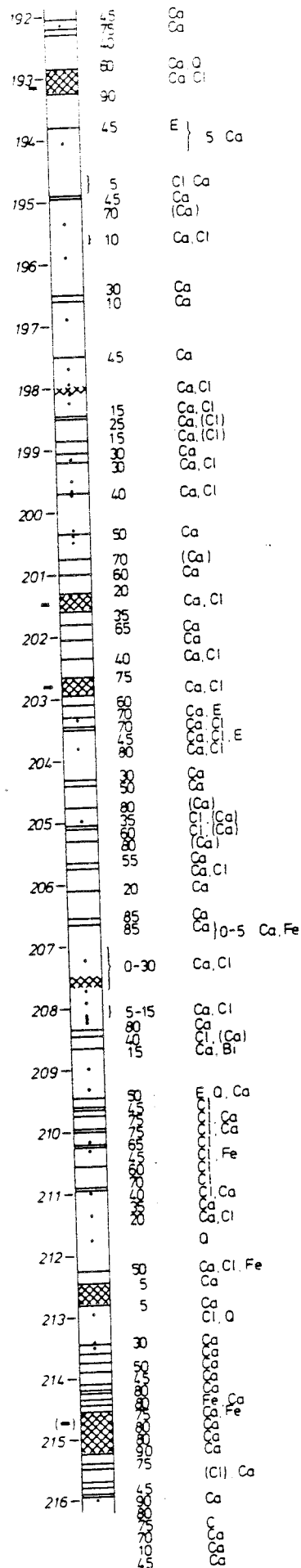
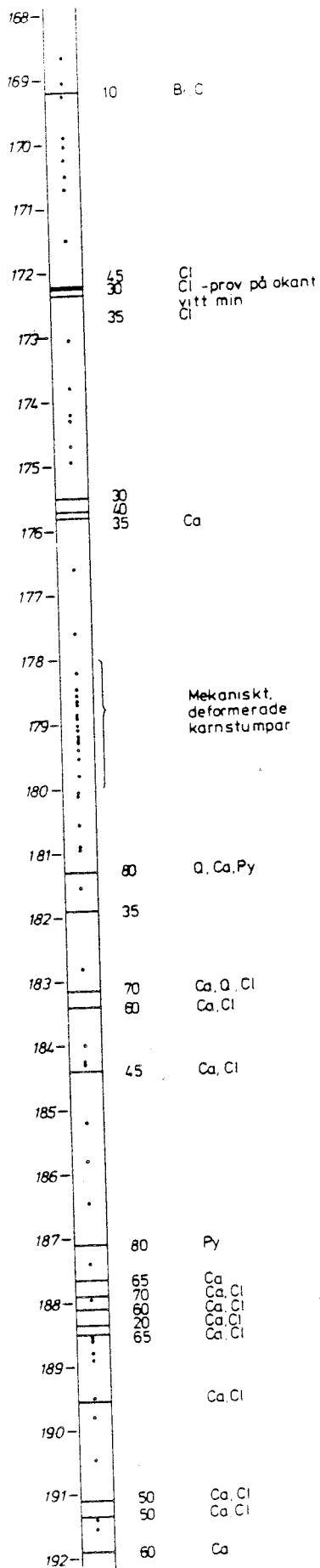
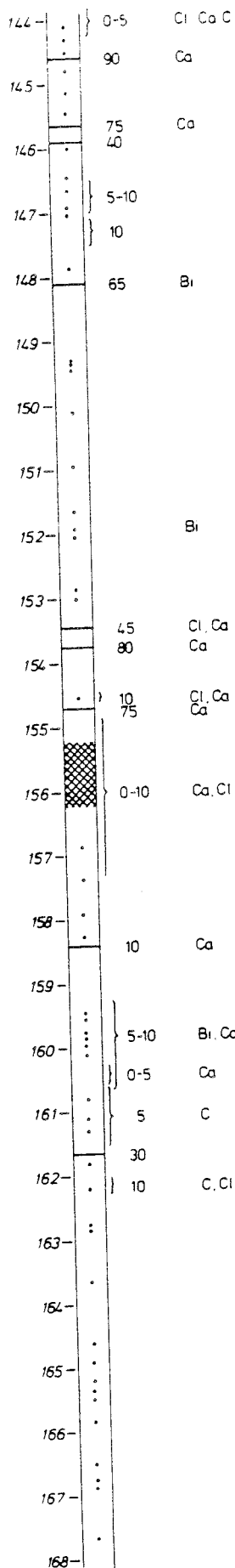
Fracture fillings, abbreviations

Bi	Biotite
C	Clay
Ca	Calcite
Cl	Chlorite
E	Epidote
Fe	Iron precipitation, rust
Py	Pyrite
Q	Quartz
T	Talc
Mylonit	Mylonite

Uppdrag KBS ta objekt 60 10







List of SKB reports

Annual Reports

1977-78

TR 121

KBS Technical Reports 1-120.
Summaries. Stockholm, May 1979.

1979

TR 79-28

The KBS Annual Report 1979.
KBS Technical Reports 79-01-79-27.
Summaries. Stockholm, March 1980.

1980

TR 80-26

The KBS Annual Report 1980.
KBS Technical Reports 80-01-80-25.
Summaries. Stockholm, March 1981.

1981

TR 81-17

The KBS Annual Report 1981.
KBS Technical Reports 81-01-81-16.
Summaries. Stockholm, April 1982.

1982

TR 82-28

The KBS Annual Report 1982.
KBS Technical Reports 82-01-82-27.
Summaries. Stockholm, July 1983.

1983

TR 83-77

The KBS Annual Report 1983.
KBS Technical Reports 83-01-83-76.
Summaries. Stockholm, June 1984.

1984

TR 85-01

Annual Research and Development Report 1984
Including Summaries of Technical Reports Issued during 1984. (Technical Reports 84-01-84-19)
Stockholm June 1985.

1985

TR 85-20

Annual Research and Development Report 1985
Including Summaries of Technical Reports Issued during 1985. (Technical Reports 85-01-85-19)
Stockholm May 1986.

Technical Reports

1986

TR 86-01

I: An analogue validation study of natural radionuclide migration in crystalline rock using uranium-series disequilibrium studies

II: A comparison of neutron activation and alpha spectroscopy analyses of thorium in crystalline rocks

JAT Smellie, Swedish Geological Co, AB MacKenzie and R D Scott, Scottish Universities Research Reactor Centre
February 1986

TR 86-02

Formation and transport of americium pseudocolloids in aqueous systems

U Olofsson

Chalmers University of Technology, Gothenburg, Sweden

B Allard

University of Linköping, Sweden

March 26, 1986

TR 86-03

Redox chemistry of deep groundwaters in Sweden

D Kirk Nordstrom

US Geological Survey, Menlo Park, USA

Ignasi Puigdomenech

Royal Institute of Technology, Stockholm, Sweden

April 1, 1986

TR 86-04

Hydrogen production in alpha-irradiated bentonite

Trygve Eriksen

Royal Institute of Technology, Stockholm, Sweden

Hilbert Christensen

Studsvik Energiteknik AB, Nyköping, Sweden

Erling Bjergbakke

Risø National Laboratory, Roskilde, Denmark

March 1986

TR 86-05

Preliminary investigations of fracture zones in the Brändan area, Finnsjön study site

Kaj Ahlbom, Peter Andersson, Lennart Ekman,

Erik Gustafsson, John Smellie,

Swedish Geological Co, Uppsala

Eva-Lena Tullborg, Swedish Geological Co, Göteborg

February 1986

TR 86-06

Geological and tectonic description of the Klipperås study site

Andrzej Olkiewicz
Vladislav Stejskal
Swedish Geological Company
Uppsala, October, 1986

TR 86-07

Geophysical investigations at the Klipperås study site

Stefan Sehlstedt
Leif Stenberg
Swedish Geological Company
Luleå, July 1986

TR 86-08

Hydrogeological investigations at the Klipperås study site

Bengt Gentzschein
Swedish Geological Company
Uppsala, June 1986

TR 86-09

Geophysical laboratory investigations on core samples from the Klipperås study site

Leif Stenberg
Swedish Geological Company
Luleå, July 1986

TR 86-10

Fissure fillings from the Klipperås study site

Eva-Lena Tullborg
Swedish Geological Company
Göteborg, June 1986

TR 86-11

Hydraulic fracturing rock stress measurements in borehole Gi-1, Gideå Study Site, Sweden

Bjarni Bjarnason and Ove Stephansson
Division of Rock Mechanics,
Luleå University of Technology, Sweden
April 1986

TR 86-12

PLAN 86 – Costs for management of the radioactive waste from nuclear power production

Swedish Nuclear Fuel and Waste Management Co
June 1986

TR 86-13

Radionuclide transport in fast channels in crystalline rock

Anders Rasmuson, Ivars Neretnieks
Department of Chemical Engineering
Royal Institute of Technology, Stockholm
March 1985

TR 86-14

Migration of fission products and actinides in compacted bentonite

Börje Torstenfelt
Department of Nuclear Chemistry, Chalmers University of Technology, Göteborg
Bert Allard
Department of water in environment and society,
Linköping university, Linköping
April 24, 1986

TR 86-15

Biosphere data base revision

Ulla Bergström, Karin Andersson, Björn Sundblad,
Studsvik Energiteknik AB, Nyköping
December 1985

TR 86-16

**Site investigation
Equipment of geological, geophysical, hydrogeological and hydrochemical characterization**

Karl-Erik Almén, SKB, Stockholm
Olle Andersson, IPA-Konsult AB, Oskarshamn
Bengt Fridh, Bengt-Erik Johansson,
Mikael Sehlstedt, Swedish Geological Co, Malå
Erik Gustafsson, Kenth Hansson, Olle Olsson,
Swedish Geological Co, Uppsala
Göran Nilsson, Swedish Geological Co, Luleå
Karin Axelsen, Peter Wikberg, Royal Institute of Technology, Stockholm
November 1986

TR 86-17

Analysis of groundwater from deep boreholes in Klipperås

Sif Laurent
IVL, Swedish Environmental
Research Institute
Stockholm, 1986-09-22

TR 86-18

Technology and costs for decommissioning the Swedish nuclear power plants.

Swedish Nuclear Fuel and Waste Management Co
May 1986

TR 86-19

Correlation between tectonic lineaments and permeability values of crystalline bedrock in the Gideå area

Lars O Ericsson, Bo Ronge
VIAK AB, Vällingby
November 1986

TR 86-20

A Preliminary Structural Analysis of the Pattern of Post-Glacial Faults in Northern Sweden

Christopher Talbot, Uppsala University
October 1986

TR 86-21

Steady-state flow in a rock mass intersected by permeable fracture zones. Calculations on case 2 with the GWHRT-code within level 1 of the HYDROCOIN project

Björn Lindbom, KEMAKTA Consultants Co, Stockholm
December 1986

TR 86-22

Description of hydrogeological data in SKBs database Geotab

Bengt Gentzschein, Swedish Geological Co, Uppsala
December 1986

TR 86-23

Settlement of canisters with smectite clay envelopes in deposition holes

Roland Pusch, Swedish Geological Co, Lund
December 1986

TR 86-24

Migration of Thorium, Radium and Cs-137 in till soils and their uptake in organic matter and peat

Ove Landström, Björn Sundblad, Studsvik Energiteknik AB, Nyköping
October 1986

TR 86-25

Aspects of the physical state of smectite-adsorbed water

Roland Pusch, Ola Karnland, Swedish Geological Co, Lund
December 1986

TR 86-26

Model shear tests of canisters with smectite clay envelopes in deposition holes

Lennart Börgesson, Swedish Geological Co, Lund
December 1986